ABSTRACT

Title of Dissertation: 3D ENGINEERING OF VIRUS-BASED PROTEIN NANOTUBES AND RODS: A TOOLKIT FOR GENERATING NOVEL NANOSTRUCTURED MATERIALS

Adam Degen Brown, Doctor of Philosophy, 2018

Dissertation directed by: Professor James N. Culver, Department of Plant Science and Landscape Architecture and the Institute for Bioscience and Biotechnology Research

Technological innovation at the nanometer scale has the potential to improve a wide range of applications, including energy storage, sensing of environmental and medical signals, and targeted drug delivery. A key challenge in this area is the ability to create complex structures at the nanometer scale. Difficulties in meeting this challenge using traditional fabrication methods have prompted interest in biological processes, which provide inspiration for complex structural organization at nanometer to micrometer length scales from self-assembling components produced inexpensively from common materials.

From that perspective, a system of targeted modifications to the primary amino acid structure of *Tobacco mosaic virus* (TMV) capsid protein (CP) has been

developed that induces new self-assembling behaviors to produce nanometer-scale particles with novel architectures. TMV CPs contain several negatively charged carboxylate residues which interact repulsively with those of adjacent CP subunits to destabilize the assembled TMV particle. Here, the replacement of these negatively charged carboxylate residues with neutrally charged or positively charged residues results in the spontaneous assembly of bacterially expressed CP into TMV virus-like particles (VLPs) with a range of environmental stabilities and morphologies and which can be engineered to attach perpendicularly to surfaces and to display functional molecular patterns such as target-binding peptide chains or chemical groups for attachment of functional targets.

In addition, the distinct electrostatic surface charges of these CP variants enable the higher-level coassembly of TMV and VLP into continuous rod-shaped nanoparticles with longitudinally segregated distribution of functionalities and surface properties. Furthermore, the unique, novel, environmentally responsive assembly and disassembly behaviors of the modified CPs are shown to act as simple mechanisms to control the fabrication of these hierarchically structured functional nanoparticles.

3D ENGINEERING OF VIRUS-BASED PROTEIN NANOTUBES AND RODS: A TOOLKIT FOR GENERATING NOVEL NANOSTRUCTURED MATERIALS

by

Adam Degen Brown

Dissertation submitted to the Faculty of the Graduate School of the
University of Maryland, College Park, in partial fulfillment
of the requirements for the degree of
Doctor of Philosophy
2018

Advisory Committee:
Professor James N. Culver, Chair
Associate Professor Edward Eisenstein
Professor Reza Ghodssi
Associate Professor Silvina Matysiak
Associate Professor Daniel Nelson, Dean's Representative

Acknowledgements

I would like to thank, first and foremost, my graduate research advisor, Dr. James N. Culver, for his guidance, his support, and his extensive patience and understanding beyond what should be expected. I would also like to thank all the members of my Ph.D. dissertation committee, Professor Edward Eisenstein, Professor Reza Ghodssi, Professor Silvina Matysiak, and Professor Daniel Nelson for their assistance and suggestions which contributed to this work.

Thank you to the experts in the Laboratory for Biological Ultrastructure, Timothy Maugel and Jan Endlich, for their assistance, guidance, and expertise in electron microscopy, which was critically important to this work for the purposes of assessing results and guiding further research.

I would like to thank all my current and former collaborators and coworkers who each helped me in their own distinct ways. From Professor Culver's lab – Dr. Sabrina Kramer, Dr. Elizabeth Royston, Dr. Xiao Wang, Dr. Tamara Collum, and Ms. Yvette Tamukong – and from Professor Ghodssi's lab – Dr. Konstantinos Gerasopolous, Dr. Faheng Zang, Dr. Xiao Zhu Fan, and Dr. Sangwook Chu.

Finally, I need to thank my family: my sister, Lauren, and especially my parents, David and Cookie Brown, for their unyielding love and support.

Table of Contents

List of Figures

List of Abbreviations

TMV, *Tobacco mosaic virus*; **VLP,** virus-like particle; **CP,** capsid/coat protein; **EDC,** 1-ethyl-3-(3-dimethylaminopropyl)carbodiimide; **TNT,** 2,4,6-trinitrotoluene; **CuAAC,** Cu(I)-catalyzed azide-alkyne cycloaddition; **NHS,** N-hydroxysuccinimide; **PEG,** polyethylene glycol; **OAS,** origin of assembly sequence; **UAc,** uranyl acetate

Chapter 1: Introduction

1.1. Background and Motivation

The core motivation of this research project is twofold: (I) to improve upon the proven potential of *Tobacco mosaic virus* to function as a self-assembling, well organized nanoparticle and (II) to use TMV as a model system to better understand how to design and control the self-assembly of protein-based nanomaterials. This motivation arose from (i) the increasing awareness of the utility of nanostructured materials for a wide array of applications, (ii) understanding of the advantages that naturally occurring, biologically based materials and methods provide for the creation of nanomaterials, and (iii) recognition that viruses in particular are an adaptable and fertile model for nanoparticle production. This section will attempt to establish these ideas in some more detail.

1.1.1. Advantages and applications of nanostructured materials

Controllable, hierarchical self-assembly of complex architectures at nanometer to micrometer length scales is an important, and potentially revolutionary, capability promised by nanotechnology. The development of successful methods for producing reliable and consistent results toward this goal will have profound implications for advancements in diverse technological areas such as the harvesting, conversion and storage of energy for clean and renewable energy usage [1-4], sensing of environmental and medical signals [5, 6], and targeted drug and medical imaging agent delivery [7-10] for improved diagnostic outcomes of intractable diseases.

The promised benefits of nanotechnology, and of the benefits afforded by nanomaterials, rest on the potential improvements to existing functions or the creation of completely new functions made possible by the nanometer length scales that characterize them. Nanometer-scale structures exist at the extreme end of the trend toward miniaturization that has dramatically improved the performance of technologies in recent decades. Radical miniaturization of functional device components reduces the overall footprint necessary for those components. This can reduce the size and of the device itself, improving portability and storage requirements, which lead to greater availability of the technology. At the same time, detrimental impacts to the environment can be alleviated by reducing both the energy requirements of the device while it is in use as well as the amount of waste associated with its disposal.

Targeted drug delivery is one example of a promising technology being made possible by the development of nano- to micrometer scale structures that may radically improve treatments for costly and tragic diseases such as cancer. One of the most effective treatments for some forms of cancer involves the administration of chemotherapeutic agents to the patient which are intended to kill or stop the growth of cancer cells which may have metastasized throughout the body. Such drugs inevitably have harmful effects on the patient's healthy cells, so treatment requires finding a compromise between the goals of attacking the cancer and not harming the patient. Targeted drug delivery seeks to improve the result of this compromise by delivering the chemotherapeutic agents to the cancer cells in a targeted manner, improving chances of reducing or clearing the cancer from the body while also reducing the side

effects that reduce the patient's quality of life. The drug delivery vehicles involved in this type of treatment need to be able to contain the chemotherapeutic agent while displaying features that will cause their preferential uptake by the cancer cells, all while remaining small enough to pass through capillaries and remain in circulation long enough for eventual uptake by the cancer cells. This last requirement necessitates the use of particles in the low micrometer scale at the most, but other considerations can make smaller, nanometer-scale particles preferable, including their greater uptake by target cells, ability to cross the blood-brain barrier, and faster drug release profile [11]. In addition, the ability to precisely control the properties of these particles can dramatically affect their effectiveness. The physical and chemical properties of the particle surface are crucially important to the targeting of cells, influencing biodistribution and accumulation profiles through cellular uptake, prolonging circulation time, and determining immune system clearance or evasion [11]. Establishing greater control over these factors, including the nanoscale patterning of particle surface properties, appears to be a crucial factor in the therapeutic efficacy of the platform.

Improved control over the patterning and architecture of nanoscale structures and materials has many other potentially revolutionary applications. Many useful biochemical processes that occur naturally within cells involve pathways of chemical reactions catalyzed by enzymes. Successfully transferring these complex networks into *in vitro* environments for energy harvesting and conversion, for chemical and pharmaceutical synthesis, or for isolation and study is an ongoing project for biotechnology and analytical biology. However, the efficient functioning of these

enzyme *in vivo* often depend on their confinement and spatial arrangement at the submicron scale to effectively couple enzymatic reaction together through control of the concentration, diffusion, stability and channeling of the enzymes, substrates, reaction-intermediates, cofactors and products. The form of this patterning can be a two-dimensional arrangement along membranes surfaces [12, 13] or a more complex three-dimensional compartmentalization within proteinaceous [14] or membrane-based capsules and vesicles. The harnessing and study these enzyme cascades in an *in vitro* environment would benefit immensely from new materials that could be used to control the spatial patterning and arrangement of enzymes at nanometer scales [15].

The essential requirement of these approaches is the ability to control the three-dimensional organization of material components at a micro- to nanometer scale in a way that allows for scalable production of these materials. Improvements in efficiency, power, novelty, and utility in a variety of other application fields are promised by the development of materials and method allowing precise control of complex nanoscale patterns and architectures.

1.1.2. Strategies for generating micro- and nanostructures

Biology offers unique solutions to current needs in nanoscale design and application. The existence of functional nanoscale structures within living biological systems provides a natural starting point for the generation of new types of nanostructured materials with tailored functions and properties in the lab or factory. Using biological molecules to create nanomaterials has the advantage all the preexisting machinery for the production of these molecules, the preexisting methods for altering those molecules, and in some cases the innate tendency of those

molecules to coassociate and organize themselves in a bottom-up manner to generate higher-order structures. Attempts to create these kinds of structures from non-biological components need to solve or avoid these issues that have already been solved in biological systems, and all successful attempts do this in ways that are sometimes distinct from and at other times inspired by the biological solutions. A few of the non-biological components and methods for the creation of non-biological nanostructured materials are inorganic nanoparticles, polymers, carbon nanotubes, and dendrimers.

Biological systems have developed an array of methods for solving problems and interacting with their environment at nanometer to micrometer length scales. Cells employ a diverse toolkit for accomplishing the activities necessary for continued existence, including fine-tuned recognition of target molecules, strong and reversible binding of those targets, chemical modification of molecular analytes through enzymatic processing, and systematic coupling of these modification through enzymatic chains which together enable them to perform such diverse tasks as pathogen recognition and elimination and harvesting of energy for further cell function. All of these tasks are accomplished in a “bottom-up” approach, through the assembly from simple monomeric units of macromolecular components with well-defined structures, surface properties, and functionalities. This bottom-up fabrication method of nanoscale functional material is of particular interest for its potential use in the creation of materials and surfaces due to its often greater efficiency and scalability when compared to traditional top-down fabrication methods [16, 17].

Bionanomaterials (nanostructured biomaterials): Nucleic acids, such as DNA, are being investigated as raw materials for the self-directed construction of complex but well defined nanoscale structures and even larger scale materials with regular nanoscale patterns, such as regular and repeated binding motifs. The use of nucleic acids as a structural building material for the construction of nanoscale materials is developing rapidly and is enabled by the structural features that allow them to function as the primary physical method of information storage in the natural world, namely the flexible yet structurally stable, arbitrarily long, covalently linked, single molecule backbones which routinely reach centimeters in length together with the non-covalent coupling mechanism between strands by extensive, sequence dependent, individual base-pairing events. The importance and ubiquity of nucleic acids have led to the development of reliable and relatively inexpensive chemical methods to synthesize oligonucleotides of arbitrary length and sequence as raw materials. Two primary approaches have emerged in the field of nucleic acid-based nanostructured materials, one using DNA alone as the basis for the creating rigid nanostructures, the other using non-nucleic-acid-based nanoparticles, which provide rigidity, coupled with DNA, which direct their arrangement and organization.

The first approach uses the regular spacing of nucleotides along the DNA backbone and the sequence specificity of noncovalent hybridization of antiparallel DNA strands via Watons-Crick base-pairing interactions to direct the self-assembly of numerous DNA strands into complex architectures with well-defined geometries. The interaction of each component DNA strand with multiple other strands allows for the emergence of rigidity in the resulting material despite the inherent physical

flexibility of its components. This method has allowed for the creation of increasingly complex two-dimensional [18, 19] and three-dimensional [20-22] structures founded on a hierarchical assembly process in which rigid tiles composed of multiple oligonucleotide strands self-assemble into larger structures by DNA hybridization of the unpaired "sticky ends" exposed at the tiles' edges (Figure 1-1A, B).

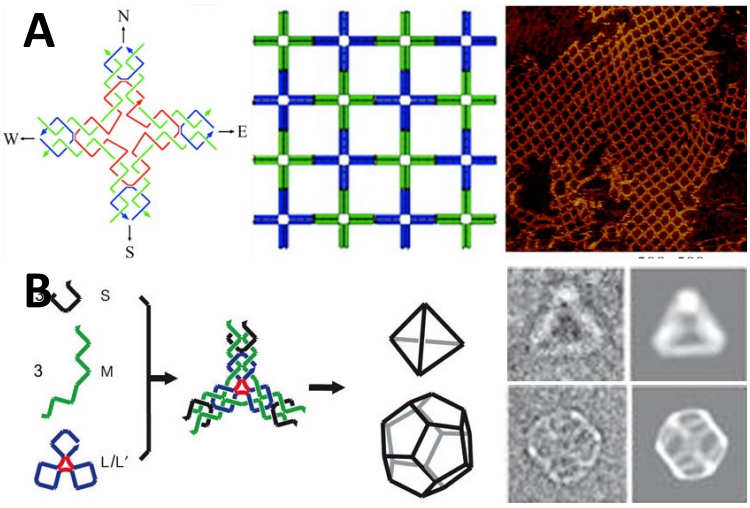

Figure 1-1: DNA hybridization-based tiled structures. (A) 2D lattice based on a tessellation of a DNA tile consisting of nine oligonucleotides. Reprinted with permission from [18]. Copyright 2003. (B) 3D wireframe polyhedral built from DNA three-point star motifs, where shape depends on the intrinsic curvature and concentration of the tile. Reprinted with permission from [20]. Copyright 2008.

In contrast to the hybridization of DNA tiles, which typically results in objects and materials with regular or periodic structure, DNA origami uses many short oligonucleotides to act as "staples" which cross-hybridize and tether distant sections of a much larger (multithousand-base long) DNA strand, inducing it to adopt some specific conformation. The assistance of computer-aided design software allows for the creation of complex two-dimensional [23] and three-dimensional [24-26] DNA origami structures (Figure 1-2). The structural complexity afforded by the method of DNA origami has several drawbacks. The conformational reactions require precise ion concentrations and very long annealing times (up to one week) and can

still result in low yields of properly folded conformations, necessitating further gel purification steps to obtain high quality samples [27].

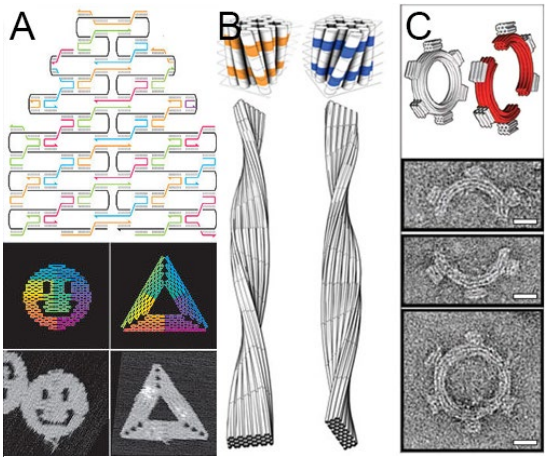

Figure 1-2: DNA hybridization-based origami structures. (A) 2D origami structures. Reprinted with permission from [23]. Copyright 2006. (B) Twisted 3D DNA Bundles and (C) curved DNA structures Reprinted with permission from [25]. Copyright 2009

The second approach uses surface-bound oligonucleotides to spatially arrange rigid nanoparticles. A typical method uses designed oligonucleotides with either 3′ or 5′ terminal thiol groups which are subsequently templated onto the surface of colloidal gold nanoparticles through gold-thiol interactions. Very dense oligonucleotide monolayers can be established on the nanoparticle surface when high ionic strength solutions, which can screen the mutually repulsive negative charges of the oligonucleotides, are employed [28]. Hybridization of the surface-bound oligonucleotides to those of adjacent nanoparticles can induce the formation of various superlattice structures, when spherical nanoparticles are used [29, 30], or alternative configurations by either controlling the controlling the templating of the oligonucleotides onto the nanoparticles [31] or by using anisotropic nanoparticles [32].

Strategies for forming nanomaterials from protein

One of the most versatile classes of components in biology's toolkit and a prime candidate source for bottom-up fabrication of novel functional materials are proteins, which accomplish diverse roles as structural scaffolds as cytoskeletal

components and viral capsids, molecular recognition sensors as receptors and antibodies, and chemical processing catalysts as enzymes. Proteins represent a more complex class of materials than nucleic acids, and so their use as the foundation for the construction of nanostructured biomaterials has several advantages. While nucleic acids are generally comprised of a relatively small number of fundamental building blocks (A, C, G, T, and U ribo- and/or deoxyribonucleotides), which can limit the number of combinations and specificity of chemical features, limiting the material's potential for complex functionality, proteins are built from a broader set of building blocks, twenty (or more) amino acids with a wider variety of physical and chemical properties. This gives protein a much larger set of possible combinations of sequences, expanding the structural and functional workspace/set of possible states. The specific nature of the 1° (amino-acid sequence) structure of the protein determines the 2° (local conformational folding), 3° (global conformational folding), and 4° (coassociation of multiple peptide chain) structure in complex but deterministic ways, the prediction of which is the focus of intense effort and continual improvement. This enhancement of possible structures and functions compared to nucleic acids is reflected in the broader set of roles naturally relegated to proteins in their native cellular and organismal environments. Additionally many of the distinct chemical groups present in the various amino acid side chains can be independently targeted for specific uses, making proteins more chemically tractable than nucleic acid-based nanostructures. Proteins are also extremely genetically tractable, as modification of the gene encoding the protein by uncomplicated and routine laboratory techniques can produce the molecular instructions for production of that

protein in any of numerous common cellular expression systems. Modifications to protein structure therefore benefit from the same processes that enable the generation of the raw materials for DNA-based nanostructures. This section will review some of the research into methods for creating nanomaterials from protein components.

Fusion proteins for symmetrical self-assembly: Some proteins naturally form symmetrically arranged complexes from multiple identical copies. Usually, these quaternary protein assemblies comprise dimers, trimers, tetramers, etc. which are assembled into regular polyhedral shapes, such as tetrahedrons, hexahedrons, octahedrons, dodecahedrons, and icosahedrons. A general method for combining the natural ability/tendency of proteins to self-assemble into small regular polyhedral in order to generate more complex nanostructured materials was described by Padilla et al. [33] wherein two proteins that separately form multimeric symmetrical assemblies with other copies of themselves are used to create a rigidly fused protein that will self-assemble with other copies of itself in more complex ways derived from the self-associating tendencies of its components. Using this method, nanoscale protein cages [34] and a highly porous protein cube [35] were designed.

Three-dimensional domain-swapped oligomers: The method of three-dimensional domain swapping involves replacing an individual structural domain from one protein monomer with the same domain from a second monomer. In this way the two monomers assemble together when the new domain of the first monomer associates with the second monomer to complete its native assembly. This method has been successfully utilized to design and construct new dimers and fibrous oligomers [36], protein polymers built from cytochrome *c* [37], myoglobin heterodimers [38] and a

Zn-SO_4-encapsulating nanocage consisting of a domain-swapped cytochrome cb_{562} dimer [39].

Self-assembling modules of designed coiled-coil peptides: Many protein-protein interactions involve associated domains of alpha-helical coiled coils. These interactions between amphipathic α-helices lead to a wide variety of protein assemblies [40]. Several researchers have incorporated these domains to guide the self-assembly of various nanostructured biomaterials, including a self-assembling cage from coiled-coil peptides [41] and self-assembling peptide nanotubes with a variety of predetermined inner channel diameters and chemistries from α-helical barrel building blocks [42]. The latter of these, the peptide nanotubes, displayed some tenability with respect to longitudinal assembly between the subunits and lateral associations between nanotubes [43]. Finally Sciore *et al* reported a simple, generalizable method for the assembly of protein cages from short de novo designed coiled-coil domains [44].

Computationally designed self-assembling artificial proteins: Advances in structure prediction [45] and design principles for de novo proteins [46, 47] have enabled a general computational approach for the design of self-assembling protein structures [48, 49]. The approach involves the design of low-energy protein-protein interfaces combined with a symmetrical repetitive architecture to drive the assembly of large scale arrays of designed protein subunits using RosettaDesign calculations. Variation of the symmetric architecture can produce protein arrays extending in one, two, or three dimensions. …designed and produced a "self-assembling icosahedral nanocage from 60-subunit trimeric protein building blocks" [50] and "megadalton-scale

icosahedral protein complexes from two-component 120-subunit proteins with atomic-level accuracy" [51]. In the latter, the researchers designed, produced, and experimentally characterized 120-subunit icosahedral protein nanostructures from two co-assembling components that were comparable in mass (1.8-2.8 MDa) and size (24-40nm diameter) to small viral capsids. [10 different designs, each with one of three different icosahedral architectures produced protein nanostructures closely matching computational models] These artificial proteins assemble in vitro from independently purified components and allows for the electrostatic charge-based packaging of small molecular cargo.

All of this recent work in novel protein-based nanomaterials is an extension of the set of naturally occurring proteinaceous nanostructures developed through the evolutionary process of trial and error and employed as a fundamental component of all living systems. A remarkably successful and extensive refinement process has produced all of the examples of existing structural proteins found in the natural world. These diverse structural proteins exhibit a wide variety of finely-tuned capabilities and properties that can not only provide exemplary inspiration for entirely novel protein designs but can also act as the established foundation for the development of new proteinaceous nanomaterials through relatively minor alterations either pre- or posttranslation.

1.1.3. Viruses as bionanomaterials

One class of protein-based biological nanostructures that offer particular suitability as potential platforms for the creation of novel biomaterials is viruses. Virus particles are nanoscale structures created by the organized macromolecular

assembly of one or several viral proteins packaging a nucleic acid genome. Viruses take advantage of the structural, molecular recognition and functional capabilities of protein for the purposes of host cell recognition, cell invasion and infection, extracellular stability, and packaging and containment of a cargo load in the form of their RNA or DNA genome. This unique combination of properties has made viruses a productive foundation for the development of a wide range of engineered applications including targeted drug delivery [52-54], biosensing [55], and energy storage [56, 57]. What follows is a review of the literature that treats viruses as materials

Several plant viruses have been investigated as nanoscale templates for the development of new materials and applications. Plant viruses share features that make them attractive as the basis for the fabrication of biomaterials. They are simple and often highly stable particles that self-assemble from defined protein subunits with remarkable uniformity of size and shape. The repetitive/iterative nature of the viral capsid makes it useful for the concentrated and organized display of functional groups in the form of native or engineered amino acid side chains, which can serve as functionalizing entities in their own right or as sites for chemical attachment of other molecules or sites for the nucleation of inorganic materials. The ability of viruses to self-assemble and to remain monodisperse in solution allows for the processing and analysis of these nanoparticles as a bulk material [58]. The three dimensional structure of many plant viruses is known, often to a high degree of atomic precision, allowing for the identification of functional groups available for targeting or the rational design for the introduction of new functional groups to optimal locations

within or on the viral nanoparticle. These design alterations to the viral nanoparticles is made possible by the encoding of the viral nanoparticle's component materials in its genome, allowing for the use of standard and well established methods of genetic modification. Finally, plant viruses can be produced relatively inexpensively and renewably at large scales [17].

As is the case with viruses in general, plant viruses typically have one of two primary morphologies: icosahedral or helical. Viruses of each type are being investigated as biological scaffolds in materials applications. The two morphologies are characterized by different structural geometries and properties that can be useful for different applications. Icosahedral viruses have a large inner chamber enclosed on all sides by the capsid proteins that surround and protect the viral genome. This inner chamber provides a location for the loading and storage of cargo, such as therapeutic or imaging molecules. Many helical viruses have an inner channel located along their central axis which is not for the containment of the genome, which is instead sandwiched between successive layers of the helically-arrayed protein, but is rather necessitated by steric considerations. This inner channel also provides a potential location for the loading of cargo, although the lack of closure at either end needs to be addressed if the cargo is to remain contained. Both types of virus allow for the display of various types of useful signals or functional agents, such as peptides, proteins, fluorescent molecules, or chelating groups [59-63]. Generally, icosahedral viruses have a greater ratio of loadable volume to (inner or outer) surface area, while helical viruses have greater surface area to volume ratio.

Icosahedral plant viruses:

Red clover necrotic mosaic virus (RCNMV) is a structurally simple icosahedral virus in the *Tombusviridae* family, whose members "possess unusually stable and robust capsids" [64]. The capsid of RCNMV consists of 180 identical copies of the capsid protein subunit, which contains an inner cage consisting of RNA and protein, and each virion particle contains around 390 (±30) Ca^{2+} ion and roughly 420 (±25) Mg^{2+} ions, or slightly more than four divalent cations per CP. CryoEM and three-dimensional (3D) image reconstruction were used to determine that RCNMV CP undergoes conformational changes upon depletion of its divalent cations, as would be expected upon relocation of the virion to the cytosol of a host cell. This conformational change causes the opening of pores through the capsid shell sufficiently large to allow the leakage of encapsulated ssRNA. This modulation of pore opening and closing by sequestration from and re-exposure to sufficiently high concentration of divalent cations was successfully exploited to enable the loading of imaging or therapeutic molecules, namely the fluorescent dyes rhodamine and luminarosine and the chemotherapeutic agent doxorubicin [65]. Notably, successful loading was only obtained with these positively or neutrally charged molecules and not with the negatively charged dye fluorescein, hypothesized to be due to interactions with the negatively charged RNA genome that is still present. Furthermore, the conjugation of N-cadherin-targeting peptide sequences to the surface of doxorubicin-loaded RCNMV particles caused increased their uptake by HeLa cells and increased toxicity to those cells [66].

Cowpea chlorotic mottle virus (CCMV), a member of *Bromoviridae*, similarly has a capsid of 180 identical CP subunits that bind to divalent cations. Upon sequestration of those divalent cations CCMV undergoes swelling and pore-opening, similarly to RCNMV but in a pH-dependent manner [67]. This response appears to be due to the electrostatic repulsion caused by negatively charged acidic residues at the Ca^{2+}-binding site, and it only occurs at or above pH7, which is thought to be due to the abnormally elevated pK_a of a single residue, Glu81, to around 7 due to its proximity to two other negatively charged amino acids, Asp153 and Glu111, against which it develops a repulsion upon protonation at higher pH in the absence of Ca^{2+} [68]. This swelling and poration is reversible and represents another possible strategy for loading and unloading of target molecules.

Cowpea mosaic virus (CPMV) is another icosahedral virus under development as a functional nanoparticle. The virion is 30 nm in outer diameter and is composed of a "large" (41 kDa) and a "small" (23 kDa) capsid protein. CPMV was the first plant virus to be developed as a peptide-presentation system, made possible by the identification of sites within the coat proteins that would be allow surface exposure of inserted peptide sequences based on detailed three dimensional assembled protein structures [69-72]. The most common point of insertion is within a surface exposed loop of the small CP (the "S protein") which results in the surface display of 60 copies of the inserted sequence per virion. It was determined that this method of display of short antigenic peptides increased their immunogenicity for the production of antibodies [73]. Similar display of certain peptides has been used to

deposit silica or an iron-platinum alloy onto the surface of CPMV for the development of inorganic featured nanoparticles [74, 75].

Filamentous plant viruses:

One category of virus of particular interest is filamentous plant viruses. These viruses are notable for their simple structure, consisting of a single nucleic acid molecule encapsulated by multiple identical copies of a single coat protein subunit, and their characteristic elongated form providing a high aspect ratio and large surface area per unit volume. The characteristic properties of filamentous plant viruses, specifically their simple composition from a single, repeated CP subunit, present them as ideally suitable candidates to act as model systems to investigate the mechanisms that drive assembly of molecular subunits into higher order structures.

Potato virus X (PVX): Carrette et al. replaced the CP gene for PVX with a gene for a fusion protein consisting of the CP fused at its C-terminus to Candida antarctica lipase B separated at the gene level by a sequence ("2A") which is known to sometimes terminate protein translations [76]. This resulted in PVX particles arrayed with catalytically active enzyme that retained infectivity and were able to reproduce *in vivo* in the host.

Steinmetz *et al.* focused on PVX as a model virus to explore the potential use of rod-shaped viruses for biomedical applications such as targeted drug delivery and imaging [63]. While the amino acid sequence of PVX's 25 kDa CP is known (and known to contain 11 lysines, 10 aspartic acids, and 10 glutamic acids as potential bioconjugation targets), its crystal structure is not known, obscuring the precise location of bioconjugated elements and inhibiting design-based modifications.

However attempts to couple biotin to carboxylate residues were unsuccessful while amine-based labelling was successful, indicating the surface-accessibility of the lysine residues and the surface-inaccessability of the carboxylates. Bioconjugation methods including amine modification and "click" chemistry were established to functionalize PVX rods with biotin, fluorescent dyes (fluorescein, OregonGreen 488, and AlexaFluor 647), and PEGs of various molecular weights. The variously labelled hybrid nanoparticles were characterized to determine labelling efficiency. Labelling was determined to be highly efficient when bioconjugating a single fluorescent dye with 70-90% of CPs labelled, while doubly fluorescently labelled rods showed lower labelling efficiency (25-40%) but also used lower initial concentration conditions. PEG labelling showed lower efficiencies, with 20% and 40% of CPs labelled with PEG1000 and PEG2000, respectively. The higher labelling efficiency of the larger PEG, which may be surprising due to the expectation of steric effects inhibiting labelling, was hypothesized to be due to the increased hydrophilicity of the longer polymers assisting the coupling reaction. Cell interaction studies showed differential uptake of hybrid fluorescently labelled, PEGylated PVX particles by HeLa cells dependent on both which fluorescent dye was attached as well as the size of the conjugated PEG molecule, with PEG blocking uptake of OregonGreen 488-labelled particles but not of AlexaFluor 647-labelled particles and the larger PEG2000 labels even increasing uptake relative to PEG1000-labelled particles.

Papaya mosaic virus (PapMV) is a member of *Potexvirus* that has been used to display a binding peptide (DPAPRPR) with specificity for the resting spores of the fungus *Plasmodiophora Brassicae*. The resulting nanoparticles showed high avidity

for the spores, allowing for the detection of these fungal spores, which had previously caused difficulty for detection using standard enzyme-linked immunosorbent assay (ELISA) due to unspecific cross reactions between fungal cell walls and the antibodies that these viral nanoparticles were designed to replace [77].

1.1.4. Tobacco mosaic virus as a model rod-shaped virus for nanomaterial synthesis

TMV is one of the most extensively studied and best characterized filamentous plant viruses. The TMV virion is a rigid but hollow tube-shaped rod, 18 nm in diameter with a 4 nm diameter inner channel, consisting of roughly 2130 CP subunits arranged in a helix with a pitch of 23° with 16⅓ CPs per turn enveloping a single strand of plus sense RNA [78]. The length of the RNA genome limits the length of the assembled virion to roughly 300 nm. The CP has a molecular weight of 17.5 kDa. Each CP subunit consists of a chain of 158 amino acids with four main alpha helices arranged radially in the assembled virion and connected by two inner loops and one outer loop with both the N- and C- terminus exposed on the outer surface of the assembled virion.

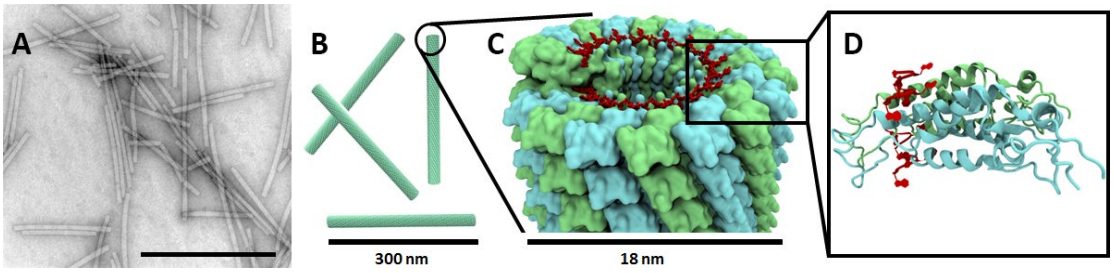

Figure 1-3: (A) TEM image of TMV, (B) models of full-length TMV rods, (C) magnified view of the 5' end of a TMV virion, and (D) representation of two adjacent copies of the TMV CP with adjacent fragments of genomic RNA

TMV enters a host cell passively through a wound to the cell wall. Upon reaching the cytoplasm, the relatively high pH and low calcium concentration initiates

disassembly of the coat protein from the 5′ end of the genomic RNA due to the relative lack of guanines in the third position at this end of the RNA [79]. The exposed 5′ end of the RNA is then free to bind to host ribosomes, which strip the RNA of bound CP as it is translated in a process of co-translational disassembly. Newly formed TMV CP monomers begin to associate into dimers, trimers, and pentamers, which then assemble into flat protein disks. Upon interaction with newly formed genomic TMV RNA, the disks undergo a conformational change into a "lock-washer" (short helical) configuration. As the RNA is situated in an RNA binding groove near the disk's inner channel additional disks of coat protein are added to the growing rod's 5′ end and the remainder of the RNA is drawn up through the inner channel until the full-length rod is formed [80].

TMV is a particularly attractive substrate for the creation of nanoscale materials. Detailed physical knowledge of TMV, including precise 3-D structural information [81, 82], virion assembly mechanism, and biochemical properties are understood in unique detail [65, 66, 83]. A full-length cDNA clone of the virus is available, allowing the design and creation of modified viruses. It is purifiable in large quantities from infected host plants, and its stability under a wide range of environmental conditions facilitates its incorporation into systems and devices [84]. While icosahedral viruses boast large interior chambers for cargo packaging and delivery, rod-shaped viruses like TMV have high-aspect-ratio geometries and large protein copy number per particle volume that make them ideal substrates and scaffolds [84]. The rod-shaped TMV has a high-aspect-ratio geometry (300 nm length by 18 nm diameter) and large protein copy number (~2130) per particle that makes it

an ideal substrate for the integration of tunable high-surface-area materials or densely arranged motif displays into functional devices. These properties have driven research into the use of TMV for the development of diverse applications, including anti-reflective photochemical electrodes, super-hydrophobic surfaces, improved energy storage, and transducer surfaces for sensing applications [16, 17, 85-88].

1.2. Thesis Contributions

1.2.1. Development of self-assembling, nucleic-acid-free *Tobacco mosaic virus*-like particles

Despite the many advantages/potential toward the development of nanoscale functional material components conferred by/inherent in the use of filamentous viruses in general and TMV in particular, the use of "live" virus in this area of research has several drawbacks/disadvantages, including the need for plant growth facilities for virus production, the extended production time of plant-based infection and generation of virus, the risk of genetic recombination eliminating or altering intentional changes made to the virus, interference or resistance to structural/functional alterations to the virus due to the necessary incorporation of genomic RNA, and retention of infectivity of the viral product. These disadvantages are eliminated by the development of a virus-like particle based on the TMV CP, which self-assembled from protein components produced in bacteria and assembling without any incorporated genomic or non-genomic nucleic acids.

This dissertation establishes the changes sufficient for the design and generation of this new type of virus-like particle which solves the aforementioned

problems. This method uses structural data that identifies pairs of amino acids with similar charges that generate repulsive forces between adjacent viral capsid protein subunits, which discourage quaternary coassembly of the subunits into virus particles without the stabilizing incorporation of genomic RNA. These negatively charged amino acid residues are eliminated by alteration of the nucleic acid sequence that encodes the capsid protein. By also optimizing the gene for translation in bacteria and transforming that gene into an *E. coli*-based bacterial expression system, the resulting protein product reliably generates VLP which can be more rapidly modified and produced than virus, without incorporated RNA, and which retains the robust range of stability of the virus upon which it is based. Furthermore, modifications made to the CP to functionalize the resulting nanoparticle are retained or, in the case of larger peptide fusion products encoded in the CP gene, enhanced by means of eliminating loss of the modification through genetic recombination.

Work toward the accomplishment of this aim was contributed by Lindsay Naves and Xiao Wang. This work was published in *Biomacromolecules* as "Carboxylate-Directed *In Vivo* Assembly of Virus-Like Nanorods and Tubes for the Display of Functional Peptides and Residues" (2013)

1.2.2. Development of VLP-forming capsid protein variants with unique environmentally responsive disassembly and reassembly behavior

One advantageous property of biologically based nanomaterials is the tunability of the self-directed bottom-up assembly process. Biological systems are dynamic by necessity and so need to be responsive to environmental changes. This

requires them to have control over the disassembly of nanostructural features in addition to their assembly and to direct these behaviors in response to environmental stimuli. This can be accomplished by the direct action of an environmental factor on key elements of the nanostructure that underlie the assembly mechanism. This type of control over assembly and disassembly of VLPs would greatly extend the usefulness of VLP-based nanomaterials by allowing for a mechanism for restoring the components of the nanomaterial to a pre-assembled state for reorganization of the system or reuse in another system as well as generating additional potential applications by allowing for environmentally sensitive structural and behavioral responses of the system. In the case of TMV, disassembly is triggered by environmental changes encountered upon entry to a host cell. A change in hydronium ion concentration (pH) and other dissolved ion (such as Ca^{2+}) concentrations directly and indirectly alter the electrostatic charge-based interactions between adjacent CP monomers. By modifying the residues responsible for these interactions in a deliberate way, the character of the aggregate intersubunit interactions is also modified in ways that shift the effect of pH and solution salinity on particle assembly stability. These targeted modifications generate TMV CP variants with unique surface charge profiles and dynamic responses to changes in pH and/or concentration of dissolved ions.

This work and the following work were presented at the 15th Annual Conference on Foundations in Nanoscience: Self-Assembled Architectures and Devices in Snowbird, UT (2018).

1.2.3. Multifunctional chimeric VLP-virus nanorods with longitudinally differentiable regions using controlled self-assembly of protein components

TMV and VLP nanorods are versatile components for functionalizing surfaces and fluids, but each nanorod is composed of identical copies of a single CP or a homogeneous mixture of CPs when combined with leaky stop codon readthrough, so any modification to the underlying CP structure is present along the entire length of the resulting nanorod, generating relatively simple nanostructures that are functionally undifferentiated along their axial dimension. The ability to vary the properties of these nanorods along the axial dimension would expand their range of potential applications and power of use by introducing an additional dimension of organizational complexity. This feature would allow for the combination of multiple additional functional capabilities into each nanorod, conferring added functionalities such as capping of VLP for selective cargo molecule containment and environmentally controlled release, improved combination of target sensing and signal transduction functions along the spatial optimal portions of the nanorod, and spatially segmented tethering of enzymes for control of enzyme cascades for energy harvesting or chemical processing.

This research combines the unique electrostatic surface charge profiles at the ends of various VLP rods produced from engineered TMV CP with the unique assembly behaviors of those rods to develop methods for generating scalable batch production of complex rod-shaped nanoparticles composed of discrete, well ordered sections of differentiably addressable and functionalizable CP.

Portions of this work were presented at Gordon Research Conference for Virology in Ventura, California (2015) and the American Society for Virology Conference in Blacksburg, VA (2016)

1.3. Literature Review

The following section will review some of the most characteristic work in the fields of research most relevant to the project presented in this dissertation. The section will begin by addressing viruses generally with a focus on plant viruses in particular and Tobacco mosaic virus specifically. The remainder of this section will review research and principles covering the structure and assembly of TMV, and the modification made to TMV and other viruses to create novel nanofeatured materials through altered assembly, patterning, and functionalization.

1.3.1. Modifications affecting assembly

An understanding of the processes and conditions underlying TMV self-assembly has allowed for targeted changes to alter the particle's physical properties. These include changes to the CP, to the RNA scaffold around which the CP assembles, or to solution conditions driving assembly and disassembly. The resulting changes range from the shapes and dimensions of the particles produced (from short disks to micrometer-length wires), to their shape (from branched rods to spheres) to the distribution of functional groups along the length of the rod.

One general method for structural TMV modification exploits the ability of disassembled TMV CP to reassemble *in vitro* in the presence of single-stranded RNA containing an origin of assembly sequence (OAS) motif [89]. CP with modifications that prevent assembly of virus *in vivo* can be incorporated into rods by initiating

assembly *in vitro* using a mixture of modified and unmodified CP. This method was used to incorporate various amounts of CP with surface-exposed, C-terminal hexahistidine (His6) tags which had resisted virion formation *in vivo* [90]. Similarly, this method was used to coassemble bacteria-expressed CP, which lacks N-terminal acetylation and will not assemble with RNA *in vitro*, and plant-expressed CP, which is acetylated and does reassemble, into stable virions and in specifiable proportions [91]. Furthermore, various CPs with distinct functionalities (bioconjugation sites, peptide tags, etc.) can be organized in discrete sections along the length of the particle by sequential introduction of the different CP variants to the RNA scaffold *in vitro* due to the assembly process which progressively adds CP to the RNA scaffold from the OAS near the 3′ end towards the 5′ end [92]. Because the length of the TMV rod is primarily constrained by the length of the genomic RNA scaffold it contains, changing the length of that RNA scaffold can be used to control the length of the resulting nanoparticles either *in vitro* [93] or *in planta* [94]. The use of branched nucleic acid scaffolds has even been used to introduce kinked or branched structures instead of linear rods, creating “nanoboomerangs” and “multipods” [95].

Of particular significance to the research presented in this document, a method of ordering the longitudinal composition of TMV nanorods into discrete sections was reported by Geiger *et al.* This was accomplished by disassembling purified modified TMV and using the directional assembly of the CP onto the genomic RNA [92]. In these experiments, TMV modified by the addition of either a cysteine residue to the N-terminus of the CP ORF (S3C) or by the addition of lysine to the C-terminus (T158K), termed TMV_{Cys} and TMV_{Lys} respectively, was disassembled into

constituent CP, which was then subsequently incubated with genomic wild-type TMV RNA or a linearized infectious plasmid containing the genomic RNA in a serial manner to allow assembly of first one and then the other modified CP onto the RNA. This resulted in hybrid TMV particles with typical lengths dictated by the RNA core material but with different functionalities present along the longitudinal dimension of the rod, as determined by the modifications made to the component CP and verified by TEM of chemically conjugated enzymes. One drawback of this method is the bidirectional nature of TMV CP assembly onto the RNA scaffold. While the addition of CP onto the 5′ end of the forming rod occurs more quickly and easily than addition to the 3′ end, combined with the location of the OAs nearer to the 3′ end of the RNA genome, results in the extension of the nascent rod primarily in the 3′ to 5′ direction, the slower addition of CP to the 3′ end results in rods which are not strictly ordered in CP composition (Figure 1-6).

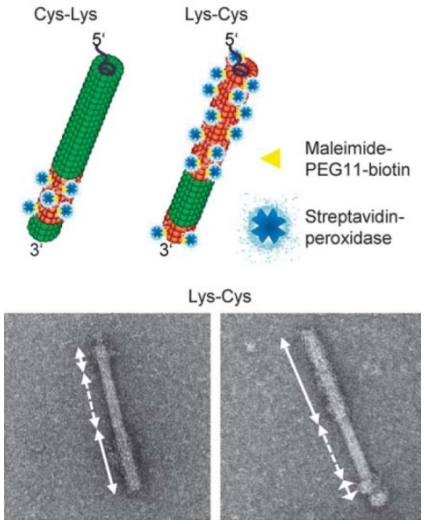

Figure 1-4: Sequential reassembly of two different TMV CP variants onto the RNA scaffold to produce nanorods with distinctly addressable regions. Reprinted with permission from [92]. Copyright 2013.

Plant viruses depend on the quaternary assembly of structural capsid proteins around the genome to protect it from environmental degradation. However the genome needs to be made available to host ribosomes upon entry into the host cell's intracellular environment to initiate the infection and reproduction process. This bimodal status of either stabilized or destabilized macromolecular assembly dependent on environmental conditions has been shown to be controlled, at least in

part, by clusters of carboxylate-containing residues which interact at intersubunit interfaces [96, 97]. These negatively charged residues generate electrostatic repulsion between adjacent capsid subunits in the cytoplasm of a host plant cell, but this repulsion can be offset by the presence of calcium ions or hydronium ions, leading to a stabilized particle in the extracellular environment.

One general method to alter particle assembly is primarily driven by engineered changes to the CP gene to manipulate the normal assembly behavior. By altering the amino acid residues located at the interface of adjacent CP monomers or at the protein-RNA interface, the dynamics of particle assembly can be altered. TMV mutants with enhanced stability of the macromolecular capsid protein assembly and inhibited/reduced disassembly proclivities were generated by systematically substituting out the carboxylate-containing residues aspartic acid (D) and glutamic acid (E) implicated in intersubunit interactions with neutrally-charged but similarly sized carboximide-containing residues asparagine (Q) and glutamine (N), respectively [96-98]. The two clusters that had been implicated in repulsive intersubunit interactions were (1) E50 and D77, which interact between capsid subunit situated adjacent to one another along the virus rod's axial dimension, and (2) E106 which interacts with the E95-E97-D109 amino acid triad in a lateral direction. Mutants with the E50Q, E106Q and combinations of E95Q/E97Q/D109N mutations showed reduced *in vivo* infectivity and *in vitro* cotranslational disassembly indicating stabilization of the capsid protein macroassembly. Mutants were also characterized as having lower $OD_{260/280}$ ratios, indicating macromolecular assembly of capsid protein without incorporation of RNA (genomic or otherwise), and variation of rod length,

including rods both shorter and longer than individual wild-type TMV particles. The E50Q mutation alone has been used more generally to promote particle assembly and stability for longer particle lengths [99] and when incorporating destabilizing CP alterations [100].

Another tactic introduces covalent bonding between adjacent CP subunits to confer stability to helical protein assemblies. One method introduced a cysteine to the flexible loop composing the surface of the virion inner channel at the low-radius portion of the assembled particle [101]. This cysteine (T103C) could interact with either of the identically positioned cysteines located on the neighboring CP subunits situated laterally to it. The resultant disulfide bonds stabilized the formation of helical rods under conditions which limit wild-type CP assembly to the formation of disks. Additional work introducing cysteines to the N-terminus (positions 1 and 3, located at the high-radius, outer surface of assembled disks or rods) in addition to the aforementioned inner loop cysteine T103C further allowed for the organization of disks or rods into various regular arrays or bundles depending on solution pH and ionic conditions [102].

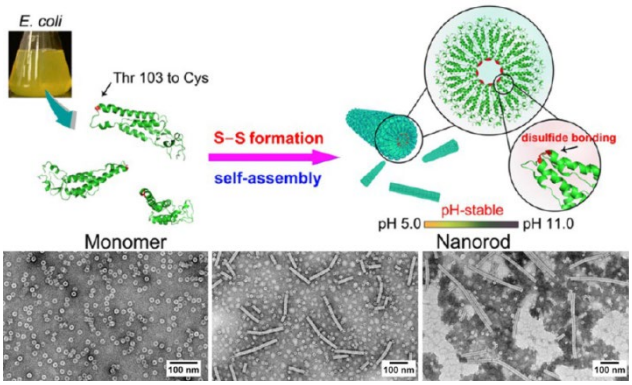

Figure 1-5: Introduction of a cysteine near the inner channel surface to create stabilizing, covalent disulfide bonds between adjacent CP. Reprinted with permission from [101]. Copyright 2013 American Chemical Society.

Other mechanisms to control TMV nanoparticle assembly and morphology depend on manipulating interactions between adjacent CP subunits. One significant

and well-studied interaction is an electrostatic repulsion between carboxylate-containing residues. Because the negative charges of those residues are pH-dependent, and because their interaction is influenced by the absence or presence of soluble ions, solution pH and ionic strength conditions can be used to promote assembly or disassembly. This can be used to generate particles with alternative shapes and aspect ratios. TMV CP, either purified and isolated from its genomic RNA or expressed and purified from bacteria or yeast, forms a mixture of short rods, disks and monomers at neutral pH and low ionic strength. Increasing the ionic strength of the solution (from 100 to 400 mM acetate) promotes the assembly of a four layer disk consisting of two bilayer disks facing opposite directions arranged in a "head-to-head" orientation [103, 104]. Alternatively, lowering the solution pH below ~5.5 induces CP to assemble into rods by protonating and neutralizing the carboxylate groups, eliminating their mutual repulsion [96, 105], allowing the hydrophobic interactions between layers of CP to drive assembly. Because these carboxylate groups are also exposed at the ends of the virus rod, their interaction inhibits the "head-to-tail" assembly of two TMV rods. Lowering the solution pH promotes the coassembly of TMV rods into long nanofibers whose structure can be stabilized and fixed by the surface deposition and polymerization of an appropriate molecule. TMV retains a negative surface charge above its isoelectric point (around pH 3.3 [106]), so positively charged polymer precursors accumulates on the long TMV fibers that form when the pH is near 5. Soluble, micrometer-scale, polymer-coated TMV nanofibers that remain stable at neutral pH have been achieved by surface deposition and polymerization of aniline [107, 108], pyrrole [109], and dopamine [110].

Polymerization of the aniline on the surface of TMV facilitated the head-to-tail attachment even at neutral pH, although the morphology of the resulting hybrid material was controlled by the pH of the reaction, with short bundles produced at very low pH(=2.5), long bundles produced at pH5, and long disperse nanofibers at pH6.5 [108, 109]. Although this method achieves end-to-end assembly of TMV, it does so indiscriminately with respect to head-to-tail order, and the resulting nanofiber has a continuous polymer coating, which could interfere with previous functionalizations of the TMV particles themselves.

1.3.2. Patterning and positioning TMV on surfaces and integrating TMV into devices

Attachment or deposition of virus onto surfaces is a critical prerequisite for the implementation of the virus's novel capabilities as components of functional devices. Selective or directed deposition of the virus onto specific surfaces, and specifically in designated patterns, can also enhance the virus's effectiveness in certain applications. Toward this end, several methods have been developed that can quickly pattern TMV over large surfaces for subsequent use.

One simple method of aligning virus rods on a surface utilizes fluid and air flow, wherein an aqueous solution of TMV is removed from a surface either by blow-drying the droplet or by capillary forces using filter paper [111]. TMV left behind are oriented in the direction of fluid flow due to shear forces within the fluid at the surface boundary. Surfaces with strong TMV interactions, such as highly polar surfaces, are amenable to the blow-drying method, while surfaces with weaker TMV

interactions, such as carbon, benefit from the lateral suction of the liquid. These methods represent a relatively simple means of generating aligned virus on a surface.

Another convective method of depositing TMV onto a surface was developed that enables deposition in a variety of particle orientations and thicknesses [112]. In this method, a liquid suspension of TMV is dragged over the surface substrate by the movement of a parallel glass slide, with an assembly front at the leading edge of the droplet and a drying front at the trailing edge. The roughness of the resulting TMV deposition depends on the surface energy of the substrate, with increasing water contact angle correlating with increasing surface roughness. Variation of virus concentration and assembly speed can be used to controllably vary the particle orientation, packing density, and thickness of the resulting viral deposition, with four observed deposition regimes: (1) incomplete monolayer with parallel orientation, (2) monolayer with parallel orientation, (3) multilayer with disordered orientation, and (4) multilayer with antiparallel orientation.

An alternative method of depositing TMV onto surfaces using a genetic modification of the virus creates a more robust attachment between the rods and the surface while also generating a vertical orientation of the virus relative to the surface. This genetically modified form of the virus, TMV-1cys, contains a single cysteine residue inserted within the N-terminal domain of the CP open reading frame. As part of the CP N-terminal region, the cysteine is located at the outer surface of the assembled virus rod, where it can form bonds with various surfaces including gold, stainless steel, Teflon® (PTFE), SU-8, Si, and SiN [56, 85, 88, 113, 114] through the interactions of those materials with cysteine's sulfhydryl/thiol group. However the CP

N-terminal region is partially shielded by the C-terminal arm. This partial obscuring of the cysteine likely inhibits the direct contact of the cysteine sidechain's thiol group with the surface except at the virus's 3′ end, where the thiol has greatest exposure. The result is the spontaneous vertical attachment of TMV-1cys from its 3′ end to these materials upon incubation with an aqueous solution of the virus, radically increasing the theoretical ratio of utilizable and exposed virus surface area per substrate surface area compared to previous method of attachment with parallel surface--virus orientation. Due to the selectivity with respect to surface material composition for attachment of TMV-1cys, patterned deposition of a TMV-1cys-binding material onto a surface can direct virus-deposition patterning. TMV-1cys has also been deposited onto silicon and SU-8 three-dimensional microstructures, further increasing the functional virus surface area per footprint surface area beyond that afforded by the perpendicularly oriented surface attachment of TMV-1cys.

Standard microfabrication methods can be used to pattern TMV-1cys on a surface after virus deposition. Lift-off is a technique where a patterned photoresist mask defines areas where a subsequent layer, such as metal, will be removed at the end of the process. This process has been demonstrated to be compatible with TMV-1cys, both uncoated and metal-coated [115]. For uncoated TMV-1cys, either acetone and ultrasonication or a standard photoresist developer diluted with sodium phosphate buffer to reduce the pH to one within TMV's range of stability was used to dissolve the photoresist mask, which had already been flood exposed prior to the virus deposition process. This process resulted in very well-defined patterning of the virus, limited only by the contact lithography critical dimension (2 μm).

A final approach for the surface attachment and patterning of TMV utilizes DNA hybridization methods [116]. This approach exploits the normal method of TMV virion assembly whereby TMV CP, in monomer, oligomer, and assembled disk forms, assembles itself around the genomic RNA. Silicon wafers were prepared using polymer blend lithography allowing exposed silicon regions to be functionalized by the attachment of linker DNA that binds via nucleic base pairing to strands of TMV genomic RNA. Incubation of the prepared surface with a solution of TMV CP generates assembly of surface-attached virions by assembly of CP onto the surface-attached RNA. The virus/VLPs are present only in areas initially treated to bind the DNA linkers, but despite the physical point of attachment of the rods to the surface, the rods were observed to lie flat on the silicon surface in randomly distributed orientations.

1.3.3. TMV Surface Functionalization

TMV, as a nanoparticle with a defined and repetitive architecture, can act within systems as a nanoscale scaffold for the anchoring, arrangement, and display of biochemical motifs. For some applications, the native functional groups displayed on the surface of the wild-type virus are sufficient to achieve the desired ends. However one important capability afforded by virus particles is the customizability of their surface. A variety of genetic and post-translational modifications have been developed to enable TMV to function as a general purpose scaffold for the display of an enormous variety of molecules and functional groups.

A common theme of research in this area is the recruitment of TMV as a nanoparticle capable of circulating in the blood and selectively targeting certain

tissues for uptake and delivery of either therapeutic, prophylactic or imaging/reporting molecules (or of both in the case of theranostic technology). For targeted drug delivery, the attachment of (chemo)therapeutic agents to the TMV inner or outer surface can be combined with the display of moieties such as carbohydrates or proteins that target uptake by a tumor or other tissue together with other molecules, such as PEG, to escape detection by the immune system or clearance by the liver. Alternatively the "highly ordered, repetitive, quasicrystalline display" of antigen epitopes when displayed on the TMV surface provides an enhanced immunogenicity for vaccine applications or the production of antibodies when detection by the immune system is intended [117]. The primary modifications explored in this review are summarized in Table 1.

The amino acid side chains exposed on the surface of virus and virus-derived particles provide a variety of reactive sites for the chemical conjugation of desired molecules and moieties, whether these amino acids are naturally present or artificially introduced. Specifically, two TMV variants, altered by the addition of a single cysteine (TMV-1cys) or lysine (TMV-1lys) residue to the N-terminal region of the CP, have proven to be reliable scaffold for the conjugation of small fluorescent molecules. TMV-1cys can be decorated with molecules containing a maleimide functional group through the well-established thiol-maleimide reaction generating a covalent bond, while TMV-1lys can be similarly decorated via a reaction between the amide of lysine and an NHS-ester functional group. These two variants, TMV-1cys and TMV-1lys, were fluorescently labelled with maleimide-fluorescein and NHS-ester-fluorescein, respectively [118]. Measurement of fluorescence/TMV mass

Table 1: Overview of TMV Surface Functionalization Strategies

Location on TMV	TMV Alteration	Purpose	Functional group	Activity	Specific uses
Inner channel	None	Site for conjugation of functional molecules	Glutamic acids (Glu97, Glu106)	Electrostatic interactions	Cationic photosensitizer [119], phenanthriplatin [8]
				EDC-activated amide attachment,	Fluorescent dye (Cy5 [120]), cisplatin [121], MRI contrast agents [9]
Outer surface			Tyrosine (Tyr139)	Azo-coupling of diazonium salts	Fluorescent dyes: (Cy5 [120], rhodamine B [122]), folic acid [122], doxorubicin [122], PEG [122, 123], MRI contrast agents [9], carbohydrates [121]
	Genetic alteration		N-terminal lysine	NHS-attachment	PEO_4, biotin, protein (GFP), peptide (canine papillomavirus fragment) [124]
			C-terminus proximal lysine (Thr158Lys)		Fluorescent dye (Cy5[120]), PEG [125], peptides [125]
			N-terminus proximal cysteine (S3C or S1_Y2insC, i.e. "1Cys")	Maleimide attachment	Fluorescent dyes (Texas Red and Atto 488)[92], PEG [92], enzymes (HRP [92], glucose oxidase [126])
		Inherent functionality		Thiol-metal interactions	TMV surface attachment, metal deposition [88]
			Peptides	Target binding	TNT-binding [127]
				Antigen display	FLAG-tag [128]
				Receptor binding	RGD [129, 130]

indicate that each TMV-1cys and TMV-1lys virion displayed ~1850 and ~1400 fluorescein molecules, respectively, corresponding to a fluorescein labelling of ~85% and ~65% respectively of each of the ~2130 CP subunits comprising each virion. The presence of a fraction of CP in each sample without bound fluorescein was confirmed with matrix-assisted laser desorption/ionization time-of-flight mass spectrometry (MALDI-TOF MS). The reduced fraction of fluorescently labelled (fluorescein-bound) TMV-1lys CP subunits was hypothesized to the due to steric hindrance due to the larger size of the NHS-ester group relative to maleimide.

Similarly, phenol groups naturally present in the sidechains of surface exposed tyrosine residues in wild-type TMV have be shown to be functionalizable by binding oligo-aniline (OANI) motifs [131]. This involved a three-step bioconjugation protocol that attached the terminal alkynes of OANI to the phenol groups on the TMV rod surface to produce OANI-labelled TMV (TMV:OANI). To prevent aggregation and bundling of TMV:OANI, dimethyl sulfoxide can be added to the nanoparticle solution to inhibit reaction between OANI units, similar to the use of DTT to prevent crosslinking of TMV-1cys by the creation of disulfide (cystine) bonds.

The functional groups present and solvent-exposed on the surface of unmodified TMV include a tyrosine residue (T139), whose phenol group is exposed on the outer surface, and two glutamic acid residues (E97 and E106), whose carboxylate groups are exposed on the surface of the inner channel. Bioconjugation to the exterior tyrosine's phenol can occur by azo-coupling through the use of diazonium salts, while the inner channel glutamic acid residues can be activated by 1-ethyl-3-(3-dimethylaminopropyl)carbodiimide (EDC) and coupled to amine-linked

target molecules via an amide bond [123]. Further strategies to increase the range of products and efficiency of bioconjugation to the external tyrosine include the azo-coupling of an alkyne group, allowing the Cu(I)-catalyzed azide-alkyne cycloaddition reaction (CuAAC), a type of "click" chemistry [132], and the further addition of β-cyclodextrin by CuAAC, allowing the strong but noncovalent attachment of adamantyl-coupled molecules [122].

A lysine inserted at the CP N-terminus similarly allowed for bioconjugation to the outer surface of TMV through a reaction between the lysine's amide group Dual attachment by independent targeting of the outer and inner surfaces of the TMV allows for separate functionalization of these two surfaces. Given the potential of TMV for use for theranostic, targeted drug delivery, or imaging purposes, bioconjugated elements that have been selectively bound to TMV include fluorescent dyes Surface-exposed functional groups provide selective sites for chemical bioconjugation, broadening allowable modifications while avoiding assembly disruptions that sometimes result from genetic modifications. Naturally occurring bioconjugation sites include an outer-surface-exposed tyrosine (T139) and two inner-channel-accessible glutamic acids (E97 and E106). Bioconjugation to the tyrosine's phenol can occur by azo-coupling using diazonium salts, while the inner-channel glutamic acids are activated by 1-ethyl-3-(3-dimethylaminopropyl)carbodiimide (EDC) and coupled to amine-linked targets via an amide bond [123]. The azo-coupling of an alkyne group to the exterior tyrosine allows the use of Cu(I)-catalyzed azide-alkyne cycloaddition reactions (CuAAC), a type of "click" chemistry [132],

simplifying further modifications. The addition of β-cyclodextrin by CuAAC, allows the noncovalent attachment of adamantyl-coupled molecules [122].

Independent targeting of TMV's tyrosines and glutamates allows heterologous functionalization of their distinct surfaces. Given TMV's potential drug delivery and imaging applications, bioconjugated molecules include fluorescent dyes [120, 122], paramagnetic contrast agents for MRI [9], poly(ethylene glycol) to tune circulatory clearance rates [122, 123], carbohydrates [121], folic acid [122] and peptides (cRGD) [91] to direct receptor-mediated endocytosis, and pharmaceutical agents including doxorubicin [91, 122] and cisplatin [121]. Additionally it was shown that the negative charges provided by the glutamates (E97 and E106) exposed along the inner channel of the virus are alone sufficient for the non-covalent loading and retention of ~800 copies of a triply cationic porphyrin-based photosensitizer per virion [119] or ~2000 copies of the doubly cationic DNA-binding anticancer drug candidate phenanthriplatin per virion (approximately one molecule per CP) with subsequent release of phenantriplatin shown in acidic environments [8].

To expand the range of methods for functionalizing TMV and the possible targets of binding, several modifications to the TMV CP to introduce new functional groups at the virus surface have been made. A genetic insertion encoding one or more cysteine residues near the N-terminus of the CP provides several advantages. The surface-exposed thiol groups allow for improved metal deposition on the virus surface [114] including confluent Ni, Co, Pt, Pd coatings of tunable thickness. The orientation of the cysteine directs the perpendicular attachment of TMV rods to surfaces of gold, stainless steel, Teflon® (PTFE), SU-8, Si, and SiN [56, 85, 88, 113,

114]. The cysteine also enables the use of well-established reactions between thiol and maleimide as an alternative method of bioconjugation to the external surface of TMV. This method has been used to attach fluorescent dyes (Texas Red [133] and Atto 488 [92]) or biotinylated PEG, which allowed the subsequent attachment of streptavidin-labeled enzymes including horseradish peroxidase [92] and glucose oxidase [126] with an efficiency of approximately one thousand enzyme molecules per TMV rod, indicating that roughly half of all CP subunits bound to an enzyme molecule [126].

A lysine inserted at the CP N-terminus similarly allowed for bioconjugation to the outer surface of TMV through a reaction between the lysine's amide with an N-hydroxysuccinimide (NHS)-ester-labeled target. Smith et al. generated a library of TMV with three random amino acids and a lysine at the N-terminus and isolated an infectious and soluble clone containing the sequence ADFK [124]. Biotinylation of the lysine residue with NHS-PEO_4-biotin allowed decoration of the virus with streptavidin-linked whole proteins (GFP) and peptides (a fragment of Canine oral papillomavirus L2 protein) with a loading efficiency of 26% to function as protein antigen display scaffolds for vaccine applications [124]. Demir et al. had previously added a lysine to the C-terminus of the CP (T158K) with no other modifications for particle solubility improvement, but showed the ability to biotinylate the rods with NHS-biotin and subsequent binding of avidin [134]. Altintoprak et al. conjugated cysteine containing polypeptides between nine and twenty-one amino acids in length to the C-terminal lysine using bifunctional PEG linking maleimide and NHS groups to control and improve silica deposition homogeneity [125].

Another strategy to functionalize viral surfaces is to alter or extend the CP open reading frame (ORF) by genetic modification so that the introduced peptide sequence is located at the desired surface of the assembled viral particle. The C-terminus of the CP is an ideal site for additional peptide sequences, if it is located on the relevant surface of the assembled particle, due to a decreased likelihood of the added peptide sequence interfering with cotranslational protein folding. In general, short peptide sequences, less than ~25 amino acids in length, have the best results in being incorporated into virus/VLP/PVN structure by minimizing interference with CP folding and NP assembly [135]. However, even short peptide sequences can inhibit or even prevent virion assembly in a manner highly dependent on the particular protein sequence for reasons that may be either obvious (such as a large number of hydrophobic residues) or not easily predicted [136].

One strategy to functionalize virus particles is to genetically alter or extend the coat protein (CP) open reading frame (ORF) by genetic modification to introduce a peptide sequence at the desired surface of the assembled viral particle. The well-established crystal structure of TMV CP in the assembled state [78] indicates that the high radius region on the outer surface of the TMV virion includes the CP N-terminus, C-terminus, and a surface exposed loop containing residues 63 to 66 [114, 124, 137]. Insertions of sequences at each of these three sites have produced infectious virus that assemble into stable virions. The C-terminus of the CP has been the preferred site for additional peptide sequences due to a decreased likelihood of the added peptide sequence interfering with cotranslational protein folding. In general, short peptide sequences are most successful by minimizing interference with CP

folding and virion assembly [136]. The ability to display short (<~25 a.a. residues in length) peptide sequences enables virus-based particles to display peptide tags that can act as targets for other molecules such as antibodies or that can selective target molecules on their own, effectively transforming the virus-based particle into a multivalent biosensor. However, even short peptide sequences can prevent virion assembly in a manner highly dependent on the particular protein sequence for reasons that may be either obvious (such as a large number of hydrophobic residues) or not easily predicted [135].

Larger peptides, including proteins, as well as some smaller peptides that appear to inhibit virion assembly can also be added to the CP through extension of the CP ORF and assembled particles can be obtained provided that the particles are allowed to assemble from a mixture of augmented and unaugmented ("wild-type") CP subunits. This mixture can result from the coexpression of wild-type CP either independently or through the use of a "leaky" stop codon. Leaky stop codons have some probability of not terminating translation but instead of being read-through and producing a protein of extended length [138]. Virus-based particles so produced have the added peptide or protein fused to only some subset of their CP subunits, with a random "mosaic" distribution, and so compromise the number of peptides displayed per particle in order to allow particle assembly. Peptide additions as large as the fluorescent proteins GFP and mCherry have been added to the CP of PVX and produced assembled virions using these techniques [138, 139]. However in some cases even large peptide additions have been added to a virus CP ORF and produced virions in which every CP subunit displayed the peptide fusion domain, such as a 133

amino acid segment of protein A which was fused to the TMCP ORF and produced assembled virions that demonstrated binding of antibodies along the entire length.

A common use of this peptide display capability has been the multivalent display of epitopes for the detection of antibodies or for the production of an immune response as a vaccine component. For instance, TMV CP with a C-terminal FLAG tag (DYKDDDDK) was used to generate virus-like particles (VLPs) that were deposited on an optical disk resonator to demonstrate a highly sensitive immunosensor targeting anti-FLAG antibodies [6].

TMV peptide display can also use the specificity and high affinity with which short polypeptides can selectively target and bind molecules. Such peptide sequences can be isolated and identified from phage display libraries of short peptides used to screen for bond strength to the target analyte [140-142]. One such binding peptide with specificity to 2,4,6-trinitrotoluene (TNT) was expressed as a TMV CP fusion to generate virus-like particles. These particles were used in solution, where their binding to dissolved TNT altered the diffusion rate of TNT to an electrode, changing the peak corresponding to the oxidative reduction of TNT in response to square wave voltammetry for the purposes of TNT detection [127].

Other examples include expression of the integrin receptor target amino acid sequence arginine-glycine-aspartic acid (RGD) on the TMV surface. This allowed TMV to serve as mimics of extracellular matrix proteins with unique consistency and structural patterning to serve as a substrate for the culture of stem cells [129, 130].

The ability to express short peptide sequences as contiguous parts of the TMV CP enables the immediate use of purified virus as a highly multivalent, high-surface-

area nanoscale peptide display scaffold with no further modifications. However these genetic insertions can produce destabilizing effects. Depending on the peptide, purifiable virus yield may be low, or virus rods may fail to assemble completely form entirely for reasons not easily predicted [135]. Given the time and effort required to modify and clone a genetic TMV variant prior to discovering whether sufficient virus yield will be produced,, many groups opt instead for post-translational bioconjugation of functional groups, including peptides, to assembled virus.

1.4. Summary

1.4.1. Contribution of Research Project

This project used TMV VLPs as a model system to investigate controlled macromolecular assembly of simple protein components into more complex, higher order multimacromolecular biological nanostructures capable of diverse functions in integrated devices. This was accomplished through a multiphase project comprising (1) the development of TMV VLPs by the bacterial expression and isolation of **modified TMV CP capable of assembling in the absence of the RNA genome**, (2) the further development and characterization of **VLP-forming modified TMV CP with unique environmentally responsive assembly behavior**, and (3) the establishment of methods to use these modified CP variants to create in the form of end-to-end attachment of TMV VLPs to create **chimerical multirods by the controlled, directed macromolecular assembly of heterogeneous VLP components of differentiable function.** This project will function as model for further development of functional micromolecules with applications in targeted drug delivery, imaging, biosensing, and theranostics, combining diagnostic and therapeutic

applications in a single platform. Such research is expected to enable the development of new, low cost, environmentally responsive materials and surfaces with improved sensing, storage and release capabilities for threat and disease detection, information processing, and therapeutic application.

1.4.2. Structure of Dissertation

Chapter 1 has attempted to establish the basis for this research project by explaining its motivation and reviewing the literature establishing the state of the field. The following chapters will describe the major achievements that have been made in pursuit of its goals. Chapter 2 will describe the initial strategies that allowed for the first production of functional virus-like particles from bacterially expressed *Tobacco mosaic virus* capsid protein. Chapter 3 will introduce the further strategies that lead to the creation of multiple alternative TMV capsid protein variants with unique and divergent behaviors with respect to macromolecular assembly and will describe the use of these modified forms of TMV CP to generate particulate nanomaterials with an additional layer of architectural complexity. Chapter 4 will summarize and conclude this research dissertation and provide a direction for future research.

Chapter 2: Assembly of Virus-Like Particles from Modified *Tobacco mosaic virus* Capsid Protein[1]

2.1. Abstract

Uniform dimensions and genetic tractability make filamentous viruses attractive templates for the display of functional groups used in materials science, sensor applications and vaccine development. However, active virus replication and recombination often limit the usefulness of these viruses for such applications. To circumvent these limitations genetic modifications of selected negatively charged intersubunit carboxylate residues within the coat protein of *Tobacco mosaic virus* (TMV) were neutralized so as to stabilize the assembly of rod-shaped virus-like particles (VLPs) within bacterial expression systems. Here we show that TMV-VLP nanorods are easily purified, stable and can be programmed in a variety of configurations to display functional peptides for antibody and small molecule binding.

[1] This chapter comprises the text of the published article "Carboxylate-Directed In Vivo Assembly of Virus-like Nanorods and Tubes for the Display of Functional Peptides and Residues," written by A. D. Brown, L. Naves, X. Wang, R. Ghodssi, and J. N. Culver, appearing in *Biomacromolecules,* vol. 14, pp. 3123-3129, Sep 2013. The manuscript was written through contributions of all authors. All authors have given approval to the final version of the manuscript. Authors A. D. Brown and L. Naves contributed equally.

2.2. Introduction

Virus particles are remarkable examples of biological evolution. They consist of individual components that encode the ability to self-assemble into uniform nano-scale shapes. These traits have made viruses attractive templates for use in nanotechnology applications. Furthermore, the protein and genetic components that make up these particles display a unique level of malleability that enables both genetic and chemical modifications for the addition of novel functionalities that include vaccine epitopes, moieties for the mineralization of inorganics, and genetics for the patterning of virus particles [143-146]. Yet despite these traits the application of virus particles is often limited by problems associated with viral replication and recombination that result in the loss of the desired functionalities. In addition, size constraints dictated by the need to include replication competent virus genomes also reduce the potential application of these particles. However, many of these limitations can be circumvented by the use of virus-like particles (VLP) derived from the assembly of virus structural proteins in the absence of the virus genome [147-149]. Yet a number of virus coat proteins, filamentous viruses in particular, are not amenable to particle assembly in the absence of nucleic acid. Here we describe an *in vivo* VLP assembly system for the filamentous *Tobacco mosaic virus* (TMV) and its application for the display of functional binding residues and peptides.

TMV has served as a model virus for use in a variety of applications [150]. TMV forms a nanotube structure 300 nm in length and 18 nm in diameter with a 4 nm diameter hollow inner channel. Each particle is assembled from ~2130 identical 17.5 kDa protein subunits wraped in a helix around a single strand of plus strand viral

RNA [151]. TMV particles are stable up to 60 °C and at pH range of 2-10 [152] and are amenable to genetic modifications for the addition of novel functionalities that include inorganic binding and vaccine epitope display [150, 153, 154]. Combined, these traits make the virus a durable biological template. However, the use of infectious TMV imparts limitations associated with virus recombination and replication [154]. In addition, *in planta* production of virus particles requires specialized plant growth conditions and produces an infectious particle. These limitations often result in the loss of genetically added sequences via recombination or the inability to generate sufficient quantities of virus particles due to interference in the virus life cycle by the added sequence or peptide [155].

Previous studies have demonstrated that the TMV coat protein can be expressed and purified from *Escherichia coli* [156-158]. However, at neutral pH purified TMV coat proteins are only capable of assembling into lower order disk-shaped aggregates. Assembly of these aggregates into characteristic rod-shaped particles requires the co-expression of RNA containing the virus origin of assembly, leading to the production of VLPs containing nucleic acid [159]. Alternatively, exposure of purified coat protein to pH 5 buffer conditions is also known to induce the formation of rod-shaped particles [160]. Both of these approaches entail drawbacks that can limit the usefulness of the TMV coat protein generated VLPs. For example, recruitment to the bacterial polyribosomes can significantly disrupt the production of RNA assembled VLPs [159]. Furthermore, the presence of nucleic acid within the rod may be undesirable for some applications. Assembly through post-purification pH treatments is also problematic in that neutral pH conditions necessary

for many biological and chemical functions lead to the disassembly of these VLPs, thus limiting their use. New methods that permit the self-assembly of the TMV coat protein under biological relevant conditions are needed.

Stability of the TMV particle is modulated by repulsive carboxylate groups located on opposite sides of subunit-to-subunit interfaces [151, 161]. These negatively charged repulsive interactions are stabilized by protons and Ca^{++} ions that function as a stability switch. Specifically, within the extracellular environment excess Ca^{++} ions and protons function to negate repulsive carboxylate interactions, stabilizing the virus particle. However, lower Ca^{++} ion concentrations and higher pH of the cellular environment results in the loss of stabilizing ions and protons, leading to particle disassembly and infection. Structural and mutational studies have identified three specific intersubunit carboxylate interactions within the TMV particle [96, 151]. One carboxylate interaction occurs between Asp116 and phosphate from the viral nucleic acid. Another forms a lateral cluster of interactions at the virion inner radius between E106 of one subunit and E95, E97 and D109 of the adjacent subunit. The third occurs axial between residues E50 and D77 (Figure 2-1A). The E50 – D77 interaction has been shown to be a significant driver in helical rod assembly as mutations E50Q and D77N have been shown to block virus disassembly and produce empty virus-like helical rods during infection [96, 98, 161]. We have exploited these findings to investigate and develop an *in vivo* TMV VLP assembly system for the patterning and display of functional residues and peptides.

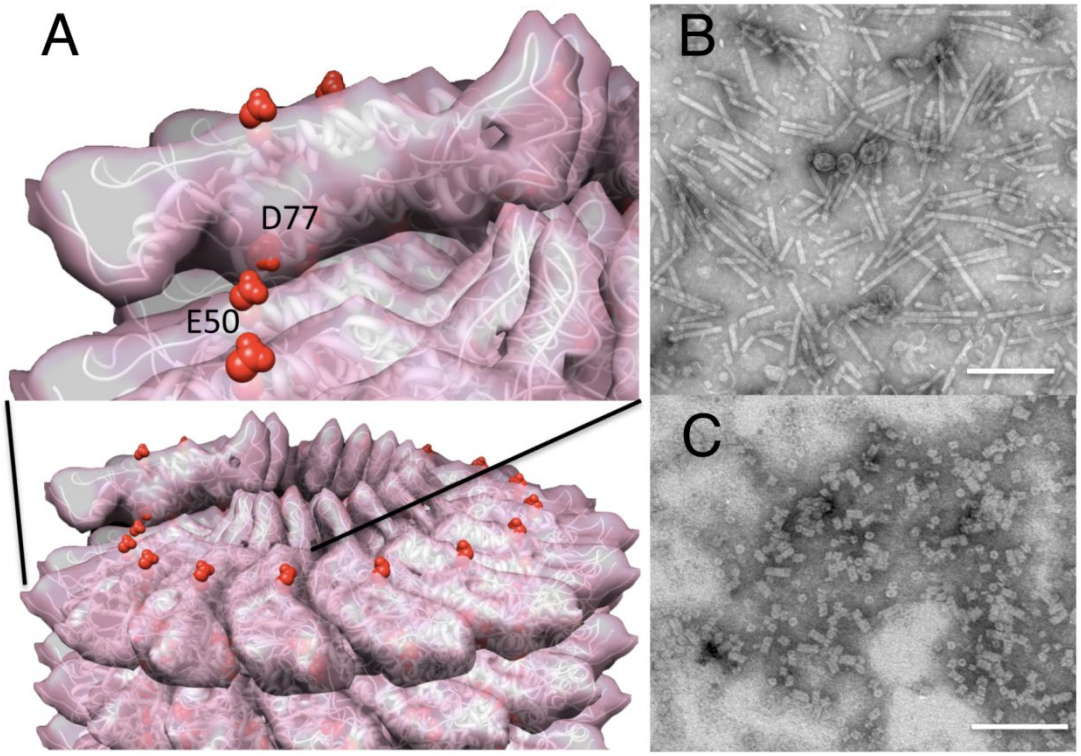

Figure 2-1: Carboxylate modifications to the TMV coat protein promote particle assembly. A, Molecular model of the rod surface showing the location of the juxtaposed E50-D77 carboxylate pair. B, Electron micrograph of crude bacterial lysates derived from the expression of the E50Q / D77N coat protein ORF. C, Electron micrograph of crude bacterial lysates from the unmodified coat protein showing only disks and short stacks of disks. Bars equal 200 nm.

2.3. Methods

2.3.1. TMV coat protein expression constructs

The TMV coat protein open reading frame (ORF) carrying the E50Q and D77N modifications was codon optimized for expression in *E. coli* (GenScript, Piscataway NJ: Supplemental Fig. 1) and inserted into the pET-21a(+) expression vector (Novagen, Madison WI) via *Nde*I and *Xho*I restriction sites. Further modifications to the N- and C-terminus of the coat protein ORF were achieved by primer based PCR mutagenesis using oligonucleotides containing additional or altered sequences (Table 1). A cysteine codon was added at position two at the N-

terminus of the coat protein ORF to produce TMV-VLP1cys for enhanced metal coatings and oriented surface-binding [162]. Sequences encoding the binding peptides for FLAG epitope (DYKDDDDK) were added to the coat protein C-terminus [163]. Sequences binding the fluorescent imaging agent Genhance^{TM} 680 (IQSPHFF) were added to the coat protein C-terminus as fusions either with or without preceding sequences encoding a "leaky" amber stop codon (TAG) or a flexible 10 amino acid linker (GGGGSGGGGS) [164], [165]. Amplified PCR products containing 5′ *Nde*I and 3′ *Xho*I restriction sites were used to ligate the modified coat protein ORFs into similarly cut pET-21a(+) vector.

2.3.2. Induction and purification of TMV-VLPs

Coat protein expression constructs were transformed into BL21 competent *E. coli* K-12. Additionally, JM109 *E. coli* cells were used for coat protein constructs containing the amber stop codon TAG. JM109 cells carry the supE44 suppressor of the amber stop codon via a tRNA mutation that transitions the GUC glutamine anticodon to AUC [166]. Transformed cells were cultured at 37^{o}C in LB broth containing ampicillin (100 μg/ml) / chloramphenicol (50 μg/ml) for BL21 and ampicillin (100 μg/ml) / nalidixic acid (30 μg/ml) for JM109 cells to an OD_{600} of 0.5. Cells were then induced by the addition of 0.1 mM IPTG and incubated overnight at 25°C. Induced cells were harvested by centrifugation at 4°C and lysed using Bugbuster^{TM} with Lysonase^{TM} according to the manufacturer's protocol (Novagen, Madison WI). Dithiothreitol to a concentration of 0.5 mM was added to the cell lysates followed by 3-5 min of sonication in a Branson 1510 sonicator (Branson Ultrasonics, Danbury CT). One third volume of chloroform was then added to the

lysates, mixed and separated by centrifugation for 10 min at 17,000 × g at 4°C. Because of the hydrophobic nature of the IQ peptide the chloroform purification step was replaced by centrifugation at 800 × g for 1 min, centrifugation of the resulting supernatant at 66,400 × g for 30 min, and resuspension of the pellet in 3 mL of 0.1 M pH 7 sodium phosphate buffer. VLPs were then precipitated by the per volume addition of 1.5% KCl and 6% polyethylene glycol for one hour at 4°C. VLPs were then pelleted by centrifugation for 10 min at 17,000 × g. The resulting pellet was resuspended by shaking overnight in 0.5 to 2 mls of 0.1 M pH 7 sodium phosphate buffer. Resuspended VLP pellets were then loaded onto a 10 to 40% sucrose gradient in 0.1 M pH 7.0 sodium phosphate buffer and centrifuged for 1 hr at 91,000 × g at 14°C. A diffuse band corresponding to the purified VLP was removed by syringe and concentrated by centrifugation for 1 hr at 92,000 × g at 4°C. The purified VLP pellet was then resuspended in 0.1 M pH 7 sodium phosphate buffer.

To visualize VLPs within bacteria, cells were induced overnight and subsequently prepared by pelleting, followed by fixing in 2% gluteraldehyde in phosphate buffered saline (PBS) with 0.29 M sucrose. Post-fixing was done in en bloc on the pelleted cells using 1% osmium tetroxide with 2% aqueous uranyl acetate. Dehydration of the pelleted cells was accomplished by treatment with solutions of increasing ethanol content (100% final). The dehydrated pellet was then embedding by solutions of propylene oxide with increasing Spurr's resin content (100% final) and curing at 70°C overnight. Expressed VLPs were visualized in whole fixed bacterial cells and in purified form using a transmission electron microscope at 80 kV.

2.3.3. VLP surface assembly and electroless plating

Purified TMV-VLP1cys was self-assembled onto 1 cm^2 gold-coated silicon chips by incubation overnight at 4°C in a 1 mg/mL solution of the purified VLPs resuspended in 0.1 mM sodium phosphate buffer, pH 7. VLP assembled chips were then dipped in a 0.158 mM solution of Na_2PdCl_4 for 30 minutes at 4°C. The surface-bound VLPs were then coated with nickel by moving the chip directly into an electroless nickel plating solution consisting of 0.05 M $NiCl_2$, 0.12 M glycine, 0.0785 M sodium tetraborate, 0.525 M dimethylamine borane complex at pH 7. Nickel deposition by reduction was allowed to proceed at room temperature until the entire surface of the chip had darkened. Nickel coatings were visualized via field emission electron microscopy.

2.3.4. Chip based enzyme-linked immunosorbent assay (ELISA)

Gold coated 1cm^2 silicon nitrate chips were submerged overnight in purified TMV1cys-VLP or TMV1cys-VLP1cys-FLAG at 4°C to facilitate oriented VLP assembly onto the gold surface. VLP assembled chips were then incubated for an additional 30 min at 4°C in Tris buffered saline (50 mM Tris-HCL, 200 mM NaCl, TBS) pH 7.0 containing 5% non-fat dry milk as a blocking agent. Chips were then rinsed three times by submersion in fresh TBS buffer. Rinsed chips were subsequently incubated for 3 hrs at room temperature in TBS containing 5% non-fat dry milk and a 1/1000 dilution of rabbit anti-flag antibody (Sigma-Aldrich, St. Louis MO). The chip was then rinsed 3 times with TBS buffer and twice with TBS buffer containing 0.05% Tween-20. After rinsing, chips were submerged in TBS with 5% nonfat dry milk containing a 1/5000 dilution of anti-rabbit IgG alkaline phosphatase

and incubated at room temperature for 3 hrs. Chips were again rinsed as described above and placed directly in a solution containing 0.15 mg/ml of 5-bromo-4-chloro-3-indoyl phosphate and 0.3 mg/ml NitroBT in substrate buffer (10 mM Tris-HCL pH 9.5, 100 mM NaCl and 5 mM MgCl-6H_2O) and incubated for 10 min at room temperature. The reaction was stopped by immersion in water and the chips dried. Color intensities of individual chips were measured using ImageJ software [167].

2.3.5. Fluorescence binding onto IQ peptide tagged TMV-VLPs

The IQ-tag modified VLPs were tested for preferential binding of the fluorescent imaging agent Genhance^{TM} 680 (PerkinElmer, Waltham MA) as follows. Purified TMV1cys-VLP-AmberFlex-IQ (0.2 mg/ml or 0.02 mg/ml) were incubated overnight at 4°C in 0.5 mL of 0.1 M pH7 phosphate buffer with or without the addition of 10 µL of 0.1 mg/mL Genhance^{TM} 680. Samples were then centrifuged at 16,000 × g for 45 min. The VLP pellets were then resuspended in 1 mL of 0.1 M pH 7.0 phosphate buffer and centrifuged again for 45 min. Pelleted VLPs were then resuspended in 0.1 M pH 7.0 phosphate buffer to a concentration of 0.5 mg/mL and 0.05 mg/mL. 200 µL of each sample was added to a black-walled 96-well microtiter plate and fluorescence intensity at 690 nm (655 nm excitation and a 665 nm cutoff) was determined using a SpectraMax M2 (Molecular Devices, Sunnyvale, CA).

2.4. Results

2.4.1. Expression and characterization of modified TMV coat protein VLPs

The TMV coat protein open reading frame was codon optimized for prokaryotic expression and synthesized either with or without E50Q and D77N substitutions (Supplemental Fig. 1). Bacterial expression of the modified coat protein open reading frames was achieved via IPTG inducible bacterial expression vectors. Induced bacterial cultures were lysed and the crude extracts analyzed for TMV coat protein expression and assembly. PAGE analysis of bacterial lysate demonstrated coat protein expression (Figure 2-2A, lane 2). Electron microscopy demonstrated the presence of rod-shaped VLPs consistent with the helical assembly of the TMV coat protein (Figure 2-1B). In contrast, the unmodified wild-type optimized TMV coat protein ORF produced only disks and stacks of disks when similarly expressed (Figure 2-1C). Subsequent thin section electron microscopy of induced bacterial cells also displayed the presence of rod-shaped TMV-like particles within the bacterial cells (Figure 2-2C).

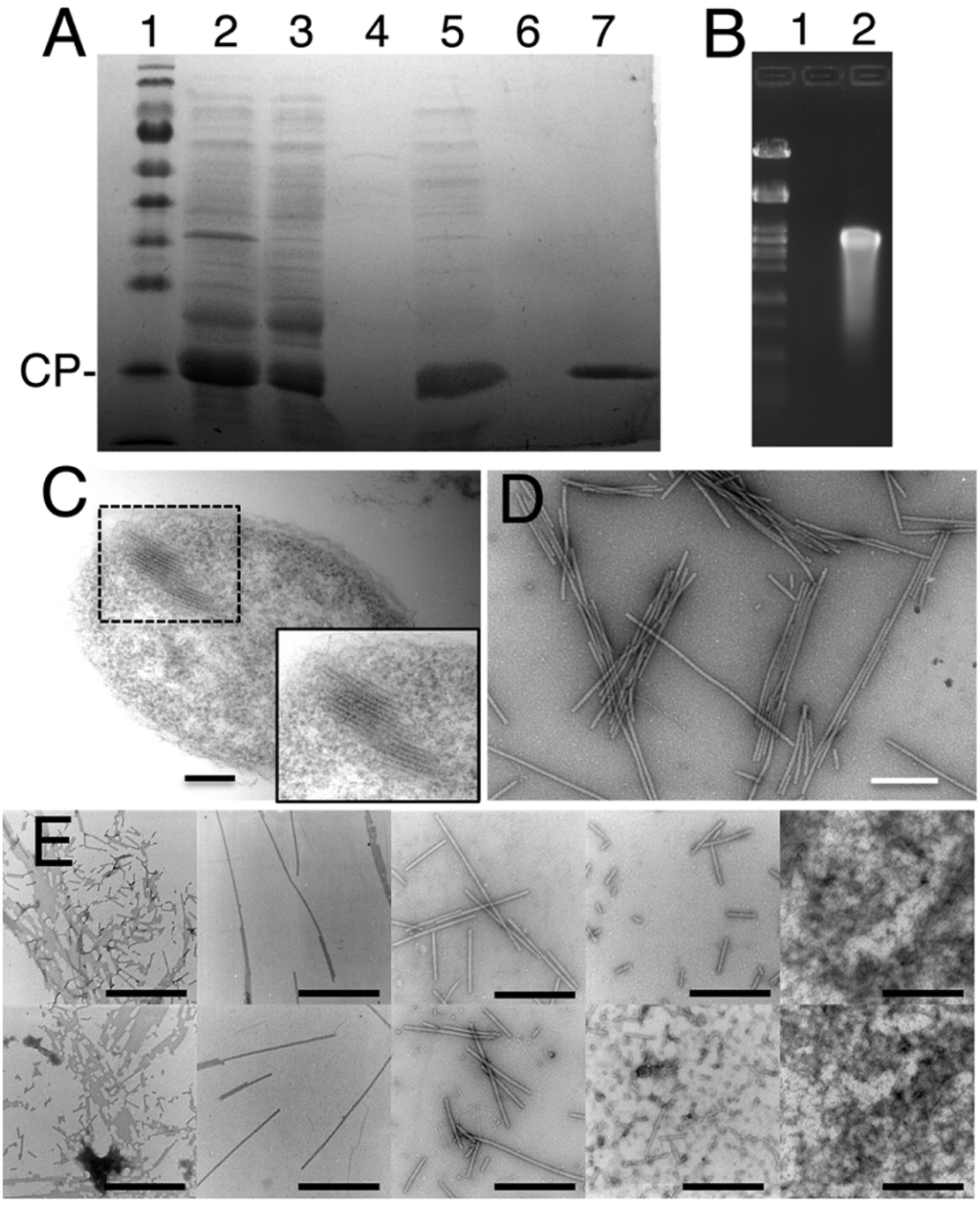

Figure 2-2: Expression and purification of TMV-VLPs from *E. coli* extracts. A, PAGE analysis of VLP purification scheme. Lane 1, protein marker; lane 2, lysed extract from IPTG induced bacteria; lane 3, chloroform clarified extract; lane 4, supernatant from PEG precipitation; lane 5, pellet from the PEG precipitation; lane 6, supernatant from the sucrose fractionation; lane 7, pellet from the sucrose fractionation. B, Agarose gel electrophoresis of RNA extracts from purified TMV-VLPs (Lane 1) and TMV virions (Lane 2). Band in lane 2 represents the TMV genome. C, Thin section electron micrograph of a fixed *E. coli* cell showing the presence of assembled TMV-VLPs. D, Purified TMV-VLPs from the sucrose gradient resuspended pellet. Bars equal 200 nm. E, Transmission electron microscope images of TMV1cys (top row) and TMV1cys-VLP (bottom row) adjusted to pH 3, 5, 7, 9, and 11 (left to right). Bars equal 500 nm.

Purification of these particles was easily accomplished via sucrose gradient centrifugation of chloroform cleared bacterial extracts. PAGE analysis from each purification step (bacterial lysate, chloroform clarification, PEG precipitation and sucrose gradient fractionation) shows the selective purification of the VLPs (Figure 2-2A, lanes 3-6) while electron microscopy of the final gradient fractions (Figure 2-2A, lane 7) shows the purity of the VLPs (Figure 2-2D). Concentrations of purified rod-shaped VLPs of over 70 mg per liter of culture were routinely obtained using this method. An analysis of purified particles indicated a width (18 nm) and inner channel size (4 nm) consistent with the virus particle. However, the length of the bacterial purified particles was highly variable with many particles substantially longer than the 300 nm virus produced particles (Figure 2-2D). Variable VLP lengths indicate an absence of RNA, which typically controls virus particle length. Subsequent nucleic acid extractions from purified VLPs confirmed the lack of nucleic acid in these particles (Figure 2-2B, lane 1). In contrast, similar nucleic acid extractions from purified virus samples produced an abundant amount of genomic viral RNA (Figure 2-2B, lane 2). Combined these findings demonstrate that the E50Q / D77N mutations are sufficient to drive the nucleic acid free assembly of the TMV coat protein within the bacterial expression system.

To determine the relative pH-dependent stability of the TMV and TMV-VLP rods, samples were exposed to a pH range of 3-11. 100 µL of 1 mg/mL TMV1cys and TMV1cys-VLP in 0.1 M pH 7 phosphate buffer were first dialyzed against 200 mL 0.1 M pH 7 Tris. The samples were then divided and dialyzed against 200 mL 0.1 M Tris adjusted to pH 3, 5, 7, 9, or 11 for 72 hours. The resulting suspensions were

examined by transmission electron microscopy. The results showed a similar stability profile for TMV1cys-VLP as compared to RNA-containing virus rods (Figure 2-2E). Both were shown to be stable at pH 5 and 7, with longer rods present at pH 5, and both exhibited fracturing of rods at pH 3 and 9. Both samples at pH 11 showed complete loss of visible structure.

2.4.2. Surface attachment and inorganic coatings of TMV1cys-VLPs

To examine the stability of the bacterial assembled TMV-VLPs we assessed their ability to be surface assembled and metal coated. Previous studies using the TMV1cys virus have demonstrated a robust ability of this virus to bind surfaces in an oriented fashion (from one end of the rod) and via electroless plating produce uniform metal coatings [162, 168]. The positioning of the N-terminus 1cys mutation directs the attachment and vertical positioning of the viral rod-shaped particles onto gold, steel, or other metal surfaces [162]. Although surface exposed, the 1cys mutation is recessed within a groove and partially covered by the C-terminal arm of the coat protein. This position inhibits direct contact between the cysteine derived thiol and metal surfaces except at the 3′ end of the virion rod where the thiol group is sufficiently exposed to make direct contact with the gold surface (A). Here we show that the addition of the 1cys mutations to the E50Q / D77N TMV-VLP ORF produces rod-shaped nanoparticles that readily assemble onto surfaces and can be

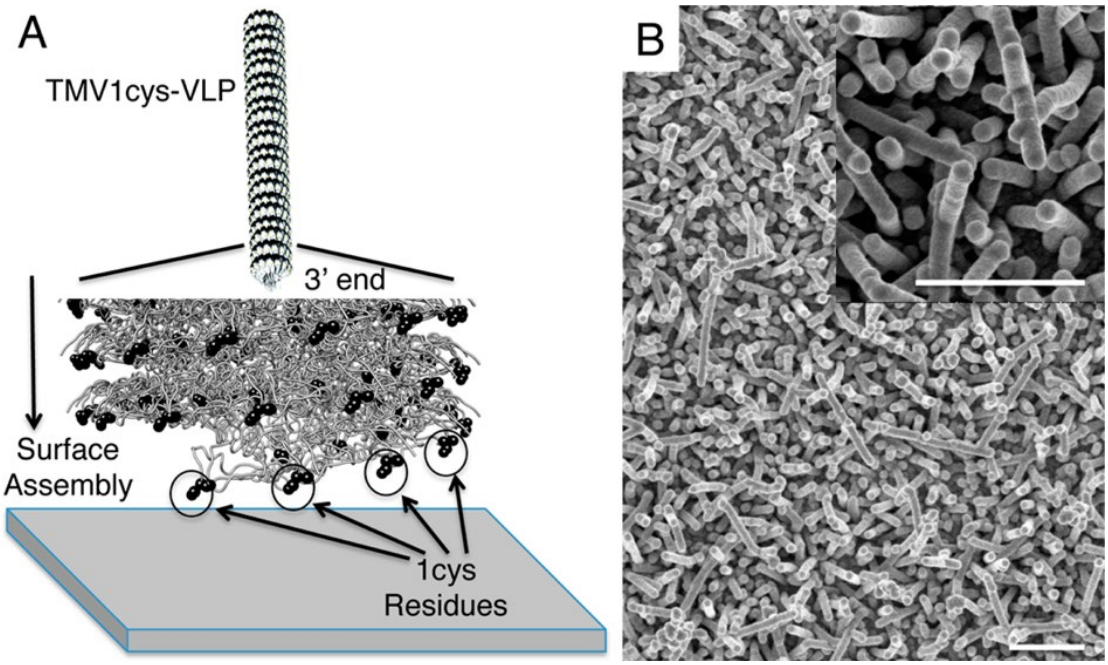

Figure 2-3: Surface binding and electroless plating of TMV1cys-VLPs. A, Molecular models showing the location and binding of the TMV1cys-VLP modification for the oriented attachment of the VLPs onto a gold coated surface. B, Scanning electron micrograph of a TMV1cys-VLP assembled surface electroplated with nickel. Bars equal 1µm.

easily metal coated using established electroless plating methods (Figure 2-3B) [162]. These findings demonstrate that even in the absence of viral RNA the E50Q – D77N VLP rods maintain robust stability during the extensive processing required for surface attachment and metallization.

2.4.3. Chip based enzyme linked immunosorbent assay

To examine the flexibility of the TMV-VLP assemblies we produced a set of modified coat protein ORFs for the display of peptides along the outer surface of the virus particle (Figure 2-4). The simplest system directly fused the peptide of interest to the C-terminus coat protein ORF so that each coat protein subunit displays the desired peptide (Figure 2-4A and B). For these experiments the eight amino acid FLAG peptide (DYKDDDDK) was fused directly to the C-terminal arm of the 1cys coat protein ORF to produce TMV1cys-VLP-FLAG. To examine the ability of

TMV1cys-VLP-FLAG assembled peptides to bind their target molecules we utilized a microchip based ELISA strategy for SiN chips [169]. TMV1cys-VLP-FLAG were self-assembled onto gold coated chips and washed with PBS buffer to remove any excess unbound virus and blocked with 5% non-fat milk to reduce background. Incubation with anti-FLAG antibody and subsequent detection via an alkaline phosphatase linked anti-antibody produced a clear color precipitant with an antibody detection limit of $<10^{-6}$ mg/ml (Figure 2-5). Control chips assembled with TMV1cys-VLP without the FLAG peptide did not show detectable color changes. These studies demonstrate the utility of the TMV1cys-VLP system for the display and surface assembly of target peptides for detection purposes.

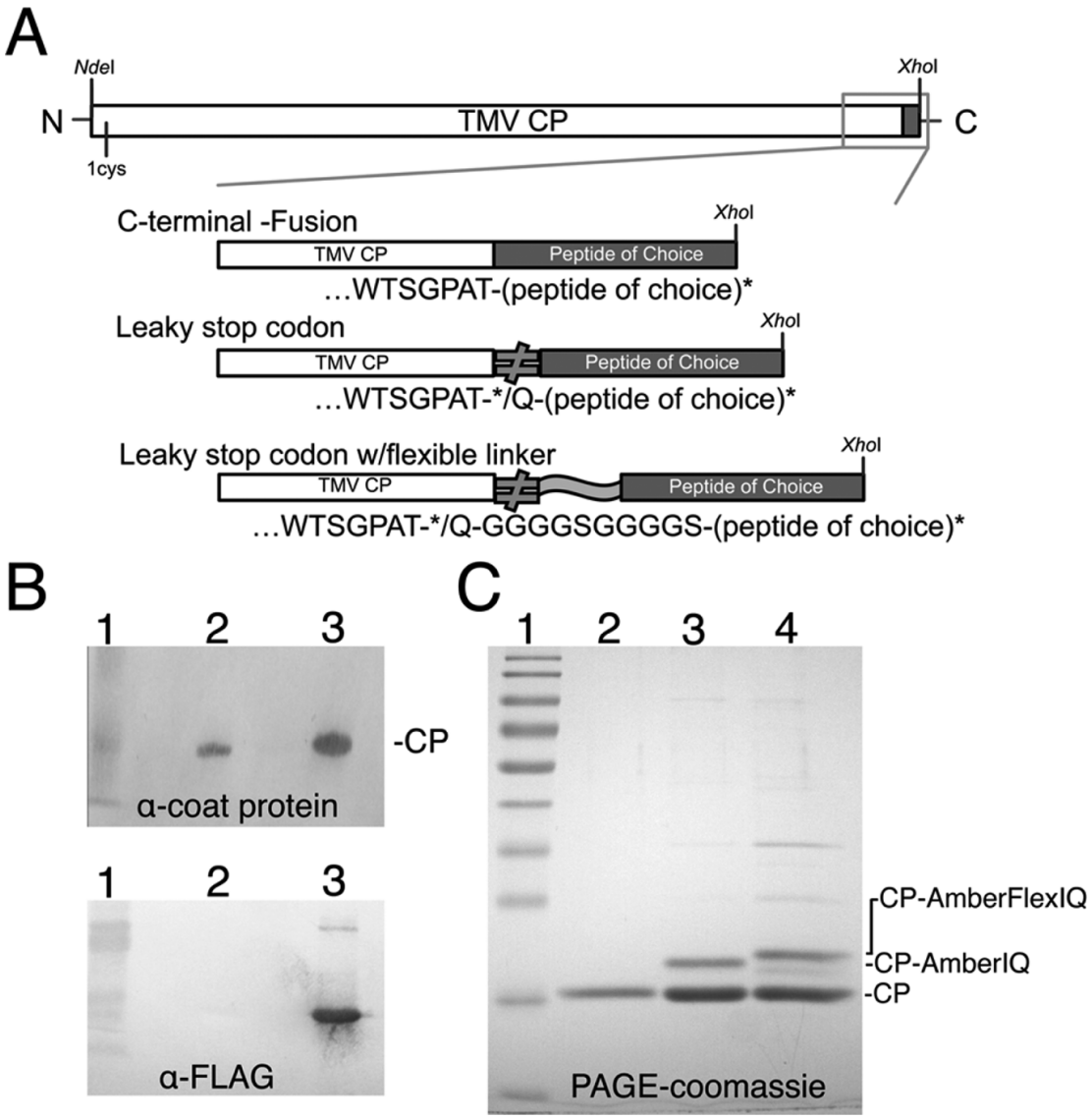

Figure 2-4: TMV-VLP expression constructs. A, Diagram of TMV ORF with three variations for the expression and display of functional peptides. B, Western blot analysis of purified TMV1cys-VLP-FLAG particles with either anti-coat protein and anti-FLAG antibody. Lane 1, marker proteins; lane 2, the unmodified TMV1cys-VLP; lane 3, TMV1cys-VLP-FLAG. C, PAGE analysis of purified TMV1cys-VLP-AmberIQ and -AmberFlexIQ constructs. Lane 1, marker proteins; lane 2, the unmodified TMV1cys-VLP; lane 3, TMV1cys-VLP-AmberIQ; lane4, TMV1cys-VLP-AmberFlexIQ.

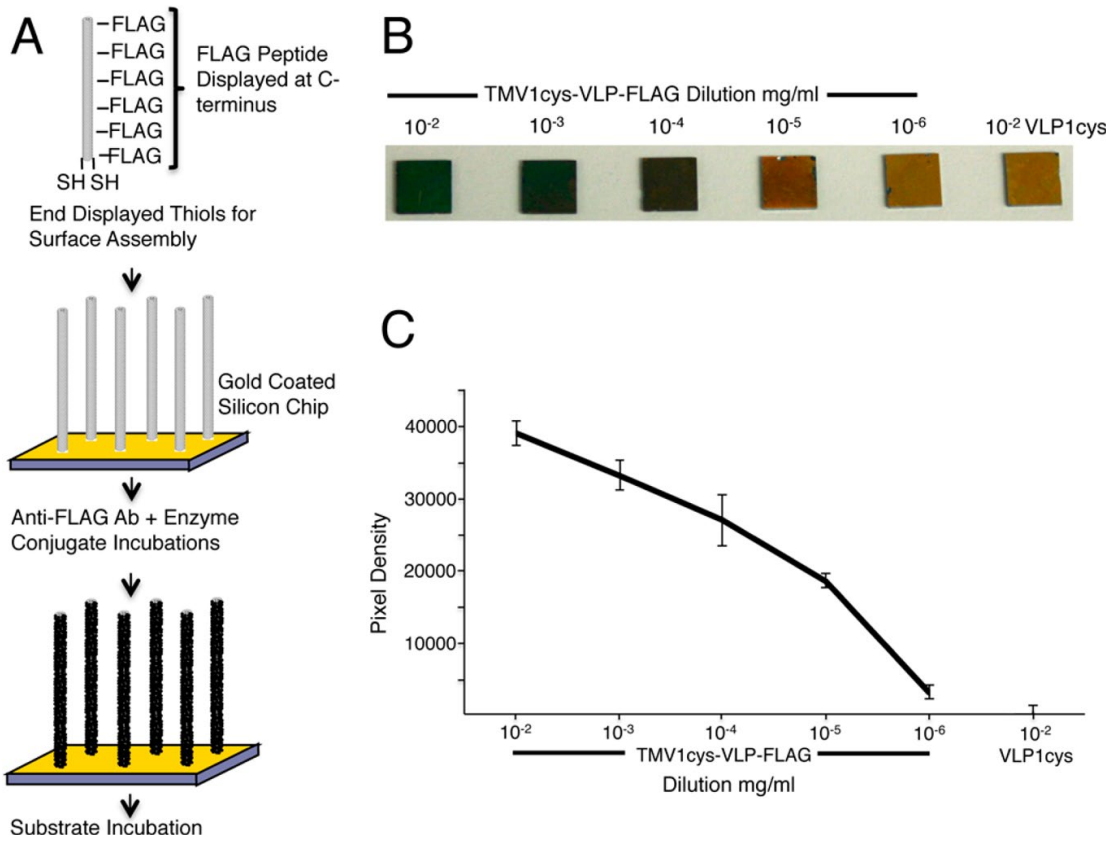

Figure 2-5: Use of TMV1cys-VLPs in a chip based ELISA detection system. A, Diagram of VLP assembly and detection system. B, Gold coated chips assembled with a range of TMV1cys-VLP-FLAG concentrations and processed as outlined in A. Note, the control chip coated with the 10^{-2} mg/ml unmodified TMV1cys-VLP did not produce a substrate reaction after ELISA processing. C, Density analysis of ELISA chips shown in B.

2.4.4. Controlled peptide display for VLP assembly small molecule detection

To further investigate the ability of the TMV-VLP system to function as a nano-scaffold for the display of functional peptides we engineered the rod-shaped VLPs to display a seven amino acid "IQ" peptide (IQSPHFF) previously identified by phage display for its ability to bind the fluorescent imaging molecule Genhance^{TM} 680 [165]. However, initial attempts to purify TMV1cys-VLP rods with the IQ peptide fused directly to the C-terminus of the coat protein ORF failed (data not shown). We speculate that unlike the FLAG peptide the IQ peptide produces

misfolding of the coat protein and / or disrupts VLP rod assembly, possibly via steric hindrance between the stacked coat protein subunits. To circumvent these potential problems an amber stop codon was added to the 3′ end (C-terminus) of the coat protein ORF (Figure 2-4A). Expression of the amber stop construct from within the bacterial supE44 suppressor system directs the occasional incorporation of a glutamine residue at the TAG stop codon due to a tRNA mutation. This produces a mixture of coat proteins both with and without the additional peptide. A second construct adding a 10 amino acid flexible linker "Flex" (GGGGSGGGGS) in front of the IQ peptide was also created as a means to further reduce any interference the IQ peptide may have on VLP rod assembly (Figure 2-4A). The small side chains of this linker produce a highly flexible peptide sequence that has been used extensively for bridging functional peptide domains [164]. Bacterial expression and subsequent VLP rod purifications produced significant quantities of these VLPs (Figure 2-4C). In particular the TMV1cys-VLP construct expressing the amber stop with flexible linker produced nearly twice the concentration of purified VLPs, ~16mg/L, in comparison to the construct with only the amber stop, ~9mg/L. For both constructs an average ~34% of the subunits derived from the purified VLP nanorods were read-through products of the amber stop codon and displayed the additional peptide sequences (Figure 2-4C, lanes 3& 4). The ability to vary the expression and display of the desired peptide provides a means to significantly reduce disruptions in VLP assembly conferred by the desired peptide.

The ability of the TMV1cys-VLP displayed IQ peptides to bind their target analyte was also investigated. Purified TMV1cys-VLP-AmberFlexIQ scaffolds were

mixed with Genhance^{TM} 680, washed and analyzed for retention of the fluorescent imaging agent. Results for the tested VLP concentrations indicate that the VLPs alone are capable of binding low levels of the fluorescent analyte in a non-specific manner (Figure 2-6). However, addition of the IQ peptide sequence, creating TMV1cys-VLP-AmberFlexIQ, produced a significant increase in retained fluorescence over the unmodified control TMV1cys-VLP (Figure 2-6). This finding indicates that the IQ peptide maintains the ability to bind its target molecule when displayed from the TMV1cys-VLP-AmberFlexIQ scaffold.

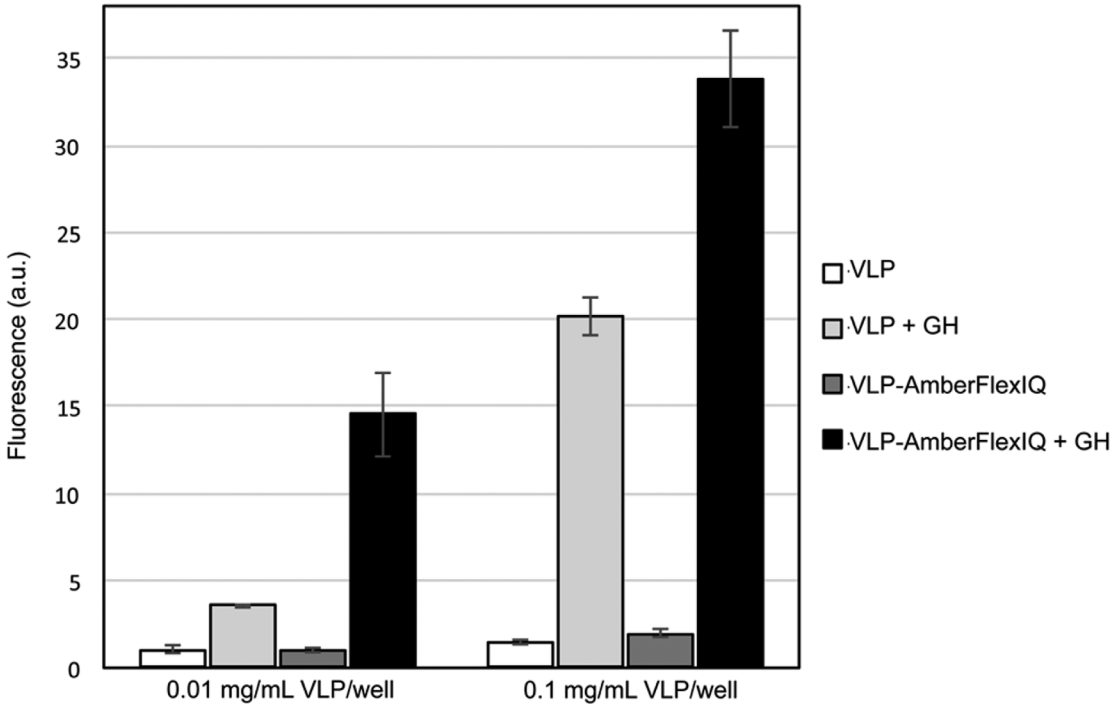

Figure 2-6: TMV-VLP directed binding of a fluorescent imaging agent. Purified TMV-VLPs at defined concentrations were mixed with Genhance 680^{TM} (GH) washed and assayed for fluorescence retention. Data is shown for the unmodified TMV-VLP (VLP) and TMV-VLP-AmberFlexIQ (VLP-AmberFlexIQ) both with and without GH treatment. Results show averaged ± standard deviation from three assays.

2.5. Discussion

In this study the known structure and assembly mechanism of TMV was used to engineer a novel *in vivo* VLP assembly system. In nature TMV occurs as a

soilborne virus and has evolved a sensitive sensing system that allows the rod-shaped particle to remain stable in the soil environment yet become unstable upon entry into a host cell. This sensing system is controlled by juxtaposed carboxylate interactions that exist between subunits [151, 161]. These repulsive carboxylate interactions represent a key factor in virion assembly and disassembly. Removal of these interactions strengthens the association of the coat protein subunits through existing hydrophobic and salt bridge interactions, significantly stabilizing the helical rod assembly [98]. Carboxylate alterations E50Q and D77N significantly shift the coat protein assembly equilibrium toward the production of rod-shaped particles, thus driving helical rod assembly even in the absence of the viral RNA. This modification permits the production of rod-shaped TMV-VLPs from a simple *E. coli* expression system and greatly expands the potential usefulness of these bio-macromolecules in a number of nanotechnology related applications.

Significantly, the ability to rapidly produce quantities of TMV nanorod VLPs directly from bacterial cultures greatly simplifies methods for the construction and purification of highly modified versions of these macromolecules. The use of this system eliminates problems such as recombination and reduced virus accumulations that can occur when the infectious virus functions as the template for the display of functional peptides and groups. Additionally, specialized plant growth facilities are not needed, making these macromolecules more accessible for use in a wider range of research settings. Furthermore, findings indicate that bacterially expressed TMV-VLPs display a similar level of stability and functionality as the plant produced viruses, including pH sensitivity, surface assembly, mineralization and sensor

functions. Thus, stability conferred by the genetic neutralization of repulsive carboxylate groups is sufficient to produce robust VLP assemblies.

For virus particles two areas of application that have been studied extensively are their use in materials fabrication and their ability to display functional groups for sensor or vaccine applications. Filamentous viruses including TMV and M13 have been developed as biotemplates for the deposition of a variety of inorganic materials [146, 150]. The rigidity of the TMV rod-shaped particle as well as its polar ends allows for the particle to be attached to a surface in vertical orientation, producing three-dimensional nano-featured substrates that significantly improve electrode function in a variety of electrode chemistries [150]. Similarly, TMV particles and coat protein have been genetically engineered to display epitopes from a variety of agents including the malaria parasite, foot and mouth disease virus and influenza A as a means to rapidly produce vaccine components [170-172]. Findings from this study clearly indicate that the TMV-VLPs are similarly capable of functioning as biotemplates for inorganic coatings as well as nanoparticles for the display of functional epitopes.

The use of bacterial phage and related systems to display and screen peptide libraries is a powerful combinatorial technology for the identification of unique peptides that confer selective binding abilities [173]. To date, phage display methods have been employed to identify numerous single chain antibodies as well as receptor peptides that bind various pathogens and toxins of importance, including heavy metals such as cadmium; toxins such as ricin, botulinum, shiga and staphylococcal enterotoxin B; and bacterial pathogens including *Escherichia coli* O157:H7 [174-

179]. Many of these receptor peptides display binding affinities in the nano-molar range and are capable of detecting their target molecules in traditional ELISA systems at the nanogram level [165, 180]. However, a considerable gap between the identification of these receptor peptides and their assembly into functional devices remains. The TMV1cys-VLP based display system represents a simple means to genetically produce these peptides in a variety of configurations and in a nanostructured format that can be patterned three dimensionally onto a variety of surfaces. Combined these attributes make this VLP system a powerful means for the controlled display of functional peptides.

2.6. Conclusion

We report here the development of a TMV-VLP display system that directs the *in vivo* production of virus-like nanorods and tubes from a simple bacterial expression system. This system is genetically tractable and produces stable rod-shaped VLPs that can be used to display functional groups and peptides in multiple configurations with potential applications in sensor, electrode and therapeutics development. This VLP system greatly simplifies the production of these rod-shaped particles, eliminating the need to produce a full-length infectious clone of the virus for production in plants. This simple, genetically tractable system for the production of TMV based nano-particles should provide greater accessibility for a wider core of researchers interested in utilizing these particles to address a variety of questions and applications.

2.7. Acknowledgements

We wish to thank Tim Maugel in the Laboratory of Biological Ultrastructure at the University of Maryland, College Park, for assistance with EM imaging and sample fixation. This work was supported by Biochemistry Program of the Army Research Office award W911NF1110138 and Maryland Agricultural Experiment Station award MD-PSLA-0275. [181]

Chapter 3: Modified *Tobacco Mosaic Virus* Capsid Proteins with Unique Environmentally Responsive Assembly Behavior for Hierarchically Ordered Nanotubes

3.1. Abstract

The creation of particles and surfaces with complex functional architectures at the nanometer to micrometer scale is a promising capability afforded by advances in nanotechnology. One strategy for generating these materials is the hierarchical, bottom-up self-assembly of nanoscale components that occur naturally in biological systems. *Tobacco mosaic virus* (TMV) is one example of a self-assembling biological system that has been studied extensively for nanoscale applications. TMV is a filamentous plant virus with a hollow, tube-shaped rod of 300nm length × 18nm diameter consisting of ~2130 capsid protein [182] subunits. Its high aspect ratio and high surface area generated from iterated copies of a single component protein make it attractive as a foundation for the design of novel nanostructured materials. Multiple acidic amino acid residues are incorporated into the viral CP, generating electrostatic repulsion between adjacent CP not only within the assembled rod, limiting assembly of virus rods without incorporated genomic RNA, but also between individual rods, encouraging their monodispersity. One pair of negatively charged, surface-exposed residues known to have particular importance to the virus's structural stability through electrostatic repulsion is composed of glutamic acid E50 and aspartic acid D77, which are shown by structural analysis to interact between adjacent CP in the direction of the virus rod's axial (longitudinal) direction. This project investigates the

effects of altering these residues on the assembly behavior of TMV CP both within individual rods for the generation of a new class of virus-like particles (VLPs) and between different members of this class for the self-directed, hierarchical assembly of more complexly structured nanoparticles. Replacing the one or both of the negative charged carboxylate residues glutamic acid (E50) and aspartic acid (D77) with neutrally charged glutamine (E50Q) and asparagine (D77N) or positively charged lysine (E50K or D77K) results in self-assembling nanotube VLPs with unique rod end charge profiles which self-direct the end-to-end coassembly of distinct VLP populations into lengthened, chimeric VLP with longitudinally ordered structure. Addition of a well-positioned cysteine residue directs the perpendicular attachment of these complex VLPs to surfaces to for the development of surface-attached nanoscaffolds with distinct surface-proximal and surface-distal addressability and functionality.

3.2. Introduction

Biologically derived macromolecular assemblies are of increasing interest for their application in nanotechnology. Nucleic acids, proteins, and complexed assemblies of these, such as viruses, have been investigated for applications including enhanced energy production, sensing, drug delivery and enzyme sequestration [183-185]. Interest in these biological components stems from their ability to self-assemble into defined nanoscale structures, to recognize and bind target analytes, to enzymatically catalyze chemical reactions, and to be manipulated genetically, permitting specific modifications to these assemblies. In addition, the bottom-up fabrication strategy afforded by the use of biological components holds the potential

to generate novel nanoscale structures and patterns with unique functions. Examples include “DNA origami” that utilize DNA base paring to direct the ordered assembly of hundreds of oligonucleotides or the use of protein–protein interaction domains to assemble peptide chains into complex geometric shapes [185-187]. Combined, these studies represent remarkable initial efforts in the development and application of designed biological assemblies.

Viruses in the form of virions represent some of the most studied and manipulated naturally occurring sub-micron self-assembly systems. As such, virus-based assembly systems have been created to encapsidate therapeutics, enzymes, pesticides and inorganics for use in a range of applications [188-190]. What make viruses particularly amenable to these studies are the molecularly scaled uniform capsid proteins that under the appropriate environmental conditions can be induced to self-assemble into defined nanoscale shapes with great fidelity. In general, modification of virion assemblies has involved the surface display of naturally occurring or genetically introduced amino acid residues or functional polypeptide chains that enable chemical cross-linking of molecules to the virion surface, the surface display of selective binding motifs or the incorporation of enzymes, nucleic acids and inorganics within the virion shell [183, 191]. These studies add functionality to existing virion structures, but efforts to re-engineer virion assembly to produce novel nanoscale structures are less well developed and in need of additional investigation.

Some of the most extensive efforts to modify virion assembly have occurred with *Tobacco mosaic virus* (TMV). TMV is a common plant virus prevalent in many

environmental systems. The TMV particle consists ~2130 identical coat proteins subunits (M.W. 17.5 kDa) packed in an 18 nm diameter helix, the layers of which sandwich a single strand of plus-sense RNA, around a 4 nm diameter channel situated along the 300 nm long longitudinal axis [151]. The two ends of the rod-shaped virion are morphologically distinct, with a concave surface at the end containing the 5′ end of the genome and a convex surface structure at the 3′ genome end. The three-dimensional structure of the CP has been resolved to 2.8 Å and 2.4 Å for a 20S disk aggregate, consisting of two stacked protein rings each containing 17 CP subunits [82, 160] and at 2.9 Å resolution for the TMV virion [151]. This structural information has led to several innovative assembly systems. Included in these systems is the design of a circular permutant from a rearrangement of the TMV CP gene with newly created N- and C-termini on the inner - rather than outer - surface, facilitating modifications to the central channel of the virion [157]. In a second system an added cysteine at inner-channel-proximal CP residue 103 was used to promote the assembly of rod shaped virus-like particles (VLP) in the absence of viral RNA [192]. The disulfide bonds responsible for stabilizing rod assemblies provide a redox-based means to control the production of virus-like protein rods. Alternatively, novel assembly systems have been developed by altering the viral RNA, which plays a critical role as a structural component of the virion. Specifically, RNAs containing TMV origin of assembly sequences (OAs) can be used to direct the assembly of TMV CPs into virus-like rods of defined lengths, heterologous CP composition or onto patterned substrates [193-195]. Furthermore the multiple-OAs-containing-RNA-directed assembly of TMV CPs can be used to produce branched virion-like

structures [196]. Combined these systems provide varying levels of control over the assembly of these virus-based macromolecular assemblies, opening up their potential as functional components in larger and more complex nano- and micro-scale structures.

Our group has previously developed a VLP assembly system based on the elimination of an assembly-destabilizing intersubunit interaction between carboxylate groups [181]. Previous studies had identified two sets of carboxylate groups generating intersubunit repulsion, composed of (i) CP residues E50 and D77 interacting between axially adjacent subunits and (ii) E106 and E95/E97/D109 located between laterally adjacent subunits, as providing the driving forces in virion disassembly [96, 151, 161]. Outside of a host cell, the relatively low pH of the extracellular environment functions to neutralize this repulsive E50 – D77 interaction, stabilizing the virion assembly. However, upon entry into the cellular environ the higher pH results in the loss of stabilizing protons and the destabilization and disassembly of the virion. By weakening these repulsive interactions, substitution mutants E50Q/D77N, E97Q, and E95Q/D109N function to stabilize the virion assembly, producing long virion-like rods *in planta* [96]. In addition, the double axially-interacting-carboxylate substitution E50Q/D77N produces long virion-like rods in bacterial expression systems [181]. The use of bacterial systems greatly enhances the speed and ease of expression for these TMV-VLPs over plant-based TMV infection systems. In addition, heterologous expression is significantly more amenable to incorporation of additional gene-level modifications since recombination events associated with virus replication do not occur in this system.

In this study, the directed modulation of TMV-VLP assembly is investigated as a means to control the production of complex hierarchical nano-rods. Genetic modifications of the TMV CP were created to modulate both the CP subunit structure and its electrostatic-charge-based intersubunit interactions to either strengthen or weaken the ability of individual CP interfaces to self-associate and to associate with other modified or wild-type CP. These modifications were created to preferentially direct assembly of CP subunits to either the 3′ or 5′ nanorod ends of TMV.

3.3. Methods

3.3.1. Design of modified TMV CP genes

The TMV capsid protein gene was modified to substitute neutrally charged or basic amino acid residues for one or more of the negatively charged acidic residues which interact with those on adjacent CP subunits. All modified forms of the TMV capsid protein used in this study were ultimately generated from copies of a DNA open reading frame (ORF) encoding the TMV CP codon optimized for expression in *E. coli* using codon utilization frequency tables. The ORF encoding the E50Q/D77N form was obtained from GenScript (Piscataway, NJ). The ORFs encoding the E95Q/E97Q/E106Q/D109N, E50Q+E95Q/E97Q/D109N, D77N+E106Q, E50K-HA, and D77H and R46G-E50H-HA were generated using Invitrogen™ GeneArt™ Strings™ DNA fragments. All additional variants were generated by sequential polymerase chain reactions using overlap extension PCR with primers encoding the designed modifications and complimentary to regions of the ORF to be modified. These included additional modifications to the carboxylate-containing sites E50, D77, E95, E97, E106, and E109, the insertion of the S1_Y2insC (hereafter denoted as

"1cys") modification by the insertion of a cysteine at position three (5′-MSYS…→5′-MSCYS…), and insertion or replacement of sequences encoding either the FLAG-tag epitope (DYKDDDDK) or the HA-tag (YPYDVPDYA) to the 3′ end of the gene, following the sequence encoding the C-terminal PAT residues. Two endonuclease restriction sites, an *NdeI* restriction site over lapping the ORF start codon and an *XhoI* restriction site at the 3′ end, flanking the ORF were included. For each ORF-interior modification, a set of PCR reactions, each using a primer pair consisting of either a forward primer containing the ORF 5′ end and a reverse primer containing the interior modification or a forward primer containing the interior modification and a reverse primer containing the ORF 3′ end, was performed using *Platinum Taq* DNA Polymerase (Invitrogen): 94 °C for 5min; 32 cycles of 94 °C for 30 s / 55 °C for 30 s / 72 °C for 1 min; 72 °C for 5 min). The PCR product from each of the two PCR reactions was gel-purified using a GENECLEAN III gel purification kit (MP Biomedicals) and used as templates for PCR with the 5′ end forward primer and the 3′ end reverse primer from the previous PCR reactions. Complete PCR products of CP ORFs were isolated and amplified using a TOPO TA cloning kit. pCR-2.0 vector, TOP10 competent cells (Invitrogen).

ORFs were excised from TA clones by restriction with *NdeI* and *XhoI* and isolated from the plasmid vector by agarose gel electrophoresis. Bands were purified using GENECLEAN III gel purification kit and purified DNA fragments were ligated into a similarly cut and purified pET-21a(+) (Novagen, Madison, WI) or pET-DUET expression vector with T4 DNA ligase. Complimentary overhangs between vector and insert were created by using the same restriction enzymes. Ligated plasmid

vectors containing the ORFs were transformed into DH5α chemically competent cells for amplification with ampicillin selection and subsequent miniprep purification. Clones containing inserted genetic material were identified using restriction hydrolysis of ORF-flanking restriction sites and were sequenced to screen for unintended mutations.

3.3.2. Bacterial expression and purification of TMV CP variants

Plasmids containing sequence-verified ORFs encoding the various TMV CPs described above were transformed into chemically competent BL21-CodonPlus *E. coli* K-12 cells. Transformations were spread onto LB-agar plates containing ampicillin (100 μg/mL) and chloramphenicol (20 μg/mL). Colonies were picked and grown in LB containing ampicillin (100 μg/mL) and chloramphenicol (20 μg/mL) at 37 °C overnight. Frozen stocks of cells containing the TMV CP constructs for continued production of modified CP were made by addition of DMSO (70 μl/mL culture) and storage at -80 °C. Cell cultures were grown at 37 °C until reaching an absorbance of 0.5 ± 0.1 at a wavelength of 600 nm. At that point the culture was induced by the addition of IPTG to a concentration of 1 mM and incubated at room temperature with shaking overnight. Induced cells were pelleted by centrifugation at 4 °C and lysed by resuspension in Bugbuster HT Protein Extraction Reagent and the addition of Lysonase according to the manufacturer's protocol (Novagen, Madison WI) and incubation at room temperature for 30 minutes. The bacterial lysate was diluted 10:1 with 0.1 M pH 7 phosphate buffer and pelleted by centrifugation at 91,000 × g for 2 hours. The resulting pellet was resuspended in 2 mL 0.1 M pH 7 phosphate buffer with pipetting and shaking overnight at 4°C. Resuspended pellets

were loaded onto a 10 to 40 % sucrose gradient in 0.1 M pH 7 phosphate buffer and centrifuged at 91,000 × g at 14 °C for either 1 hour (E50Q and D77N variants) or 15 minutes (E50K and D77K variants). The virus-like particles were removed from the center portion of the gradient, where they formed a diffuse visible band, with a syringe and transferred to ~25 mL ultracentrifuge tubes. The samples were diluted with 0.1 M pH 7 phosphate buffer to reduce sucrose concentration and centrifuged at 91,000 × g for 2 hours at 4 °C. The purified VLP pellets were resuspended in 0.1 M pH 7 phosphate buffer.

3.3.3. Determining concentration of TMV and bacterially expressed TMV CP

All determinations of disassembled CP and assembled VLP solution concentrations were made using a Thermo Fisher Scientific™ Nanodrop™ 1000. VLP samples purified from monoclonal cultures of transformed expression strains of *E. coli* (BL21 and BL21 codon plus) all showed a light attenuation peaks at around 280 nm, indicating the relative lack of nucleic acid and in contrast to purified samples of absorption spectrum of encapsidated RNA centered around 260 nm.

Determinations of TMV concentrations, which contain the genomic RNA, were made by measuring the attenuation of the TMV sample at λ = 260 nm, calculating and subtracting the attenuation due to scattering to obtain the attenuation at 260 nm attributable to absorbance alone and using the mass attenuation coefficient and path length to determine concentration using the following form of the Beer-Lambert law

$$C = \frac{(A_{260} - 2.44 \times A_{325})}{\varepsilon_{TMV,260} \times l}$$

Where A_{260} and A_{325} are the sample absorption measurements of 260 nm and 325 nm wavelength light, respectively, $\varepsilon_{TMV,260}$ is the extinction/attenuation coefficient of TMV at wavelength 260 nm, and l is the path length. The expression $2.44 \times A_{325}$ is the estimated attenuation at 260 nm due to scattering. Because neither protein nor RNA has significant absorption at 325 nm, all attenuation at 325 nm is assumed to be due to scattering. Because scattering varies with wavelength with a factor of λ^{-4},the scattering at 260 nm is related to the scattering at 325 nm by a factor of $(260^{-4}/325^{-4})$ = 2.44. The inherited mass attenuation coefficient for TMV, ε_{260}, is 3 $L \cdot g^{-1} \cdot cm^{-1}$.

The concentration of RNA-free, bacterially expressed CP was determined by measuring the optical attenuation at λ = 280 nm, calculating and subtracting the attenuation due to scattering to obtain the attenuation at 280 nm attributable to absorbance alone and using the mass attenuation coefficient and path length to determine concentration using the following form of the Beer-Lambert law

$$C = \frac{A_{280} - (1.8 \times A_{325})}{\varepsilon_{CP,280} \times l}$$

Where A_{280} and A_{325} are the sample absorption measurements of 280 nm and 325 nm wavelength light, respectively, ε_{280}, is the extinction/attenuation coefficient of the relevant CP at wavelength 260 nm (see table), and l is the path length. The expression $1.8 \times A_{325}$ is the estimated attenuation at 280 nm due to scattering. Because protein does not have significant absorption at 325 nm, all attenuation at 325 nm is assumed to be due to scattering. Because scattering varies with wavelength with a factor of

λ^{-4},the scattering at 280 nm is related to the scattering at 325 nm by a factor of $(280^{-4}/325^{-4}) = 1.815$.

The attenuation coefficients of the VLP-forming CPs were calculated using the Edelhoch method, according to which

$$\varepsilon(208)(M^{-1}cm^{-1}) = (\#Trp)(5{,}500) + (\#Tyr)(1{,}490) + (\#disulfide)(125)$$

where ε*(280)* is the molar attenuation coefficient, *#Trp*, *#Tyr*, and *#disulfide* are the number of tryptophan residues, tyrosine residues, and disulfide bonds bonds formed by crosslinked cysteine residues, respectively. The corresponding mass attenuation coefficients were obtained by dividing the molar attenuation coefficents by the mass in grams per mole of CP.

	# Trp / CP	# Tyr / CP	# S-S / CP	Molar ε ($M^{-1}\cdot cm^{-1}$)	FW	Mass ε ($L\cdot g^{-1}\cdot cm^{-1}$)
WT CP	3	4	0	22460	17420	1.289
1cys CP	3	4	0	22460	17524	1.281
R46G/E50K-E97Q-FLAG	3	6	0	25440	18405	1.382
D77K-HA	3	5	0	23950	18429	1.299

Table 2: Molar and mass attenuation coefficients at 280 nm for various TMV CPs.

3.3.4. Longitudinal coassembly of neutral carboxylate-substituted CP variants with TMV or VLP with wild-type axial carboxylates

Complexed nanoparticles with distinct and ordered longitudinal domains generated from the coassembly of a nanoparticle retaining wild-type axially interacting carboxylate residues (either infectious TMV or VLP assembled from E95Q/E97Q/D109N+E106Q CP) together with a VLP containing uncharged amino acids substituted at one rod end (E50Q+E95Q/E97Q/D109N-FLAG VLP or

D77N+E106-HA VLP) were produced by concentration of a solution containing a mixture of the component nanoparticles.

For the longitudinal coassembly of TMV and D77N+E106Q-HA VLP, 100 μg each of purified 5 mg/mL 1cys TMV and D77N+E106Q-HA VLP in 0.1 M pH 7 sodium phosphate buffer were mixed and diluted with 25 mL 0.1 M pH 7 sodium phosphate buffer in a ultracentrifuge tube. The mixture was centrifuged at 91,000 × g for 2 hours at 4 °C, at which point the supernatant was removed and replaced with 100 μL of 0.1 M pH 7 sodium phosphate buffer. The pellet was allowed to resuspend overnight at 4 °C with gentle rocking, then diluted (1:500) in 0.1 M pH 7 phosphate buffer for immunolabelling and preparation for TEM.

For the longitudinal coassembly of E95Q/E97Q/D109N+E106Q VLP with E50Q+E95Q/E97Q/D109N-FLAG VLP, 50 μL of 1 mg/mL solutions of each of the two purified VLPs in 0.01 M pH 7 sodium phosphate buffer were well mixed in a 1.5 mL centrifuge tube. The mixed sample was then centrifuged under partial vacuum until the sample volume had reduced to ~10 μL (approximately one hour). The concentrated sample was kept at 4 °C overnight before dilution (1:500) in 0.1 M pH 7 sodium phosphate buffer for immunolabelling and preparation for TEM.

3.3.5. Dialysis of samples

All dialysis was performed Spectra/Por® dialysis membrane tubing (MWCO:12-14,000, Spectrum Labs) secured to the opening of a 1.5 mL microcentrifuge tube containing 50-200 μL of plant-expressed TMV and/or bacterially expressed CP. The microcentrifuge tubes were inverted so that sample solution was in contact with dialysis film and placed in a floating microcentrifuge

holder on the surface of 500 mL of the solution to be dialyzed against, so that the dialysis tubing was in contact with the target dialysis solution. All dialysis was performed at 4 °C overnight. For all dialysis experiments, TMV or CP samples, which were initially in 0.1 M pH 7 sodium phosphate buffer were first dialyzed to 0.1 M pH 7 Tris buffer. The pH 7 Tris-buffered samples were then dialyzed against either ultrapure water adjusted to pH 7 with approximately 50 μL of 12 M NaOH per 1 L of water or 0.1 M Tris adjusted to pH 5, 6, 7, 8, or 9 with glacial HCl or 12 M NaOH.

3.3.6. Longitudinal coassembly of positively-charged carboxylate-substituted CP variants with TMV

To generate extended TMV-VLP complexed particles with distinct and ordered longitudinal components, TMV and VLP were dialyzed either separately or in admixture to solution conditions promoting disassembly of the VLP CP and then returned to conditions promoting its assembly, either by dialysis or by the addition of concentrated solution.

For assembly of D77K-HA CP onto TMV, 50 μL of a solution containing 3 mg/mL of D77K-HA CP and 0.6 mg/mL wild-type TMV (a ratio of 5:1 by mass) in 0.1 M pH 7 sodium phosphate buffer was dialyzed as described above first to 0.1 M pH 7 Tris buffer, then to 0.1 M pH 9 Tris buffer to disassemble the D77K CP, and then to 0.1 M pH 7 Tris buffer to initiate reassembly of the D77K CP onto the TMV rod end with each dialysis step taking place overnight at 4 °C. For samples treated with RNase, 0.5 μL of a 1 mg/mL stock solution of RNase A was added to the solution after the dialysis to pH 9, which was hypothesized to have exposed the

genomic RNA at the TMV's 5′ rod end, and incubated for 30 min at 37 °C before proceeding with dialysis back to pH 7.

For assembly of R46G/E50K+E97G-FLAG CP onto TMV, 50 µL of a solution containing 1 mg/mL of R46G/E50K+E97G-FLAG and 0.5 mg/mL wild-type TMV (a ratio of 2:1 by mass) in 0.1 M pH 7 sodium phosphate buffer was dialyzed first to 0.1 M pH 7 Tris buffer, then to filtered ultrapure water brought to pH 7 with NaOH to disassemble the R46G/E50K+E97G CP, and then to 0.1 M pH 7 Tris buffer / 0.3 M NaCl to initiate reassembly of R46G/E50K+E97G CP onto the TMV rod end with each dialysis step taking place overnight at 4 °C.

3.3.7. Immunolabelling and electron microscopy

To immunolabel and image samples, assembled TMV and VLP samples were adsorbed onto Formvar-coated Ni TEM grids by floating the grid on 5-10 µL droplets containing the sample arrayed on Parafilm™. Grids were washed with phosphate-buffered saline (PBS: 10 mM sodium phosphate, 150 mM NaCl, pH 7). Surfaces were blocked with Blocking Solution for Goat Antibodies (Aurion, Wageningen, The Netherlands) to reduce nonspecific binding and washed with PBS. Primary antibodies (anti-FLAG antibodies produced in rabbit, anti-HA antibodies produced in mouse, Sigma) were diluted 1:500 in incubation buffer (PBS with 0.1% Tween-20 and 0.1% Aurion BSA-c™) as needed and applied to grids at room temperature for 2 h or at 4 °C overnight. Grids were washed by placing on 50 µL drops of incubation buffer for 5 min three times. Gold nanoparticle (AuNP)-conjugated secondary antibodies (i.e. goat anti-rabbit with 10 nm AuNPs or goat anti-mouse with 6 nm AuNPs), if used, were diluted 1:50 in incubation buffer as needed and applied to grids at room

temperature for 2 h or at 4 °C overnight. Grids were washed by placing on 50 µL droplets of incubation buffer for 5 min three times and then on 50 µL droplets of 0.1 M pH 7 Tris. Grids were stained by placing them on a 5 µL droplet of 2% uranyl acetate (UAc) for 1 min. UAc was removed by wicking with filter paper, and the samples were imaged using a Zeiss transmission electron microscope (TEM) at 80 kV.

3.3.8. Light scattering assembly kinetics

Macromolecular assembly kinetics of the D77K and R46G/E50K+E97G CP from the disassembled to the assembled state upon lowering of the pH or increase of the ionic strength of the solution was observed in real time using 90° light scattering to measure the relative degree of rod formation in an aqueous solution of CP. Light scattering was measured on a Varian Cary Eclipse Fluorescence Spectrophotometer. Scattered light was measured at an angle of 90° relative to the angle of incidence using 200 µL of CP solution in a 200 µL capacity quartz cuvette and using the same value of 340 nm for the excitation and emission wavelengths. The dissociation factor D was related to the intensity of scattered light, I, by

$$D = (I_A - I)/(I_A - I_D)$$

where I_A and I_D are the intensity of scattered light for associated and dissociated forms, respectively.

For experiments examining D77K CP assembly, samples were measured by beginning recording of scattered light with baseline measurement of 175 µL of 0.1 M Tris buffer adjusted to pH 5. After 30 s, 25 µL of D77K-HA-tag CP previously dialyzed against 0.1 M Tris buffer adjusted to pH 9 was added and mixed by manual

pipetting. Light scattering was recorded for 20 minutes after mixing.

For experiments examining R46G/E50K+E97G CP assembly, samples were measured by beginning recording of scattered light with baseline measurement of 100 µL of R46G/E50K+E97G-FLAG-tag CP previously dialyzed against filtered water adjusted to pH 7 with NaOH (~50 µL 12 M NaOH / 1 L H_2O). After 30 s, 100 µL of 0.2 M Tris buffer with 0.6 M NaCl adjusted to pH 9 was added and mixed by manual pipetting. Light scattering was recorded for 30 minutes after mixing.

Data was obtained using 340 nm as both the "excitation" (incident light applied to sample from the light source) and "emission" (scattered light measured from sample) wavelength values. This wavelength was chosen after several experiments in which a scan of excitation and emission values were covaried through a range from 200 nm to 700 nm every minute during an assembly reaction of D77K-HA CP. Significant changes in scattered light was observed in the ranges from ~240 nm to ~270 nm and from ~280 nm up to 700 nm, with a dramatically reduced level of scattering observed in the region around 280 nm, presumably due to the high level of absorption by sample CP. The wavelength 340 nm was selected from the candidate ranges as determined by observation due to its use in the literature as a value previously used to study the assembly state of TMV [197, 198].

3.3.9. Surface-bound fabrication of co-assembled nanoparticles

Gold-coated silica wafers (0.5 cm × 0.5 cm), cleaned by sequential 5 min submersions in acetone, methanol, and isopropanol with agitation, were submerged in either a 0.2 mg/mL solution of 1cys TMV in 0.1 M pH 7 sodium phosphate buffer or 0.1 M pH 7 sodium phosphate buffer containing no virus overnight at 4 °C. Residual

phosphate buffer was removed by submersion of the wafers in either 0.1 M pH 9 Tris for subsequent addition of D77K-HA CP or filtered water adjusted to pH 7 (by addition of ~50 µl 12 M NaOH / 1 L water using a pH-meter to monitor pH level) for subsequent addition of R46G/E50K+E97G-FLAG CP.

For longitudinal coassembly of D77K-HA CP onto the TMV base layer: The wafers were placed gold-side-up on Parafilm™ in a 60 mm diameter petri dish. 5 µL of either 0.1 M pH 9 Tris or a 5 mg/ mL solution of D77K-HA CP previously dialyzed with 0.1 M pH 9 Tris to promote VLP disassembly was added to the gold surface by pipet and allowed to sit for 10 minutes at room temperature. Then 35 µL 0.1 M pH 5 Tris buffer was transferred to the gold surface by pipet, and the petri dish was covered with the lid and transferred to 4 °C overnight.

For longitudinal coassembly of R46G/E50K+E97G-FLAG CP onto the TMV base layer: The wafers were placed gold-side-up on Parafilm™ in a 60 mm diameter petri dish. 10 µL of either filtered water adjusted to pH7 or a 10 mg/ mL solution of R46G/E50K+E97G-FLAG CP previously dialyzed with filtered water adjusted to pH7 to promote VLP disassembly was added to the gold surface by pipet and allowed to sit for 10 minutes at room temperature. Then 10 µL 0.6 M NaCl, 0.2 M pH 7 Tris buffer was transferred to the gold surface by pipet, and the petri dish was covered with the lid and transferred to 4 °C overnight.

Excess unbound CP was washed by submersion of the wafers in 1 mL 0.1 M pH 7 Tris (for D77K-HA CP samples) or 1 mL 0.3 M NaCl, 0.1 M pH 7 Tris (for R46G/E50K+E97G-FLAG CP samples) for 5 minutes. The wafers were then placed gold-side-up on Parafilm™ in a 60 mm diameter petri dish, and a 50 µL droplet of

Aurion Blocking Solution for Goat Antibodies was gently layered onto each wafer and allowed to block for 1 hour at 4 °C. The wafers were then washed by submersion of the wafers in 1 mL 0.1 M pH 7 Tris (for D77K-HA CP samples) or 1 mL 0.3 M NaCl, 0.1 M pH 7 Tris (for R46G/E50K+E97G-FLAG CP samples) for 5 minutes, 3 times. The wafers were again transferred to Parafilm™, and 50 μL of primary antibodies (anti-FLAG antibodies produced in rabbit, anti-HA antibodies produced in mouse, Sigma) diluted 1:1000 in incubation buffer (PBS with 0.1% Tween-20 and 0.1% Aurion BSA-c™) was applied to each wafer at room temperature for 2 h or at 4 °C overnight. The wafers were again washed 3 times for 5 minutes each in 1 mL 0.1 M pH 7 Tris (for D77K-HA CP samples) or 1 mL 0.3 M NaCl, 0.1 M pH 7 Tris (for R46G/E50K+E97G-FLAG CP samples). The wafers were then submerged in 500 μL of a 1:1000 solution of secondary antibodies conjugated to horseradish peroxidase (anti-rabbit antibodies produced in goat in 0.1 M pH 7 Tris for D77K-HA CP samples and anti-mouse antibodies produced in goat in 0.3 M NaCl, 0.1 M pH 7 Tris for R46G/E50K+E97G-FLAG CP samples. The wafers were again washed 3 times for 5 minutes each in 1 mL 0.1 M pH 7 Tris (for D77K-HA CP samples) or 1 mL 0.3 M NaCl, 0.1 M pH 7 Tris (for R46G/E50K+E97G-FLAG CP samples). The wafers were then submerged in 1 mL substrate buffer (0.1 M pH 7 Tris, 0.2 M NaCl and 5 mM MgCl) containing 0.15 mg/ml of 5-bromo-4-chloro-3-indoyl phosphate and 0.3 mg/ml NitroBT. The submerged wafers were monitored for color change, and all wafers were removed and washed with 0.3 M NaCl, 0.1 M pH 7 Tris to halt colorimetric reaction after ~12 hours.

3.4. Results and Discussion

3.4.1. The role of carboxylate groups on TMV-VLP nanorod assembly

Previous studies of TMV had identified carboxylate residues whose presence and mutual interaction was key to virion disassembly in host cells [97, 199]. Within the assembled TMV virion, each CP subunit interacts with its neighbors in the axial direction through the mutually repulsive interaction of D77 and E50 while in the lateral direction residue E106 interacts repulsively with neighboring cluster E95/E97/D109 to regulate assembly (Figure 3-1B). D77 and E106 sidechains are oriented toward and exposed on the virion end containing the 5′ RNA genome terminus (5′ rod end), while E50 and E95/E97/D109 sidechains are oriented toward and exposed on the opposite rod end containing the 3′ genome terminus (3′ rod end). To further explore the role these carboxylate groups played in directing protein nanorod assembly a bacterial expression system was used to generate wild-type and substitution-variant TMV CP from an open reading frame codon-optimized for bacterial expression. Initial studies demonstrated that CP modifications E50Q/D77N produced virus-like nanorods that were of similar stability to the virus nanorods with respect to pH conditions but devoid of RNA and thus lacking constraint over particle length, exhibiting a broad distribution of values but typically between 300 and 900 nm [181] (Figure 3-2B). To examine the contributions of E50Q and D77N individually to nanorod assembly single mutations were made and the resultant CP expressed within the bacterial system. Results indicated that at pH 7 the E50Q substitution alone was sufficient to confer assembly of nanorods in 0.1 M sodium

phosphate buffer that were visually indistinguishable from the original E50Q/D77N CP (Figure 3-2D). In contrast, the D77N mutation on its own produced only two layer disks similar to the unmodified wild-type CP (Figure 3-2C). These results were consistent with previous findings that TMV with the E50Q mutation significantly reduced viral infectivity *in planta* and hindered *in vitro* translation of the embedded RNA genome with or without the D77N mutation, while the latter mutation alone did not [96].

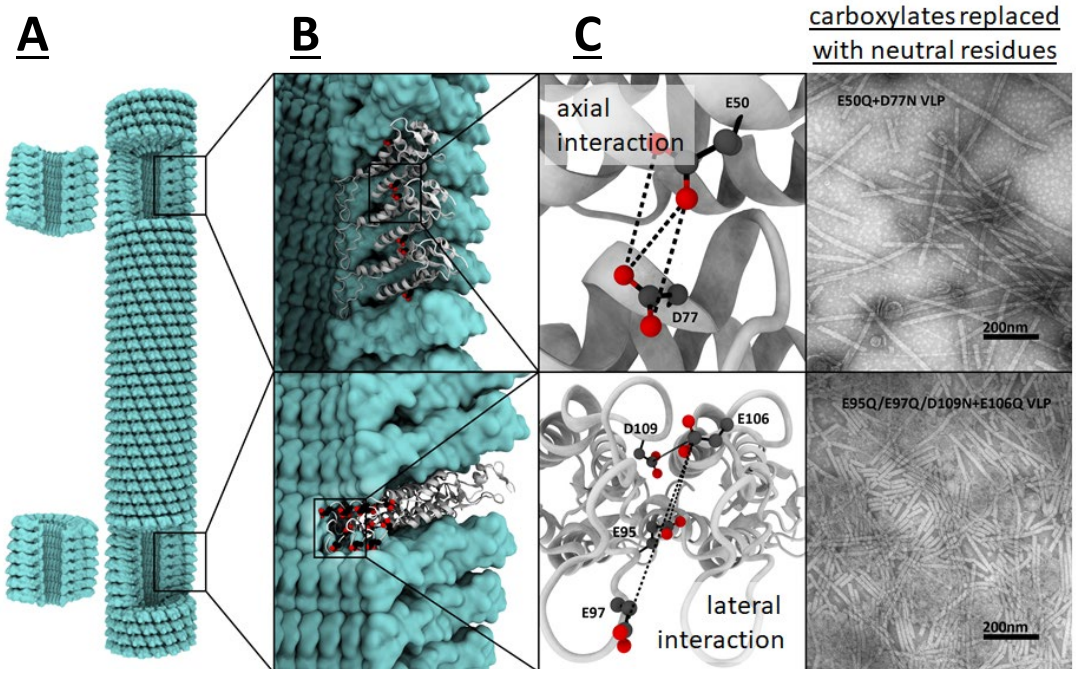

Figure 3-1: (A) Model of assembled section of TMV with sections removed to show protein assembly structure. (B) Ribbon models of three axially adjacent (top) or laterally adjacent (bottom) TMV CP subunits as located within an assembled TMV rod. (C) Ball-and-stick models of axially interacting carboxylates E50 and D77 (top) and laterally interacting E95/E97/D109 and E016 (bottom). (D) TEM images of axial-carboxylate-substituted E50Q+D77N CP VLPs (top) and lateral-carboxylate-substituted E95Q/E97Q/D109N+E106Q CP VLP.

The E50 and D77 carboxylate groups interact in the direction of the virion axis between subunits in successive turns of the rod's helical structure. There also exists a lateral interaction between E106 on one subunit and E95/E97/D109 of the next subunit within a turn of the helix at the low-radius region of the assembled

nanorod. Neutralization of just the four laterally interacting carboxylates using the substitutions E95Q/E97Q/D109N+E106Q[2] results in the self-assembly of rod-like VLPs from the bacterially expressed protein (Figure 3-1, bottom right). This indicates that the neutralization of the repulsive lateral interaction is sufficient to drive rod assembly and is consistent with the observed decrease in infectivity and translation of TMV with these same four substitutions. The combination of 3′-end-exposed E50Q with 3′-end-exposed E95Q/E97Q/D109N produced rods similar to E50Q alone. Interestingly, the addition of 5′-end-exposed E106Q to the 5′-end-exposed D77N produces rod assembly despite the reduced impact of this substitution (and lack of impact of the D77N substitution) on TMV infectivity *in planta* and translation *in vitro* relative to the E50Q (with or without D77N) and the E95Q/E97Q/D109N+E106Q substitutions. Combined these mutations demonstrate the contributions of these key carboxyl–carboxylate interactions in the control of VLP rod assembly.

[2] A note concerning notational conventions in this chapter: the amino acid substitutions made to the TMV CP in this work are generally substitutions to one or more of four sets of carboxylate containing amino acid residues: (a) axially interacting E50, (b) axially interacting D77, (c) the laterally interacting group E95, E97, and D109, and (d) laterally interacting E106. The notations for multiple substitutions within a set are separated by slashes ("E95/E97/D109"), while substitutions to different sets are given in the order just given and combined with a plus sign (hence "E50Q+D77N", "D77N+E106Q", and "E95Q/E97Q/D109N+E106Q"). Where this convention does not hold, substitutions are either uniformly separated by slashes or hyphens.

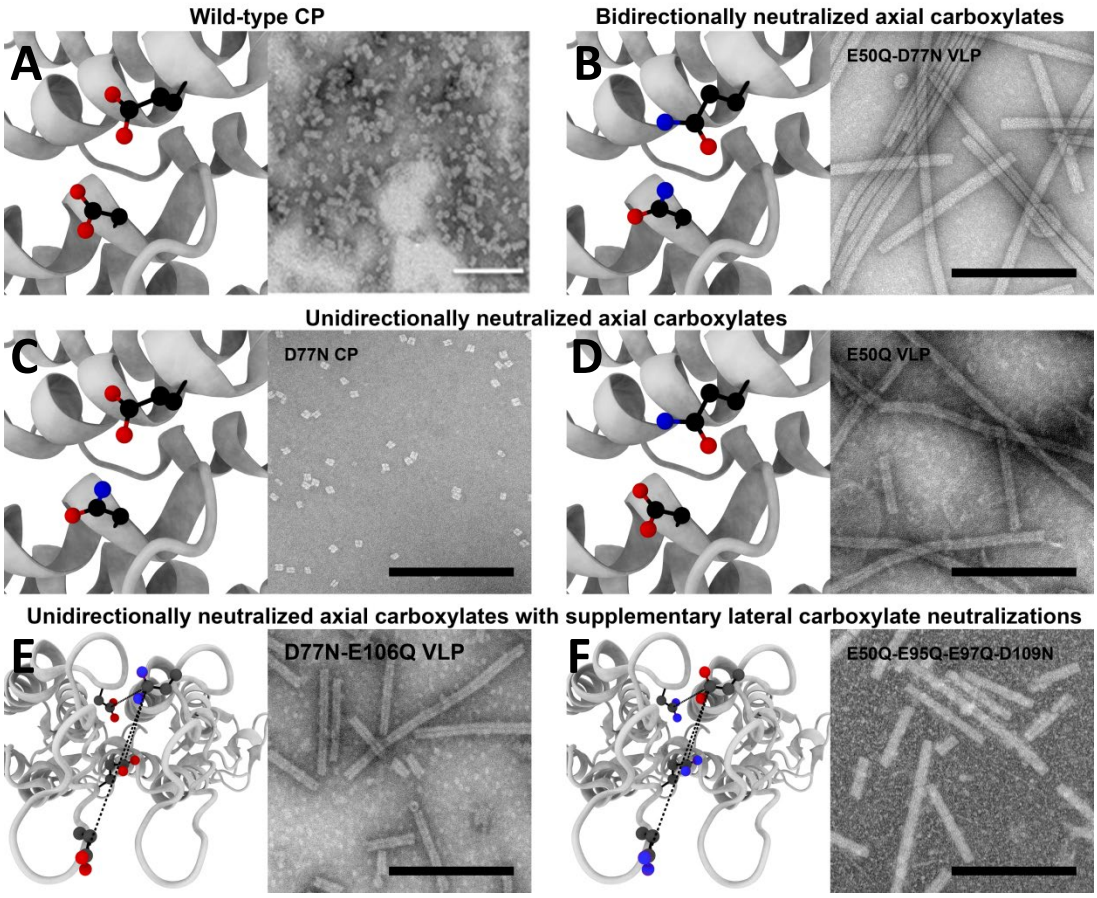

Figure 3-2: Models and TEM images of axially and laterally interacting carboxylates and substitutions. (A) Model of axially interacting carboxylates E50 and D77 present in wild-type TMV and TEM of wild-type TMV CP expressed in bacteria. (B) Model of neutralizing substitutions of axially interacting carboxylates E50Q and D77N and TEM of E50Q+D77N CP forming VLPs. (C) Model of neutralizing D77N substitution interacting with wild-type E50 and TEM of D77N CP forming bilayer disks. (D) Model of neutralizing E50Q substitution interacting with wild type D77 and TEM of E50Q CP forming VLPs. (E) Model of laterally interacting carboxylates E95, E97, and D109 interacting with neutralized E106Q substitution and TEM of D77N+E106Q CP combining this lateral substitution with the axial D77N substitution and forming VLPs. (F) Model of laterally interacting carboxylate E106 interacting with neutralized E95Q, E97Q, and D109N substitutions and TEM of E95Q/E97Q/D109N+E106Q CP combining these lateral substitutions with the axial E50Q and forming VLPs. Bars = 200 nm.

3.4.2. Co-assembly of hierarchically structured VLP–VLP and VLP–TMV complexed nanorods

Neutralization of either axial or lateral of carboxylate interactions via bi-directional axial substitutions E50Q+D77N or bi-directional lateral substitutions E95Q/E97Q/D109N+E106Q enhances intersubunit interactions and drives the self-assembly of rod-like VLPs (Figure 3-1). However unidirectional carboxylate

neutralizations are also sufficient to drive VLP self-assembly, either through the 3′-end axial E50Q substitution (with or without the 3′-end lateral E95Q/E97Q/D109N substitutions) or through the 5′-end axial D77N combined with the 5′-end lateral E106Q substitutions (Figure 3-2). Because the protein–protein interactions between the 3′ end of one TMV or VLP rod and the 5′ end of another is identical to those interactions between adjacent layers of the helix within an assembled rod, the potential for these assembly-promoting substitutions to selectively drive the "head-to-tail" assembly of rods of distinct TMV CP variant type was investigated. To this end, the 5′-end-neutralized D77N+E106Q mutant (Figure 3-3A, red) was labeled with a C-terminal HA peptide while the 3′-end-neutralized E50Q+E95Q/E97Q/D109N (Figure 3-3A, blue) mutant was labeled using a FLAG peptide. HA-labeled D77N+E50Q or FLAG-labeled E95Q/E97Q/D109N+E106Q was mixed with unlabeled TMV rods or bi-directional lateral-carboxylate-substituted E95Q/E97Q/D109N+E106Q, which retains wild-type axial carboxylates at both ends, (Figure 3-3A, green). Co-mixed samples were concentrated by centrifugation and resuspension at a ratio of 1:1 with respect to protein concentration. Results show the co-assembly of chimeric nanorods of varying lengths and relative composition, as verified by the selective immunolabelling of the FLAG- or HA-tagged CP with antibodies conjugated to gold nanoparticles and imaged by transmission electron microscopy (Figure 3-3B and C).

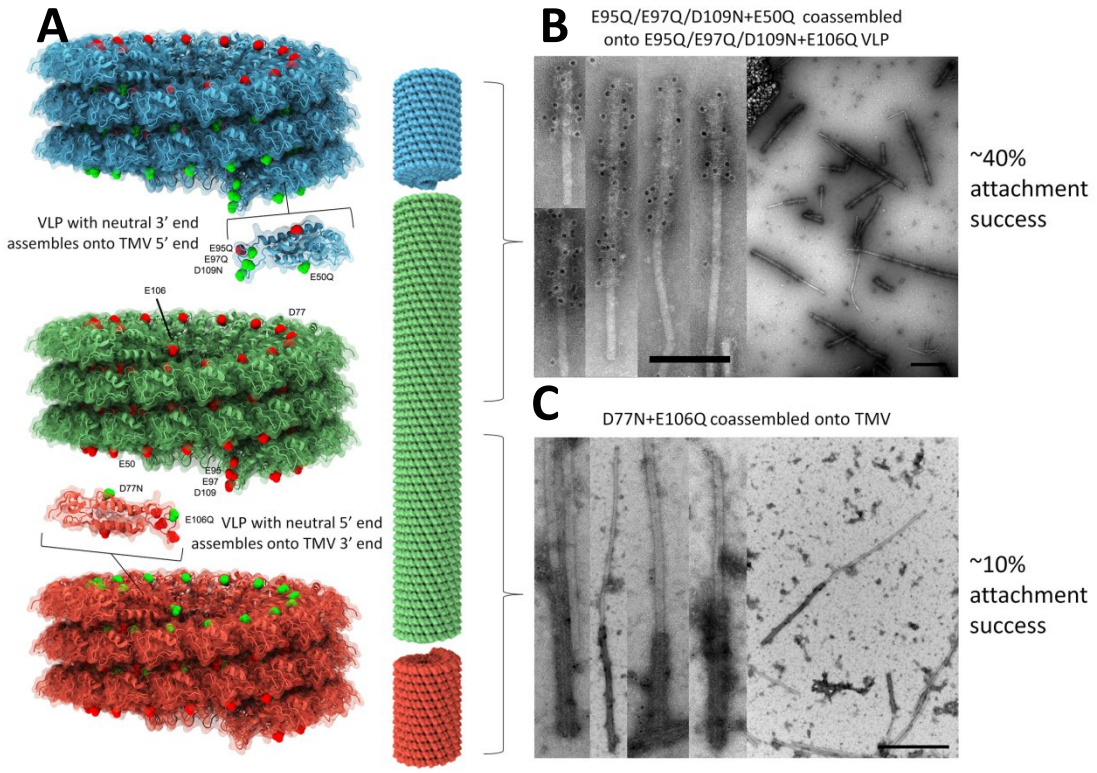

Figure 3-3: (A) Model showing schematic for selective-end-attachment of VLPs of modified CP to TMV (or VLP retaining wild-type axial carboxylates)(green, center). Neutrally charged residues (dark blue) substituted for negatively charged carboxylates (red) can be brought into proximity with wild-type carboxylates without generating destabilizing repulsion. E50Q+E95Q/E97Q/D109N VLP and CP (light blue, top) has neutralized 3′-end charges, allowing fusion to the 5′ end of TMV or a VLP with intact 5′-end carboxylates. D77N+E106Q VLP and CP (light red, bottom) has neutralized 5′-end charges, allowing fusion to the 3′ end of TMV. (B) TEM images of immunolabelled E50Q+E95Q/E97Q/D109N-FLAG VLP coassembled with unlabelled E95Q/E97Q/D109+E106Q VLP by concentrating an mixture of equal volumes of 1 mg/mL solutions of the two types of VLP in 0.01 M pH 7 sodium phosphate buffer through vacuum centrifugation to ~10% original sample volume, overnight incubation of the concentrated sample at 4 °C overnight, and dilution of the sample to the original volume with 0.1 M pH7 sodium phosphate buffer. Attachment success rate as defined by the average of the percentage of unlabelled VLP rods attached lengthwise to a labelled rod and the percentage of labelled VLP rods attached lengthwise to an unlabelled VLP rod was estimated to be ~40% based on the observation and counting of ~50 rods. (C) TEM images of immunolabelled D77N+E106Q-FLAG VLP coassembled with unlabelled TMV by ultracentrifugation of 100 µL each of 5 mg/mL solution of the two components diluted in 0.1 M pH 7 sodium phosphate buffer and resuspension of the concentrated pellet in 100 µL 0.1 M pH 7 sodium phosphate buffer. Attachment success rate as defined by the average of the percentage of unlabelled TMV rods attached lengthwise to a labelled rod and the percentage of labelled VLP rods attached lengthwise to an unlabelled TMV rod was estimated to be ~10% based on observation and counting of ~50 rods. Bars = 200 nm

The efficiency of co-assembly, as determined by the average of the percentage of unlabelled rods attached lengthwise to a labelled rod and the percentage of labelled rods attached lengthwise to an unlabelled rod, was below 50% for all combinations of 5′-end-neutralized or 3′-end-neutralized VLP with TMV or with bi-directionally laterally neutralized VLP, with 3′-end-neutralized E50Q+E95Q/E97Q/D109N CP

showing the highest co-assembly efficiency with TMV at ~40% (Figure 3-3B) and 5′-end-neutralized D77N+E106Q CP showing co-assembly efficiency of ~10% (Figure 3-3C). The low attachment efficiency among all samples could be attributed to several factors. Some of these are methodological and could perhaps be improved by refining the conditions under which the rods are mixed. The first is the absolute concentration of the TMV and VLP components in the mixture were coassembly takes place. It is known that TMV assembly in host cells and E50Q/D77N VLP assemble in bacterial cells (Figure 2-2C) where the CP exists at high concentration. The ultracentrifugation and vacuum centrifugation steps used in the coassembly of these complexed rods were intended to provide similar increases in concentration to drive their coassembly, and repeating these steps may improve results. However the coassembly of these rods also requires the component rods to meet in the correct orientation of 5′-rod-end to 3′-rod-end. This positioning of the components in three-dimensional space is presumably inhibited by the decreased mobility of the component rods compared to that of the monomers and disks that are involved in the do novo assembly of TMV and VLP rods.

The relatively lower efficiency of coassembly of the 5′-neutralized rods (D77N+E106Q VLP) onto TMV rods when compared to the coassembly of 3′-neutralized rods (E50Q+E95Q/E97Q/D109N VLP) onto VLP retaining wild-type axial carboxylates (E95Q/E97Q/D109N+E106Q VLP) requires an additional explanation. This lower efficiency of coassembly is not necessarily the result of the use of TMV versus E95Q/E97Q/D109N+E106Q VLP or of the method used to concentrate the samples to drive coassembly (ultracentrifugation versus vacuum

centrifugation)_as these other components and methods were also evaluated and found to offer no improvement [data not shown]. Instead it may be attributable to an underlying structural asymmetry in the assembly process and as influenced by the axially interacting carboxylates. The evidence for this comes from two sources. First is the evidence in the extensive literature on the assembly process of the TMV virion which shows that elongation of the rod occurs primarily through different mechanisms at each end, with elongation of the 5′ rod end occurring rapidly by the addition of preassembled CP disks or "lock-washers" while elongation of the 3′ rod end occurs more slowly by the addition of monomers, dimers, trimers, etc. [200] Another indication of an underlying structural asymmetric affecting assembly is the observation, reported above, that while the E50Q mutation alone is sufficient to drive assembly of VLPs, the D77N mutation is not, which is consistent with previous studies of the effect of these mutations on virus *in planta* [96].

3.4.3. Development of VLP CPs with novel end specific electrostatic interactions

Initial studies showed the capability of both bidirectionally neutralized carboxylates as well as asymmetrically neutralized carboxylates to allow VLP nanorod assembly and a limited ability to co-assemble onto one end of TMV or a VLP retaining wild-type axially oriented carboxylates. To improve control over the efficiency and direction (from 5′ or 3′ rod ends) of multiple-particle co-assembly, the three-dimensional structure of the E50 – D77 carboxylate pair was modeled for the placement of novel positively charged residues. Structural models indicated sufficient

rotational space within the subunit interface at residue 77 to accommodate a lysine residue with its terminal amine group positioned within 3 Å of the opposing E50 carboxyl group (Figure 3-4C). However, Structural models indicated the potential for repulsive electrostatic interference between a lysine substituted for residue E50 and residue R46 situated on the adjacent turn of an α-helix in the same subunit (Figure 3-5).

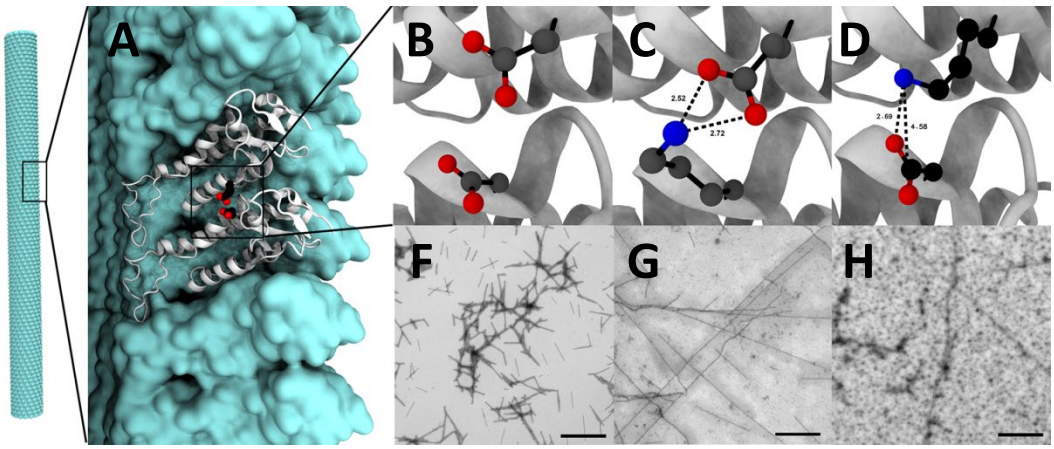

Figure 3-4: Models and TEM imgaes of postively charged residues substituted for axially interacting carboxylates E50 and D77. (A) Model of two axially juxtaposed TMV CP subunits with axially interacting carboxylates E50 and D77 represented. (B) Ball-and-stick model of wild type, axially interacting carboxylates E50 (top) and D77 (bottom). (C) Ball-and-stick model of basic residue D77K interacting with E50. (D) Ball-and-stick model of basic residue E50K interacting with D77. (F) TEM of wild-type TMV. (G) TEM of D77K VLP showing lengthened morphology. (H) TEM of R46G/E50K+E97G VLP showing lengthened morphology. Bars = 200 nm

Bacterial expression of C-terminally-peptide-tagged E50K CP and transmission electron microscopy of the bacterial lysate revealed the presence of micrometer-long loose sinusoidal or helical structures approximately 10 nm in diameter (Figure 3-5), which were interpreted as one-dimensionally aggregated E50K CP resulting from effects of the interaction between residues R46 and E50K. To eliminate the presumed electrostatic interference of R46 and to accommodate the E50K substitution an additional substitution of glycine for R46 was made, generating the R46G/E50K CP variant. Expression of this variant lacked the loose helical

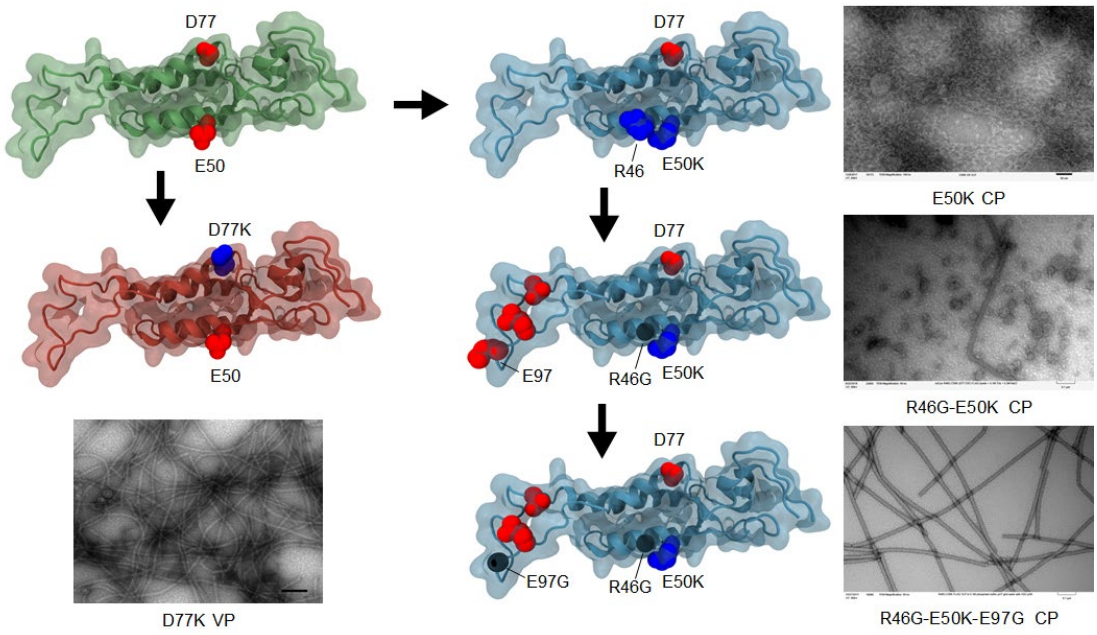

Figure 3-5: Models comparing wild-type TMV CP containing negatively charged axial carboxylates D77 and E50 (green, top left) with E50K CP (blue, top) showing proximity of positively charged E50K to positively charged R46, R46G/E50K (blue, center) showing elimination of repulsive interaction between R46 and E50K by substituting a glycine for R46, R46G/E50K+E97G (blue, bottom) showing the additional substitution of a glycine for the laterally interacting carboxylate E97, and D77K CP (red, center left). TEM images accompanying each model show E50K CP forming loose spirals instead of rods (top right), R46G/E50K showing poor VLP assembly (center right), R46G/E50K+E97G CP forming long VLP rods (bottom right), and D77K CP forming long VLP rods (bottom left). Bars = 200 nm

structures present in the E50K preparations but also indicated a poor ability to self-assemble into tight helical TMV-like rods (Figure 3-5). To improve assembly stability and VLP formation, a targeted mutation (E97G) to the destabilizing group of laterally interacting carboxylates was made to produce the R46G/E50K+E97G CP variant.

Both of these CP variants, D77K and R46G/E50K+E97G, were designed to introduce novel positive surface charges under neutral pH conditions to either the 5′ (D77K) or 3′ (R46G/E50K+E97G) CP interfaces. These positively charged D77K and E50K residues were expected to form salt-bridges with E50 or with D77, respectively, both between copies of identical modified CP, to drive assembly of homogeneous VLP, and between one end of the modified CP VLP and the opposite

end of wild-type TMV, to drive hierarchical co-assembly.

When expressed in bacteria, both of these CP variants were found to generate VLP nanorods with extensively lengthened morphologies. Transmission electron microscopy revealed VLPs composed of either D77K or R46G/E50K+E97G CP to have typical lengths on the order of 1 μm or more (Figure 3-4G and H). This was consistent with the increased stability to rod assembly that was predicted to accompany the replacement of a negatively charged residue that would generate a repulsive axial interaction with not just a neutrally charged hydrophilic residue capable of generating an ion–dipole interaction but with a positively charged residue capable of forming a salt-bridge between adjacent subunits.

In addition, each variant was found to undergo a unique disassembly response to different environmental conditions. Specifically, the D77K mutation disassembles at pH 9 while the wild-type TMV and VLP E50Q/D77N rods remain assembled under this elevated pH condition (Figure 3-6A). Additionally, restoring the disassembled D77K CP solution to pH 7 solution conditions results in the reassembly of the nanorods. Similarly, the R46G/E50K+E97G mutant CP also displays a unique disassembly behavior in response to a reduction of dissolved ion content of the ambient medium to submicromolar concentrations and a restoration of the assembled state with a subsequent increase in the ionic strength of the solution (Figure 3-7A). Interestingly, the conditions that trigger disassembly in each of these CP variants is not shared by the other: D77K VLP nanorods are primarily affected by pH and not by ionic strength while the R46G/E50K+E97G nanorods disassemble only at low ionic strength with pH having little effect (Figure 3-8).

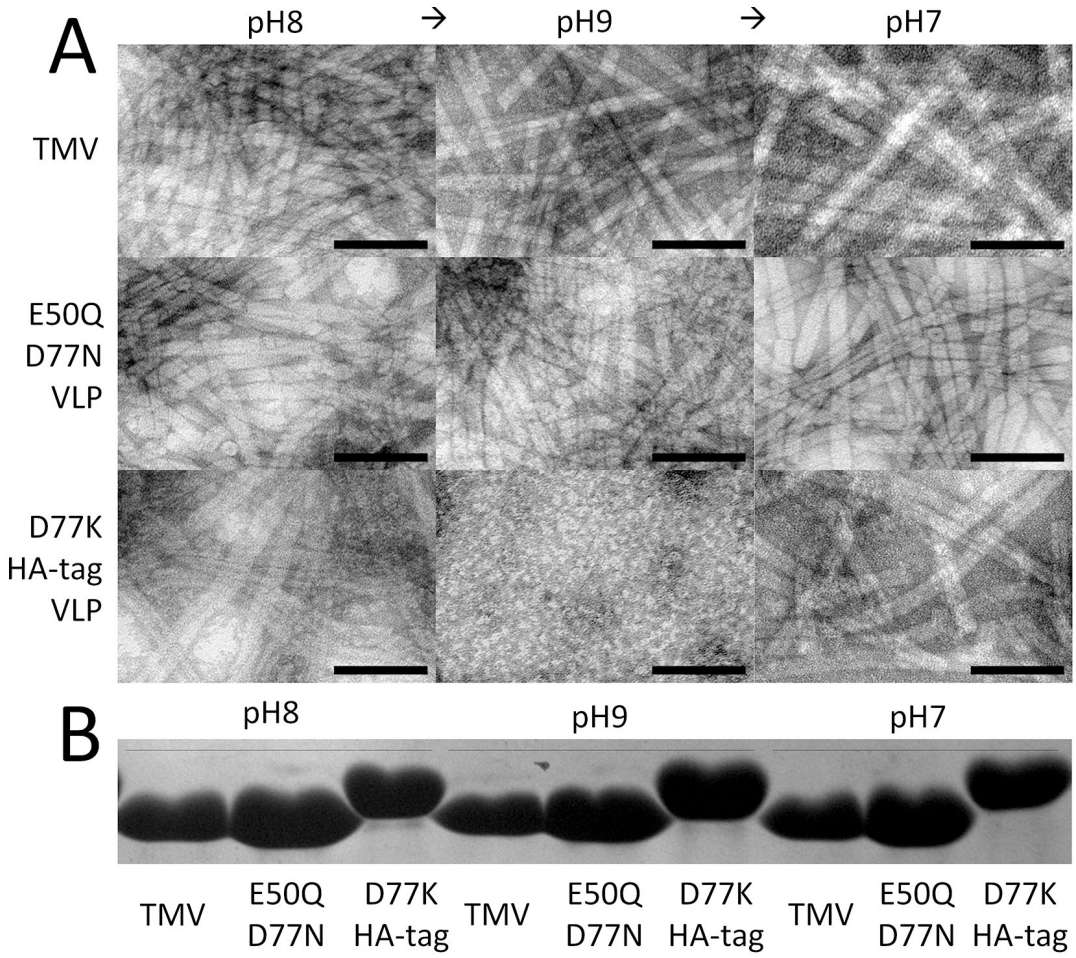

Figure 3-6: (A) TEM images of TMV (top row), E50Q+D77N VLP (middle row), and D77K-HA CP samples dialyzed to pH 8 (left column), then to pH 9 (middle column), and finally pH 7 (right column) showing stability of TMV and E50Q+D77N VLP at all pH values, but total loss of visible structure for D77K-HA CP at pH 9. All samples prepared in 0.1 M Tris buffer. (B) SDS-PAGE of equal volumes of samples from A, above, showing no detectable sample loss during the multiple dialyzation steps. Bars = 100 nm

Structural explanations for the unique disassembly behavior of the two modified CP variants must account not only for the unique disassembly response of each variant to solution conditions that do not produce the same effect in TMV or E50Q+D77N VLP but also the relative independence of disassembly response of each CP variant to the conditions that trigger disassembly in the other. Specifically, the mechanisms must explain the asymmetric responses of the two CP variants to pH and

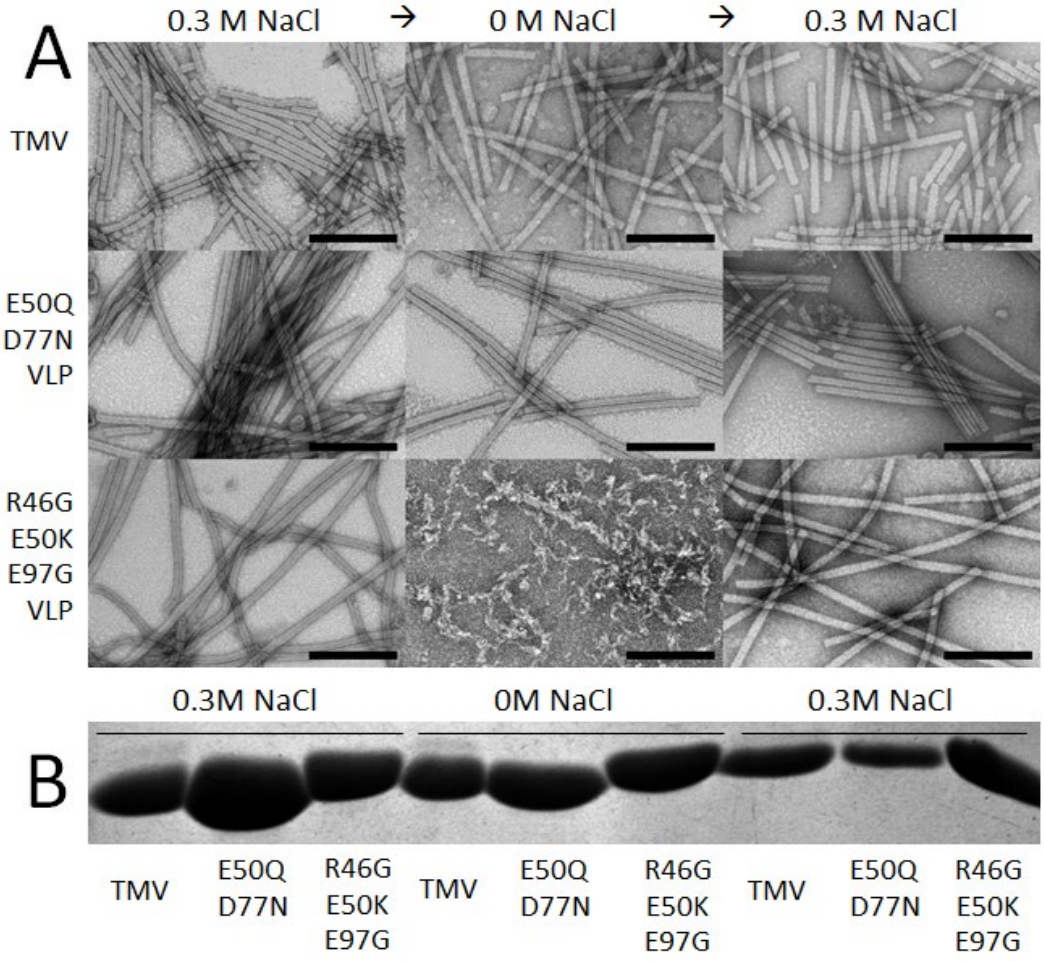

Figure 3-7: (A) TEM images of TMV (top row), E50Q+D77N VLP (middle row), and R46G/E50K+E97G-FLAG CP (bottom row) samples dialyzed to high ionic strenght conditions (0.3 M NaCl, 0.1 M Tris) (left column), then to low solute, filtered water (middle column), and finally returning to high ionic strength conditions (0.3 M NaCl, 0.1 M Tris) (right column) showing stability of TMV and E50Q+D77N VLP at all ion concentrations, but a general loss of structure for R46G/E50K+E97G-FLAG CP under very low ionic solute conditions (0 M NaCl). (B) SDS-PAGE of equal volumes of samples from A, above, showing little detectable sample loss during the multiple dialyzation steps. Bars = 100 nm

ionic strength conditions despite the similarity of the amino acid substitutions which produced them, namely, the substitution of the lysine for one or the other of the negatively charged, carboxylate-containing amino acid residues that interact axially.

The proposed mechanism for the pH-based disassembly of D77K VLP, but not R46G/E50K+E97G, is the deprotonation and subsequent loss of positive charge of the lysine sidechain's primary amine in alkaline conditions around pH 9. The pK_a of this amine group in a dilute solution of free lysine is ~10.5. However, this value

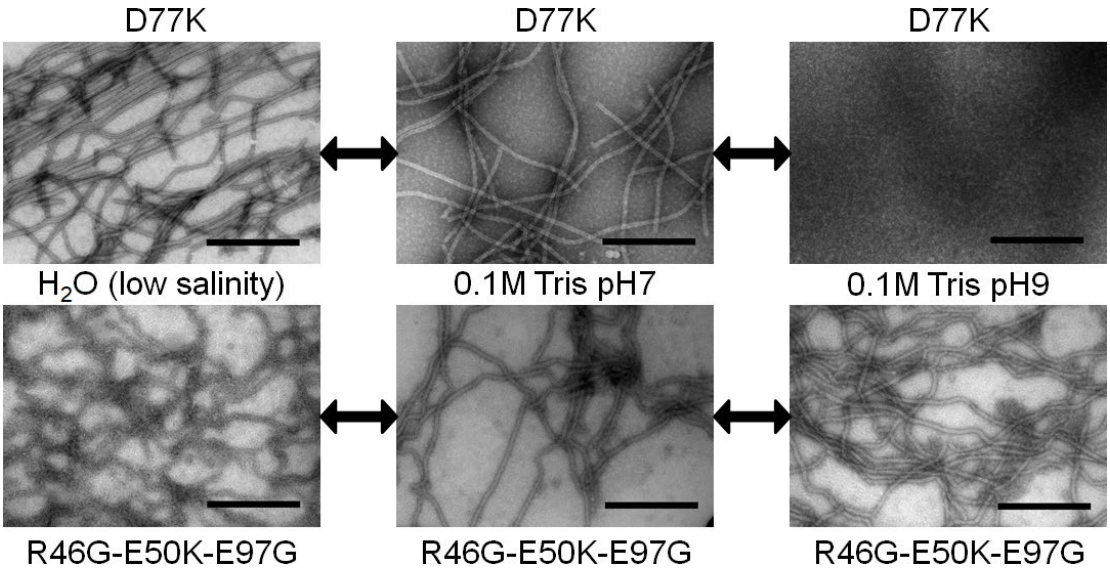

Figure 3-8: TEM images showing relative independence of disassembly conditions for the D77K and R46G/E50K+E97G CP variants. Both variants exist in an assembled state as elongated VLP rods after dialysis in 0.1 M pH 7 Tris (center images). After dialysis with filtered water (adjusted to pH 7 with ~50 µL NaOH / 1 L H_2O), D77K CP shows retention of assembled VLP structure (top left), while R46G/E50K+E97G shows significant loss of assembly structure (bottom left). Alternatively, dialysis of the samples from 0.1 M pH 7 Tris (center column) to pH 9 (right column) triggers the complete loss of virus-like particle structure in D77K CP (top right), while R46G/E50K+E97G CP retains its assembly structure. [Note: R46G/E50K+E97G samples dialyzed with 0.1 M pH 7 Tris (bottom center) and 0.1 M pH 9 Tris (bottom right) exhibit an apparently weakened, more flexuous rod structure in these images, due to the absence of the stabilizing influence of NaCl.] Bars = 200 nm

can change considerably depending on the local microenvironment of the amine group in the folded protein and within the assembled rod. The proximity of other positive electrostatic charges creates energetically unfavorable conditions and effectively lowers the pK_a of positively charged groups. The presence of a positively charge arginine, R46, in the vicinity of the lysine in D77K but not in R46G/E50K+E97G, where it was replaced with a glycine residue, may be sufficient to drive the deprotonation of D77K at pH 9 while the introduced lysine in R46G/E50K+E97G remains protonated and maintains its stabilizing axial salt bridge.

However, while a differential lowering of the introduced lysine's amine group may contribute to the two variants' different pH stability profiles, it is in itself neither necessary to explain the stability of R46G/E50K+E97G at pH 9 nor sufficient to explain the dramatic instability of D77K under the same conditions, Even allowing

the possibility that the pK_a of the lysine's amine group is sufficiently lowered in both variants to drive its respective deprotonation at pH 9, eliminating the stabilizing intersubunit axial salt bridge, structural considerations suggest that the substitution of the larger side chain volume of the substituted lysine residue for the smaller aspartic acid residue D77 would introduce a significant instability in the form of steric interference at the CP interface when deprotonated, resulting in the rapid destabilization of the TMV nanorod. In contrast, substitution of lysine for the slightly larger glutamic acid E50 within the assembled R46G/E50K+E97G rod would introduce less steric intersubunit interference, which may be further accommodated by the substation of a much smaller glycine for the bulky arginine R46 in that same variant adjacent to the lysine. Finally, even allowing for the deprotonation of the introduced lysine in both variants at pH 9 and the possibility that the difference in behavior is not due to a differential introduction of steric interference by the lysine, the behavior of the two variants is remarkably similar to the asymmetrical assembly behavior of the D77N and the E50Q CP variants, in which substitution of an uncharged amino acid residue for one of the axially interacting carboxylates acid does not generate self-assembly behavior for substitution of D77 but does for substitution of E50.

For the ionic strength-based disassembly of R46G/E50K+E97G but not D77K, structural modeling of suggests that the predicted assembly-promoting salt-bridge between the introduced lysine and the axially oriented carboxylate on the opposing subunit could be supplementally stabilized by dissolved ions. While the side chain of the E50K substitution is thought to provide a stabilizing force when

interacting with D77 on the opposing subunit, the E50K lysine is also positioned to interact with R71 of the opposing subunit, generating a repulsive interaction. This repulsive interaction may be mitigated by an ion screening effect when sufficient negative ions are present, allowing the ionic strength of the solution to control the assembly of this nanorod. The D77K lysine, however, does not interact across an intersubunit boundary with R71, and so VLP assembly would not be expected to depend on dissolved ions for charge screening.

Thus, these two mutations create distinct and orthogonal disassembly triggers, allowing the use of either pH or ionic strength as drivers in nanorod assembly and disassembly, making them ideal for controlling the assembly of chimeric VLPs.

3.4.4. Assembly kinetics

The kinetics of the environmentally dependent assembly of the CP variants D77K and R45G/E50K+E97G was investigated by measuring changes to the light scattering of solutions of CP after a sudden change in pH or ion concentration that initiates the transition from a disassembled state to an assembled one. A fluorescence spectrophotometer was used to measure the scattering of a sample of either (1) 25 µL of disassembled D77K-HA CP in a 0.1 M pH 9 Tris solution which was then diluted eight-fold with 175 µL of 0.1 M pH 5 Tris or else (2) 100 µL of R46G/E50K+E97G -FLAG CP in filtered, low ion content pH 7 water which was then mixed with an equal volume (100 µL) of 0.2 M Tris 0.6 M NaCl to achieve final solution conditions of ~ pH 7 or 0.1 M Tris 0.3 M NaCl, respectively. Samples were illuminated with monochromatic 340 nm wavelength light, and a detector located at 90° to the incident light measured the relative amount of 340 nm light scattered by the sample to

determine the assembly state of the CP in the sample. Three samples at each of three concentrations for each of the two CP variants were measured for real time assembly state. Because the absolute amount of light scattering was dependent not only on the assembly state of the CP in the sample but also the total CP concentration and the intensity of the incident light (which needed to be varied between the most and least concentrated samples to achieve adequate light scattering for each sample without oversaturating the detector), the scattering profile for each sample concentration was normalized to a measurement of the scattering at a much later time (t>2hours) when the sample was assumed to have reached a state of maximum assembly relative to the CP concentration. The results (Figure 3-10, Figure 3-11, Figure 3-13, and Figure 3-14) were generally consistent with expectations that the light scattering curves would follow a rapid initial increase corresponding to the rapid association of CP monomers or oligomers into rods due to the high availability of free CP followed by a gradual flattening as the concentration of dissociated CP decreased as well as the expectation that initial assembly rate would correlate positively with initial CP concentration.

For pH-based D77K reassembly, the light scattering measurements closely followed the expected pattern (Figure 3-11). Very low initial scattering values were consistent with electron microscope imaging data that reliably showed no discernible assembly structure in pH 9-dissociated samples.

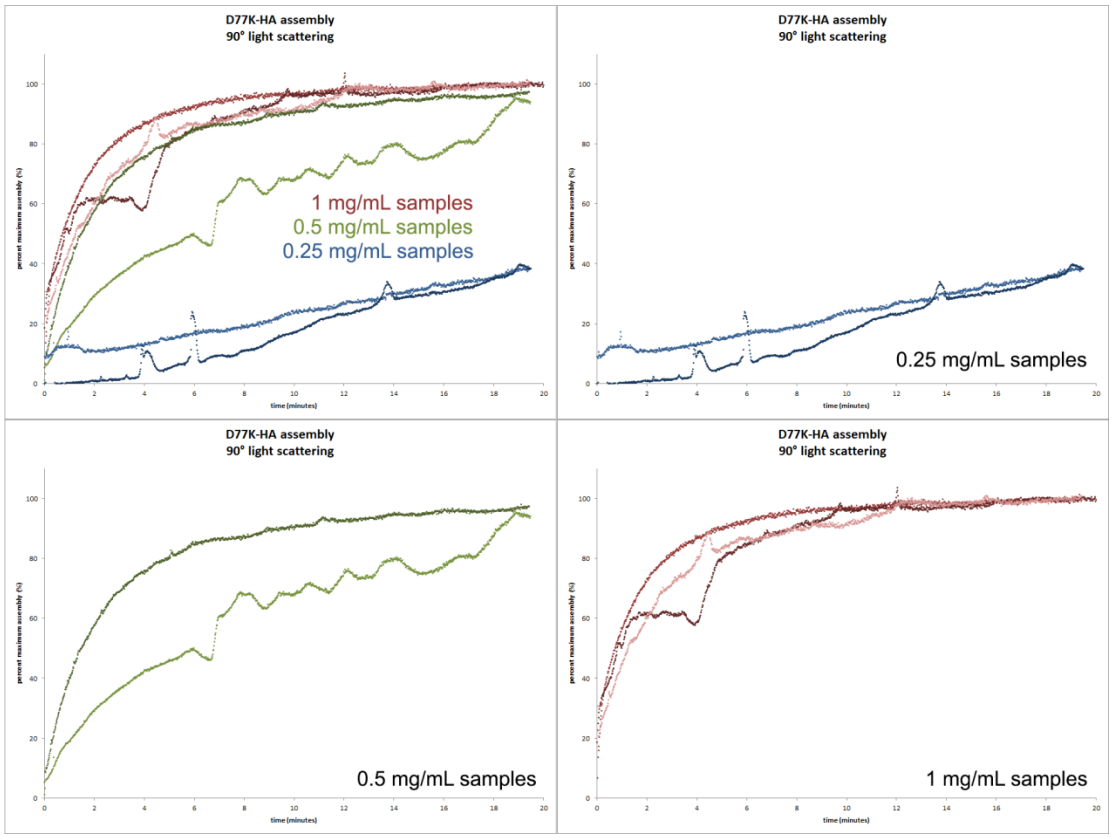

Figure 3-9 Normalized 90° light scattering curves correlating to reassembly of D77K CP from initial disassembled state after dialysis pH 9 Tris buffer with sudden adjustment to pH 7 by the 8-fold dilution with pH 5 Tris buffer at t=0. Samples were measured two or three times for final D77K-HA concentrations (after addition of pH 5 Tris) of 1 mg/mL (red), 0.5 mg/mL (green), and 0.25 mg/ml (blue). All curves were normalized relative to amount of scattering for the sample after >2hours, when it is assumed to have reached maximum reassembly state (100%).

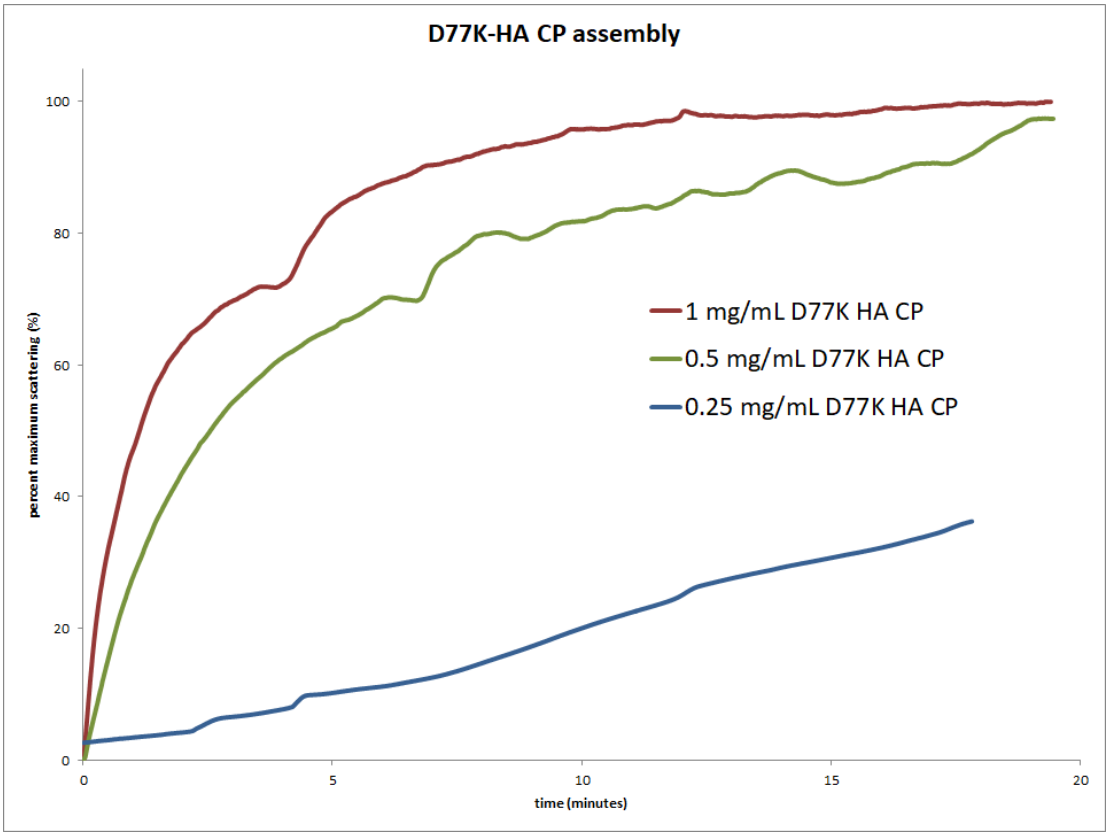

Figure 3-10: Averaged normalized 90° light scattering curves correlating to reassembly of D77K CP from initial disassembled state after dialysis pH 9 Tris buffer with sudden adjustment to pH 7 by the 8-fold dilution with pH 5 Tris buffer at t=0. Samples were measured two or three times (averaged curve shown) for D77K at concentrations of 1 mg/mL (red), 0.5 mg/mL (green), and 0.25 mg/ml (blue). All curves were normalized relative to amount of scattering for the sample after >2hours, when it is assumed to have reached maximum reassembly state (100%).

pH-based D77K-HA CP Assembly Parameters			
Concentration	50% assembly time (min)	95% assembly time (min)	Average initial assembly rate (%/sec)
0.25 mg/mL	24	46.9	0.055
0.5 mg/mL	2.4	18.2	0.49
1 mg/mL	0.95	9.5	0.82

Table 3: Assembly values derived from 90° light scattering measurements of D77K-HA CP. Averaged initial assembly rate values are averages over the first minute of assembly.

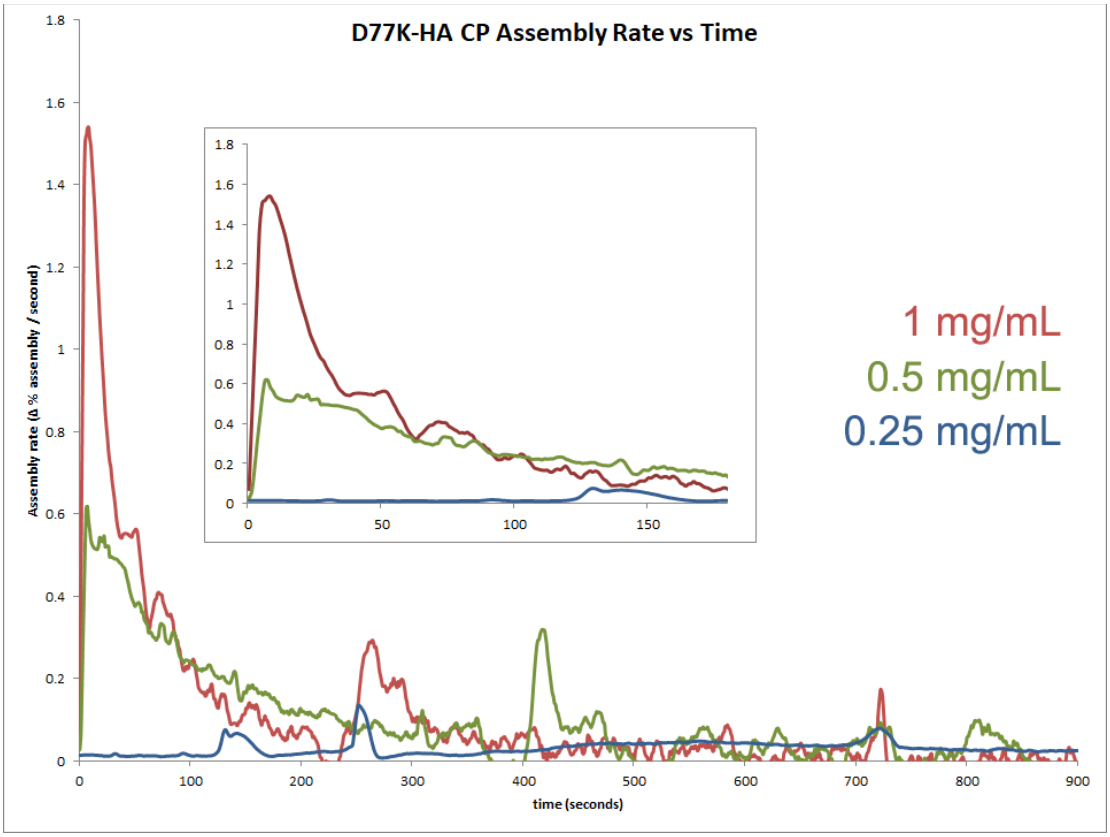

Figure 3-11: Plot of pH-based reassembly rate of D77K-HA CP versus time at three different concentrations, showing concentration dependence or rate. The y-value of each line at any point corresponds to the slope of the corresponding line in Figure 3-10.

For ionic-strength-based R46G/E50K+E97G reassembly, there were two notable deviations from the expected saturation curve (Figure 3-9). First, the initial light scattering values were significantly higher than for the D77K samples. This is consistent with the observation of some persistent intersubunit associations among R46G/E50K+E97G CP even in very low ionic strength conditions. In addition, the curves for the 0.6 mg/mL and 0.3 mg/mL samples appear to show a marked levelling off or lag phase after a rapid increase in light scattering to around 80% maximum. This lag phase is followed by a second relatively rapid increase in scattering to near 100% before again flattening. The mechanism behind this apparent two-phase process is unknown.

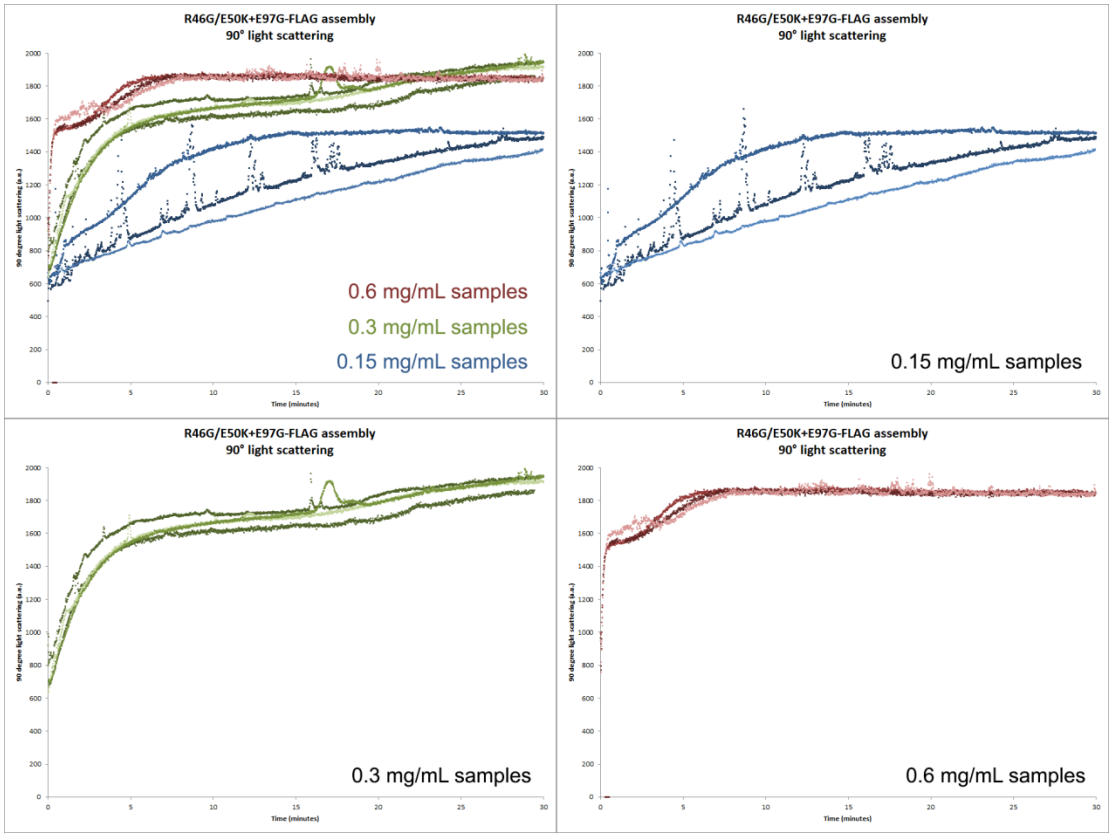

Figure 3-12 Normalized 90° light scattering curves indicating reassembly of R46G/E50K+E97G CP from initial disassembled state after dialysis with very low salinity pH 7 water after sudden adjustment to 0.1 M Tris, 0.3 M NaCl, pH 7 by 2-fold dilution with 0.2 M Tris, 0.6 M NaCl, pH 7 . Samples were measured three times for final R46G/E50K+E97G concentrations (after 2-fold dilution) of 0.6 mg/mL (red), 0.3 mg/mL (green), and 0.15 mg/ml (blue). All curves were normalized relative to amount of scattering for the sample after >2hours, when it is assumed to have reached maximum reassembly state (100%).

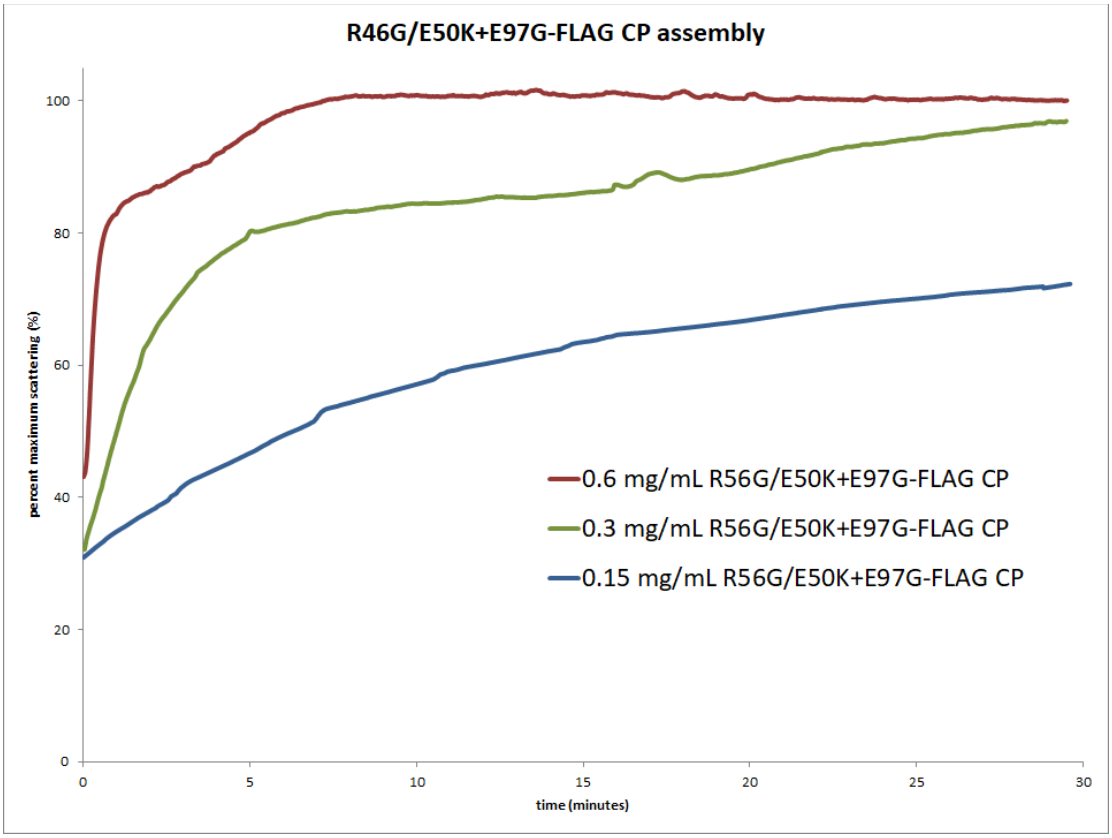

Figure 3-13: Averaged normalized 90° light scattering curves indicating reassembly of R46G/E50K+E97G CP from initial disassembled state after dialysis with very low salinity pH 7 water after sudden adjustment to 0.1 M Tris, 0.3 M NaCl, pH 7. Samples were measured three times (averaged curve shown) for R46G/E50K+E97G at concentrations of 0.6 mg/mL (red), 0.3 mg/mL (green), and 0.15 mg/ml (blue). All curves were normalized relative to amount of scattering for the sample after >2hours, when it is assumed to have reached maximum reassembly state (100%).

Ion-based R46G/E50K+E97G-FLAG CP Assembly Parameters			
Concentration	50% assembly time (min)	95% assembly time (min)	Average initial assembly rate (%/sec)
0.15 mg/mL	16.8	61	0.08
0.3 mg/mL	2.0	26	0.31
0.6 mg/mL	0.14	4.7	0.58

Table 4: Assembly values derived from 90° light scattering measurements of R46G/E50K+E97G-FLAG CP. Averaged initial assembly rate values are averages over the first minute of assembly.

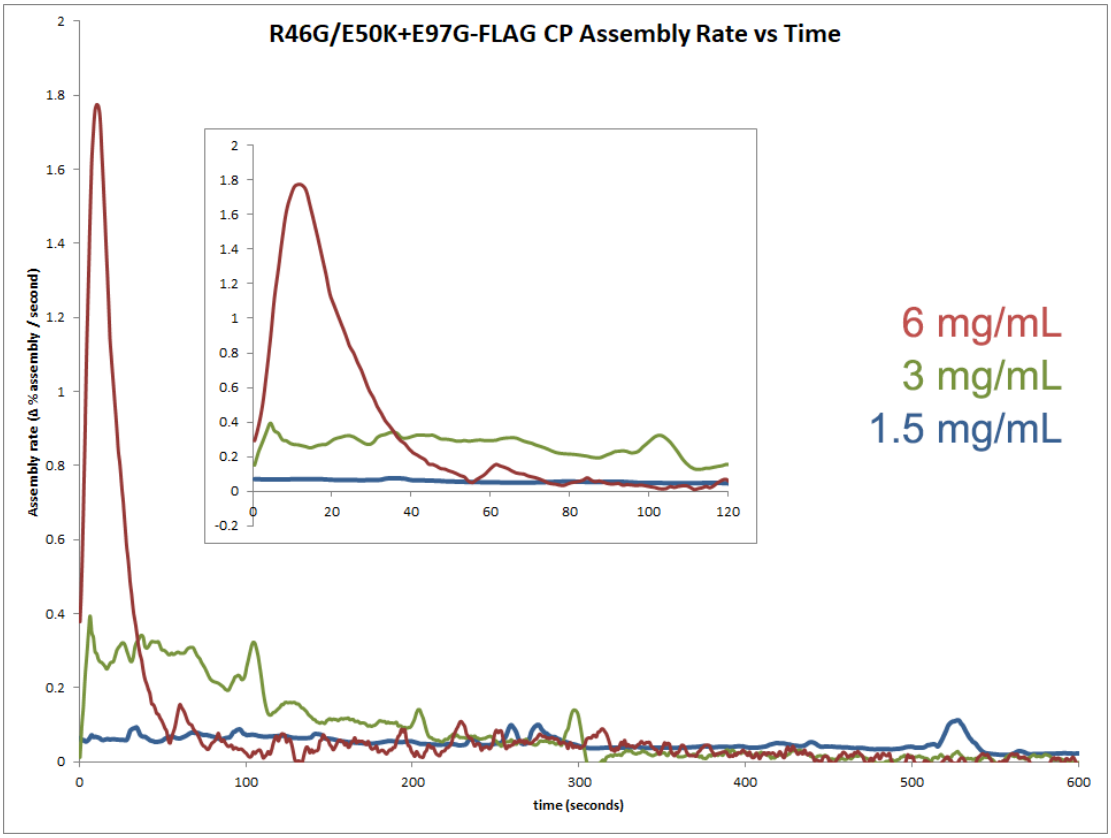

Figure 3-14: Plot of ionic strength-based reassembly rate of R46G/E50K+E97G-FLAG CP versus time at three different concentrations, showing concentration dependence or rate. The y-value of each line at any point corresponds to the slope of the corresponding line in Figure 3-13.

3.4.5. End-directed assembly of VLP subunits through novel electrostatic interactions

The unique pH and ionic strength assembly profiles of D77K and R46G/E50K+E97G, respectively, were investigated as a means to direct CP assembly onto TMV at either the 3′ end (for D77K) or the 5′ end (for R46G/E50K+E97G). While the amino acid substitutions to these CPs were expected to guide this directional assembly onto TMV, the extensively lengthened morphology of the VLPs they form hinders the co-assembly process. However the unique disassembly–reassembly behavior of these particles provides a method for eliminating the homogeneous structure of the long rods and enables their recombination with the

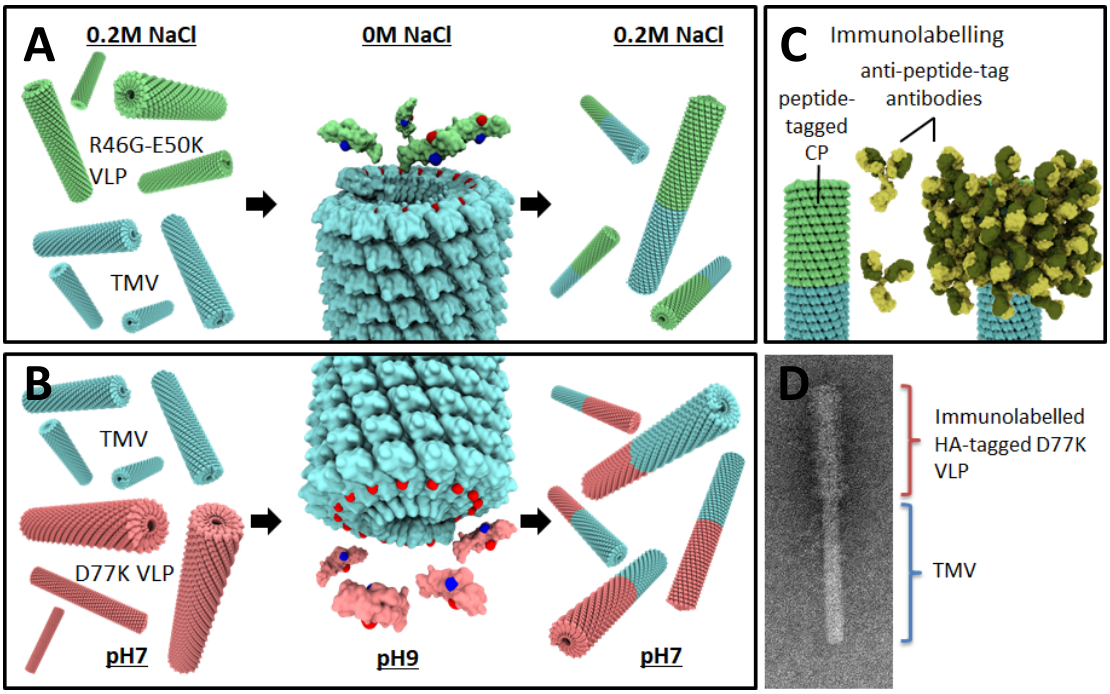

Figure 3-15: Illustrative, schematic models and TEM of pH- and ionic strength-based disassembly–reassembly mechanism for hierarchical assembly of VLP-TMV complexed rods. (A) Ionic strength-based disassembly and reassembly of R46G/E50K+E97G CP onto TMV. (B) pH-based disassembly and reassembly of D77K CP onto TMV. (C) Schematic of differential immunolabelling of protein tagged CP with anti-tag antibodies. (D) TEM of D77K-HA CP co-assembled onto a TMV rod with anti-HA-tag immunolabelling of the D77K CP.

TMV particles. For these experiments the 5′-end-substituted D77K mutant was labeled with a C-terminal HA peptide tag while the 3′-end-substituted R46G/E50K+E97G mutant was labeled using a FLAG peptide tag. Solutions containing unlabeled TMV and modified CP VLPs were combined and dialyzed against solution conditions to cause disassembly of the modified CP VLPs. For D77K-HA VLP, this entailed dialysis to pH 9 (Figure 3-10B), for R46G/E50K+E97G, dialysis to filtered water adjusted to pH 7 (Figure 3-10A). Buffer conditions for these mixtures were then adjusted back to pH 7 or increased salinity (300mM NaCl) by dialysis to initiate reassembly of the D77K or R46G/E50K+E97G CP, respectively. Samples were then immunolabelled with anti-FLAG or anti-HA antibodies and imaged by TEM.

Results from attempts with D77K-HA CP clearly show consistent and efficient

co-assembly of D77K-HA CP onto one end of the unlabelled TMV (Figure 3-11A). The resulting hybrid unlabeled TMV – D77K-HA VLP nanorods had a high degree of uniformity of length and were cleanly segregated into unlabeled and labelled sections by the anti-HA antibodies. The relative uniformity of length raised concern that the TMV's RNA genome was playing a structural role in the coassembly of the D77K-HA CP. The mechanism of TMV infection of a host cell is known to involve the exposure of the RNA 5′ end by selective disassembly at that rod end due to increased pH level upon entry into the cell interior. To test whether the D77K-HA CP was reassembling around the TMV RNA exposed by partial disassembly of the rod during dialysis to pH 9, RNase A was added to the combined TMV and VLP sample after dialysis to pH 9. Samples were they dialyzed back to pH 7, immunolabelled and imaged. The resulting hybrid nanoparticles displayed a broader distribution of lengths than samples not treated with RNase A with lengths exceeding those expected if the TMV's genomic RNA was the primary factor driving coassembly (Figure 3-11C).

D77K VLP pH-based assembly onto 3’ end

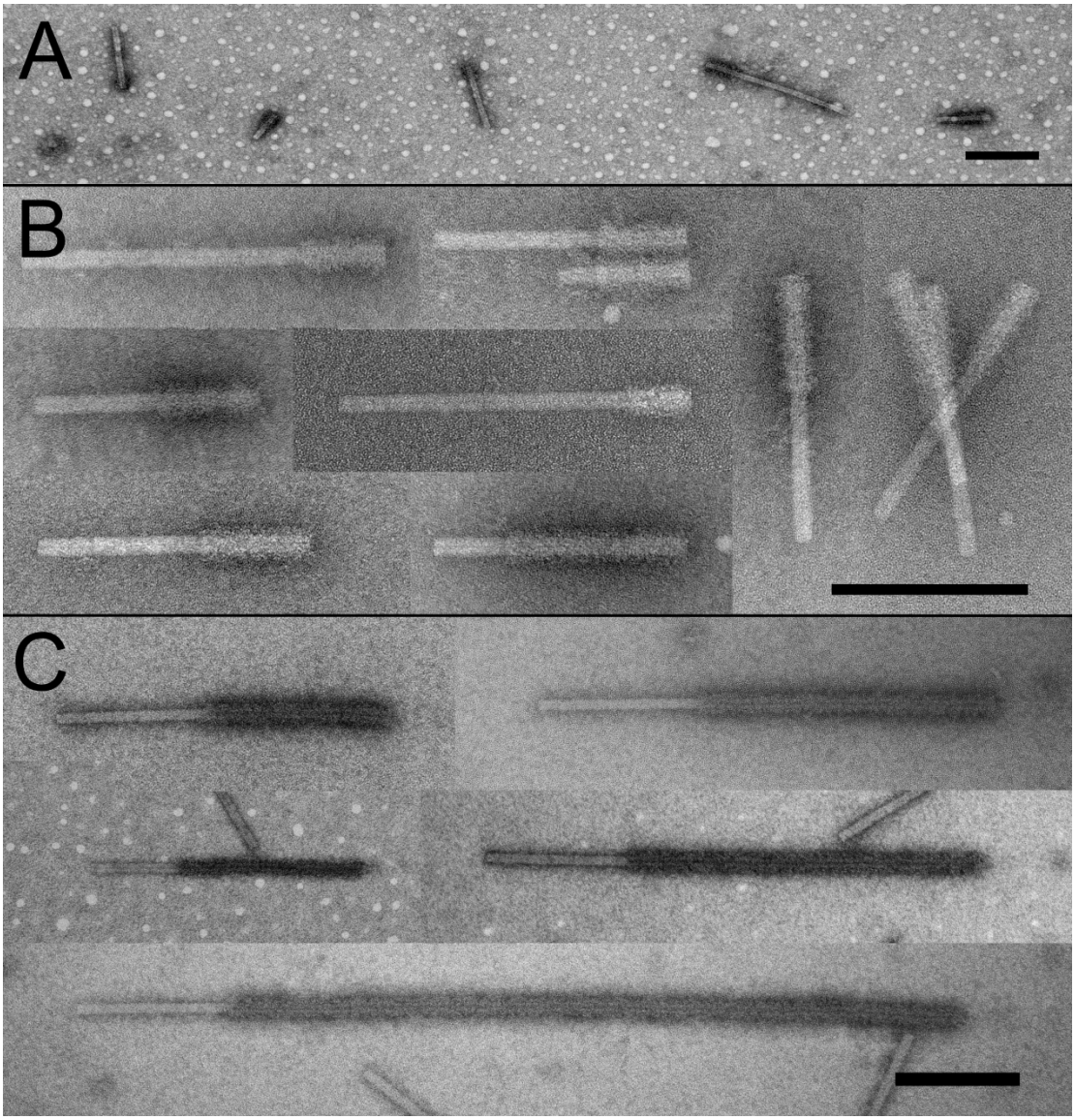

Figure 3-16: TEM images of longitudinally ordered TMV–VLP hybrid nanorods resulting from pH-based VLP disassembly/reassembly. All samples were prepared by the 2:1 mixture of 5 mg/mL solutions of D77K-HA VLP and TMV in 0.1 M pH7 Tris buffer, dialysis against a pH 9 solution of 0.1 M Tris buffer overnight at 4 °C, and then dialysis back to pH 7 with 0.1 M Tris buffer overnight at 4 °C. (A) and (B) Immunolabelled D77K-HA CP extending the lengths of unlabeled TMV with no RNase treatment. (C) Immunolabelled D77K-HA CP extending the lengths of unlabeled TMV treated with RNase (0.5 µL / 50 µL solution) for 30 minutes at 37 °C after dialysis to pH 9, showing lengths beyond those expected by RNA-scaffold-assisted assembly. Bars = 200 nm

Coassembly of R46G/E50K+E97G-FLAG CP onto TMV by the depletion and subsequent replenishment of dissolved ions also showed positive results. Samples taken from the low ionic strength conditions appeared to show coassembly of TMV

with the R46G/E50K+E97G-FLAG CP, but with the R46G/E50K+E97G-FLAG CP exhibiting the loose and fragmented structure evident from previous samples dialyzed to low ionic strength conditions (Figure 3-12, left side). The reintroduction of ions by addition of an equal volume of 0.4 M NaCl resulted in stabilization of the modified CP (Figure 3-12, right side). In contrast to the hybrid nanoparticles created using D77K CP, R46G/E50K+E97G–TMV hybrid nanoparticles mainly retained the lengthened morphology of the unhybridized VLPs, perhaps due to incomplete disassembly.

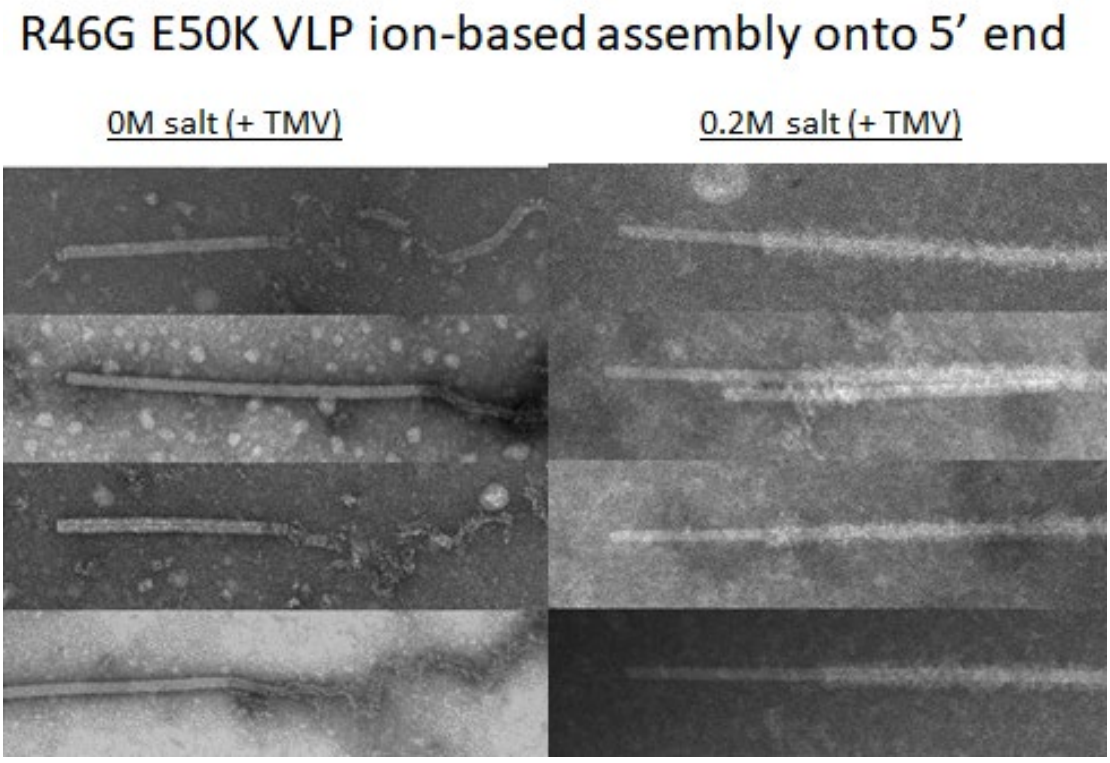

Figure 3-17: TEM images of longitudinally ordered TMV–VLP hybrid nanorods resulting from ionic-strength-based VLP disassembly/reassembly. Immunolabelled but unstructured R46G/E50K+E97G-FLAG CP extending the lengths of unlabeled TMV in low ionic strength conditions (left). Immunolabelled and well-structured R46G/E50K+E97G-FLAG CP extending the lengths of unlabeled TMV in 0.2 M NaCl solution

3.4.6. Surface-bound fabrication of co-assembled nanoparticles

To investigate the potential for integration of longitudinally differentiated protein nanoparticles into functional devices by surface attachment via the 1cys mutation (the addition of a cysteine residue proximal to the N-terminus), attempts were made to "grow" coassembled nanoparticles by sequential deposition of components onto a gold-coated silicon substrate. The gold surfaces were incubated in buffer with or without TMV-1cys, which is well established to attach itself to gold. A substantial number of TMV particles attach in an orientation perpendicular to the surface with what is thought to be the 3′ virion end serving as the point of attachment, based on molecular models. The surfaces were washed and incubated with a blocking solution. They were then washed briefly in filtered water and a small volume of R46G/E50K+E97G-FLAG CP disassembled by ion depletion was deposited on the surface. R46G/E50K+E97G-FLAG CP reassembly was initiated with the introduction of concentrated salt solution. The chips were then washed and immunolabelled with horseradish peroxidase-conjugated antibodies to visualize the presence of FLAG-tagged CP via color change (Figure 3-13B). Because R46G/E50K+E97G-FLAG CP lacks surface cysteine residues, it is assumed that its presence on the chip will either be due to non-specific adsorption or through interactions with a substrate layer of TMV-1cys (Figure 3-13A). Results indicate a correlation between the initial deposition of TMV-1cys and retention of FLAG-tagged CP, consistent with the hierarchical co-assembly of R46G/E50K+E97G-FLAG onto the surface-distal 5′ end of the surface-bound TMV-1cys, as predicted by structural modeling.

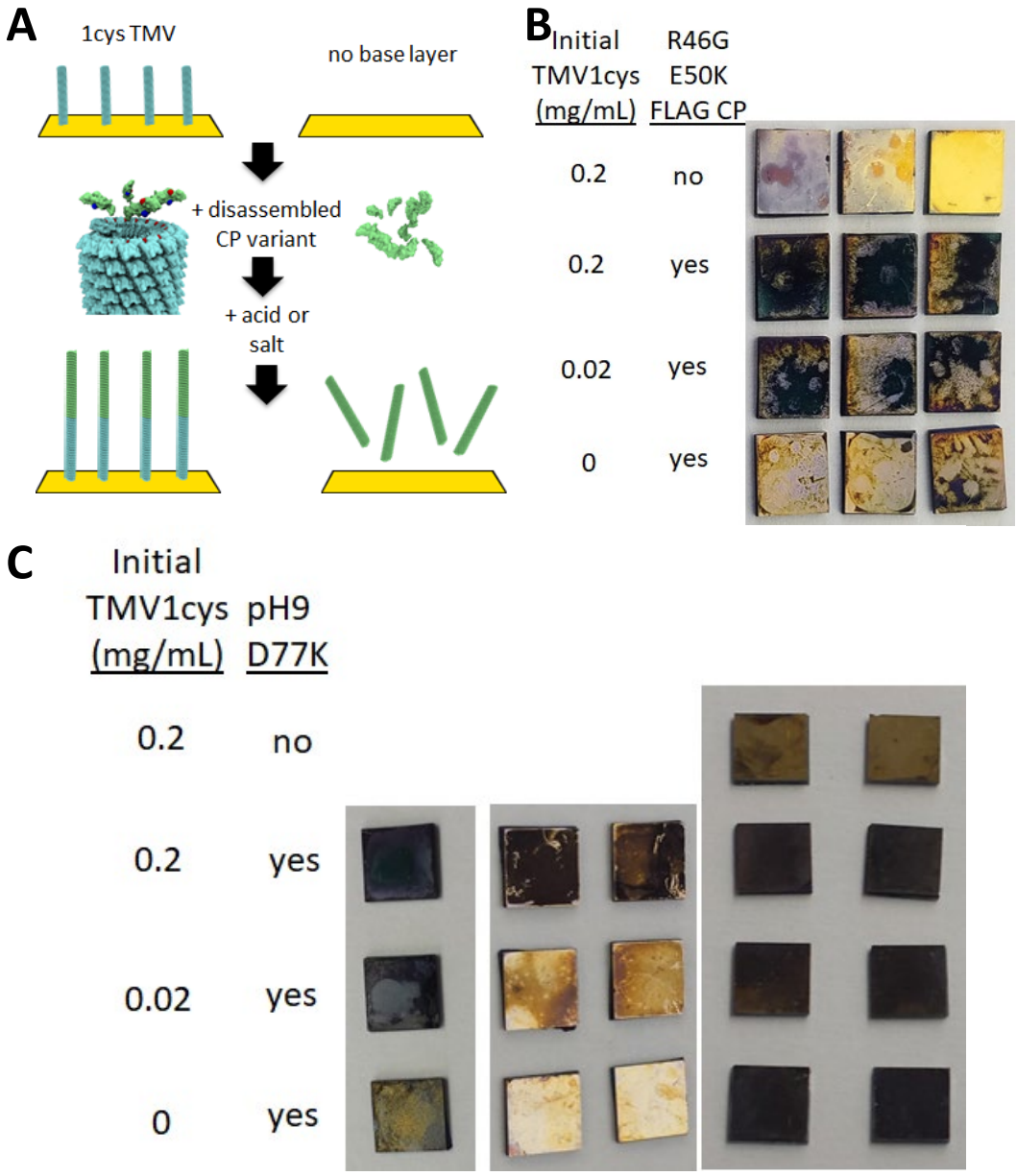

Figure 3-18: (A) Schematic of surface-bound "growth" of coassembled hybrid nanoparticles with D77K or R46G/E50K+E97G VLP only attaching to the gold surface through coassembly on a TMV-1cys intermediary base layer. (B) Results of TMV-1cys and R46G/E50K+E97G-FLAG CP surface-bound coassembly, in which TMV-1cys was first deposited on to gold-coated silica wafers followed by disassembled R46G/E50K+E97G-FLAG CP in water, followed by an equal amount of Tris with salt for a final concentration of 0.3 M NaCl, 0.1 M pH 7 Tris to initiate reassembly of the CP onto the free ends of the surface bound TMV. The presence of FLAG-tag labelled R46G/E50K+E97G CP was evaluated by colorimtric change catalyzed by alkaline phosphatase conjugated to antibodies targeting the FLAG-tag. (C) Results of TMV-1cys and D77K-HA CP surface-bound coassembly, in which TMV-1cys was first deposited on to gold-coated silica wafers followed by disassembled D77K-HA CP in water, followed by an 7-fold addition of pH 5 Tris for a final pH of 7 to initiate reassembly of the CP onto the free ends of the surface bound TMV. The presence of HA-tag labelled D77K CP was evaluated by colorimtric change catalyzed by alkaline phosphatase conjugated to antibodies targeting the HA-tag.

Similar results, however, were obtained with similar experiments using the pH-based disassembly and then surface-attachment reassembly of D77K-HA CP. Surfaces incubated first with the highest concentration of TMV-1cys before having disassembled D77K-HA CP deposited and reassembled by the addition of low pH buffer gave the strongest indication of retained HA-tagged CP. Samples negative for initial TMV-1cys deposition or D77K-HA CP addition gave weak color change responses. This is consistent with the longitudinal coassembly of D77K-HA CP with TMV-1cys but not consistent with models of the orientation of surface-bound TMV-1cys and models of the orientation of attachment of D77K CP to TMV. According to these models, D77K CP should compete for attachment to the 3′ end of TMV-1cys with the gold surface.

3.5. Conclusion

In this work, knowledge of the native structure and mechanism by which TMV regulates virion assembly was used to engineer a novel system for the generation of hierarchically assembled, complex nanoparticles. TMV capsid protein has several surface-exposed residues with carboxylate-containing sidechains. In the assembled virion, where many copies of the capsid protein are stacked in a repeating helical pattern, these residues are placed in close proximity to others on the neighboring copies of the capsid protein. Throughout the typical infection and reproduction cycle of the virus the ambient environmental pH and ionic conditions outside the host system can serve to moderate the destabilizing interaction between juxtaposed carboxylates, while inside a host cell environmental conditions allow the repulsive interactions to favor partial virion disassembly to initiate virus reproduction. Two key

carboxylate-containing residues involved in this process are the glutamic acid E50 and the aspartic acid D77, which interact between CP oriented along the virion axis. Previous work had established that neutralization of both of these residues by substitution with the similarly sized but neutrally charged glutamine (E50Q) and asparagine (D77N) produced a CP which would assemble into RNA-free virus-like particles at neutral pH. Here, it was shown that E50Q alone is sufficient to drive this assembly, while D77N alone is not. Additionally, the neutralization of a second set of carboxylate containing residue, E106 with E95/E97/D109, between laterally adjacent CP subunits, will also generate VLP, and the combination of the lateral E106Q substitution with the non-assembling D77N substitution can restore VLP-forming assembly behavior. It was also shown that the destabilizing axial interaction can be replaced by a stabilizing interaction between a positively charged and a negatively charged residue by substitution of a lysine (K) for either E50 or D77, producing supermicrometer length VLPs that uniquely disassembly under low ionic strength or low pH solution conditions, respectively. Finally, it was shown that the unique combination of negative, neutral, or positive charges at the 5′ and 3′ ends of each of the VLPs formed by these CP variants can be used to selectively direct the head-to-tail assembly of TMV with VLP containing compatible or complementary end charges. In the case of single-end-neutralized VLPs D77N+E106Q and E50Q+E95Q/E97Q/D109N, results showed that this coassembly occurred with low efficiency, but that the unique pH- or ionic strength-based disassembly and reassembly behavior of the lysine substituted mutants D77K and R46G/E50K+E97G could be used to selectively assembly these CP variants onto one end of TMV in an

efficient and reproducible manner to generate hybrid nanoparticles with different functional capabilities distributed in discrete, well-ordered sections along the particle's longitudinal axis.

Chapter 4: Conclusion

4.1. Summary of Research and Accomplishments

In this dissertation research, a system of modifications to *Tobacco mosaic virus* (TMV) capsid protein (CP) was developed to explore the mechanisms underlying the assembly behavior of these naturally occurring nanoparticles and to selectively generate novel nanoparticles with alternative functional morphologies and complex architectures. Initially building on previous research into TMV assembly, targeted changes to the amino acid sequence of the CP gene through genetic modification successfully resulted in the first reported self-assembling TMV virus-like particles (VLPs). Further modifications to alter the directionality and strength of intermolecular CP–CP interactions resulted in the successful development of library of CP variants that self-assemble into VLPs with alternative functional morphologies, with unique electrostatic surface charge profiles, and with either broad environmental stabilities or with dynamic, environmentally sensitive disassembly and reassembly behavior. Finally it was shown that the unique properties and behaviors of these novel, alternative VLP-forming CPs can be exploited to drive higher-order assembly behaviors to generate TMV-based nanoparticles with another dimension of structural complexity. This resulted in the successful creation of hybrid VLP–TMV nanoparticles with longitudinally ordered and differentiable function.

Technological innovation at the nanometer scale has the potential to confer significant improvements to a wide range of applications, and *Tobacco mosaic virus* (TMV) had been proven to be a useful substrate for the construction and development

of functional nanomaterials. However, TMV as a platform for functional nanoscale materials had several limitations including long production times, the high risk of loss of engineered function through genetic recombination, and a structurally based homogeneity of function along the length of the nanoparticle.

Initial efforts sought to alleviate these limitations through the creation of TMV virus-like particles (VLPs). Based on the knowledge that TMV CP contained several negatively charged, carboxylate containing residues (aspartic acid ("D") and glutamic acid ("E")) that interacted repulsively between adjacent copies of the CP within the assembled rod to moderate its structural stability, a CP variant with two neutralizing substitutions (E50Q and D77N) was expressed in bacteria to create the first RNA-free, TMV VLP composed of protein alone. This VLP was characterized, and found to be nearly indistinguishable from TMV in terms of stability across a range of pH conditions and function. These particles can be functionalized by the extension of the N- or C-terminus with peptide chains for analyte target binding, epitope display or bioconjugation sites with less concern for loss of function due to genetic reversion. Addition of the N-terminal 1cys mutation enabled its vertically oriented attachment to surfaces for device integration and metallization via electroless plating for high-surface area electrodes. The primary notable difference from TMV was the broader distribution of particle lengths due to the lack of length-determining RNA.

Based on this initial success, a library of modified TMV CP variants were created which differentially altered the two known sets of carboxylates that interacted between adjacent CP subunits to inhibit assembly: (i) the 5′-rod-end-oriented D77

which interacts in an axial direction with 3′-end-oriented E50 and (ii) the 5′-end-exposed E106 which interacts laterally with the 3′-end-exposed E95/E97/D109 cluster. The modifications were made to investigate the effects of eliminating these repulsive interactions – through substitutions of neutral residues for the negatively charged carboxylate residues versus creating attractive interactions by substituting positively charged residues – and to investigate how the direction of these new interactions affected assembly – by comparing substitution of one member of a set of interacting carboxylate pair to substitution of the other member(s) of the pair. It was found that neutralizing one member of the axially interacting carboxylate pair (E50Q) but not the other (D77N) was sufficient to drive VLP assembly. It was found that neutralization of the laterally interacting carboxylate group (E95Q/E97Q/D109N+E106Q) without altering the axially interacting pair was also sufficient to drive assembly and that the addition of the laterally-interacting substitution E106Q to the nonassembling D77N substitution was sufficient to drive VLP-assembly. Finally, it was found that the positively charged axial carboxylate substitutions D77K and E50K (with compensatory R46G and E97G substitutions) further stabilized macromolecular assembly, generating very long VLP particles that exhibited unique and reversible disassembly behavior under conditions of high pH and low ionic strength, respectively.

This set of independently assembling VLP constructs differed from one another in the distribution of electrostatic charges at the two separate VLP rod ends. Whereas the wild-type TMV virion has negative charges which are brought into proximity upon the approach of the 3′ end of one virion to the 5′ end of another,

generating a net repulsive interaction and inhibiting fusion of the two particles into a single large rod, the newly created VLP rods were engineered to display various combinations of electrostatic charge profiles at the two rod ends. These included negative (E50), neutral (E50Q), or positive (E50K) charged residues exposed at the 3′ end of the VLP and negative charge (D77), neutral (D77N), or positive (D77K) charged residues at the 5′ end.

The last part of this research focused on using this engineered feature of the newly created VLP-producing CP to investigate the potential for the directionally specific coassembly of heterogeneous CP types into single particles with longitudinally separable functions. While the use of the end-charge-neutralized VLP containing E50Q or D77N were found to have inefficient coassembly capabilities with TMV, the lysine substituted variants containing E50K or D77K were predicted to perform better based on modelling and assembly data for these variants in isolation. The unique disassembly behavior of these VLP-forming variants was exploited to develop methods to direct the reassembly of these component CP subunits onto one end of TMV in an efficient and reproducible manner. This resulted in the development of an assembly system capable of generating hierarchically structured nanorods with longitudinally differentiable functional capabilities that can be integrated into devices via surface attachment for advancing a range of applications that would benefit from the improvement of structural control over scalable fabrication of nanoscale materials.

4.2. Challenges and Future Directions

This dissertation research presents a new system for the fabrication of nanoparticles with unique and complex assembly behaviors and architectures. However some challenges need to be overcome before the potential for this system is fully realized. These include control of particle lengths of VLPs and of components of longitudinally ordered TMV+VLP or VLP+VLP complexes, understanding particle stability with respect to the significance of dynamic equilibrium and of the role that divalent cations may play, and establishment of methods for longitudinally ordered double end assembly. Double end assembly to create well-ordered, longitudinally differentiable, three component nanoparticles is theoretically feasible, but has not yet been shown, and the system would be improved by methods to achieve the more complete disassembly of the R46G/E50K+E97G CP VLP, whose incomplete disassembly currently limits the ability to limit the length of the coassembled nanoparticles produced using this CP variant as a component.

The current work establishing the components and methods for fabrication of longitudinally ordered nanoparticle complexes emerged from the earlier successes in manipulating intersubunit interactions for the purposes of moving from the use of TMV as a functionalizable nanoparticle platform requiring plant-based fabrication to a VLP-based platform with all the advantages that platform provides. However, the fabrication of the nanoparticle complexes detailed in this dissertation has still incorporated TMV as a component of those complexes. To fully realize the advantages of VLPs as an alternative to a plant-based virus platform, it is envisioned that continuation of this work will move to a fully VLP-based fabrication process.

However, attempts to replicate successes in the fabrication of longitudinally ordered TMV+VLP complexed nanoparticles without TMV and using only VLP and CP components have generated less robust and more inconsistent results. These attempts have generally entailed replacing the RNA-containing TMV component of the complexed nanoparticle with the RNA-free E95Q/E97Q/D109N+E106Q VLP. This VLP, in which all and only the laterally interacting carboxylate containing residues have be substituted with analogous residues with uncharged hydrophilic sidechains, was viewed as a plausible substitute for TMV due to its retention of the axially oriented carboxylates E50 and D77, which were understood to play a more important role in the longitudinal coassembly of multiple nanorod components. The problems encountered in these attempts to replace TMV with E95Q/E97Q/D109N+E106Q VLP point to some of the difficulties and challenges that will need to be overcome to move to a fully virus-free protein-based system platform.

First, the relative lack of control over the length of the assembled particles in VLP when compared to TMV is compounded when attempting to combine various VLPs in a longitudinally discrete and well-ordered manner. The RNA genome encapsidated by TMV provides a well-established method for controlling the length of the viral nanoparticles. In the fabrication of TMV+VLP complexes, the RNA scaffold can not only be used to control the length of the TMV portion of the longitudinally ordered TMV+VLP complex, but it could also provide a mechanism for control of the length of the VLP portion of the complex. The mechanism detailed in this work, which uses solution conditions to trigger the disassembly and subsequent reassembly onto one end of TMV of the lysine-substituted CP variants

D77K and R46G/E50K+E97G, is thought to proceed either by the use of one end of the TMV as a nucleation point for the addition of disassembled monomers directly or else as a point of attachment for disks or short barrels of the modified CP after they have formed in solution. Which of these mechanisms occurs has not yet been determined and may depend on which end of the TMV rod is being extended. It is plausible in theory, although it has not yet been shown in practice, that the relative abundance of TMV and modified CP could be used to provide some control over the length of the VLP portion of the complexed nanoparticle as process goes to completion and the disassembled CP is depleted from solution. When E95Q/E97Q/D109N+E106Q VLP is substituted for TMV, though, the relationship between the relative abundance of E95Q/E97Q/D109N+E106Q CP in solution and the number of VLP rod ends it supplies as nucleation points for the assembly of D77K or R46G/E50K+E97G is no longer tightly constrained. This uncertainty would be expected to be carried over into an additional lack of control over the length of the D77K or R46G/E50K+E97G portion of the complexed nanoparticle.

Another significant challenge that may be caused by the lack of an RNA scaffold, which may help explain the inconsistent results obtained so far using RNA-free components, is the role that RNA may play in maintaining a static equilibrium with respect to assembled particle stability, as opposed to a dynamic equilibrium. While the RNA scaffold of TMV and the strengthened intersubunit attraction afforded by the introduction of salt bridge-like interactions in elongated VLP composed of the lysine-substituted variants D77K and R46G/E50K+E97G provide mechanisms for maintaining stability of assembled particles once formed, it is likely

that shorter VLP with weaker intersubunit interactions are in a state of constant flux, with monomers or disks disassembling from one end and reassembling on the other as well as longer rods fracturing and shorter rods fusing. This could negatively impact the stability of complexed nanoparticles with these VLP as components, as the VLP which provide their rod ends as nucleation points for the directed assembly of other VLP components subsequently fracture or disassemble and reassemble as non-complexed VLP.

The use of only virus-like particle components, without included virus components, has some clear advantages, and yet particle stability and control over the length distribution of the component segments of the hybrid nanorods, as well as their total length, are necessary for their functionality in diverse applications, including the study and use of spatial arrangement and segregation of enzymatic cascade components for energy harvesting, sensing, or chemical fabrication purposes. Several options are available. One potential solution is the use nongenomic RNA to act as a scaffold for the support of bacterially expressed CP to provide length control and particle stability as referenced in the introductory chapter of this dissertation [90-93]. This method for controlling and stabilizing individual particles could be combined with the methods developed here to guide interactions between particles and to fabricate well-ordered and stable nanoparticle complexes. An additional method which is currently being explored to control length and may be effective for many purposes is the use of microfluidics to progressively “grow” these nanoparticles on a surface layer by layer.

Another important factor that this work does not address is the use of divalent cations such as Ca^{++} as a stabilizing agent for VLP assembly. The presence of calcium ions in the extracellular environment is known to stabilize the TMV rod by mitigating the destabilizing effects of the intersubunit carboxylate interactions. The moderated addition of Ca^{++} in controlled amounts could provide a simple and convenient method to stabilize the more labile and dynamic VLP components.

Appendix: Methods

4.2.1. TMV coat protein expression constructs

The TMV coat protein open reading frame (ORF) carrying the E50Q and D77N modifications was codon optimized for expression in *E. coli* (GenScript, Piscataway NJ: Supplemental Fig. 1) and inserted into the pET-21a(+) expression vector (Novagen, Madison WI) via *Nde*I and *Xho*I restriction sites. Further modifications to the N- and C-terminus of the coat protein ORF were achieved by primer based PCR mutagenesis using oligonucleotides containing additional or altered sequences (Table 1). A cysteine codon was added at position two at the N-terminus of the coat protein ORF to produce TMV-VLP1cys for enhanced metal coatings and oriented surface-binding [162]. Sequences encoding the binding peptides for FLAG epitope (DYKDDDDK) were added to the coat protein C-terminus [163]. Sequences binding the fluorescent imaging agent Genhance^{TM} 680 (IQSPHFF) were added to the coat protein C-terminus as fusions either with or without preceding sequences encoding a “leaky” amber stop codon (TAG) or a flexible 10 amino acid linker (GGGGSGGGGS) [164], [165]. Amplified PCR products containing 5′ *Nde*I and 3′ *Xho*I restriction sites were used to ligate the modified coat protein ORFs into similarly cut pET-21a(+) vector.

4.2.2. Induction and purification of TMV-VLPs

Coat protein expression constructs were transformed into BL21 competent *E. coli* K-12. Additionally, JM109 *E. coli* cells were used for coat protein constructs

containing the amber stop codon TAG. JM109 cells carry the supE44 suppressor of the amber stop codon via a tRNA mutation that transitions the GUC glutamine anticodon to AUC [166]. Transformed cells were cultured at 37^{o}C in LB broth containing ampicillin (100 μg/ml) / chloramphenicol (50 μg/ml) for BL21 and ampicillin (100 μg/ml) / nalidixic acid (30 μg/ml) for JM109 cells to an OD_{600} of 0.5. Cells were then induced by the addition of 0.1 mM IPTG and incubated overnight at 25°C. Induced cells were harvested by centrifugation at 4°C and lysed using Bugbuster™ with Lysonase™ according to the manufacturer's protocol (Novagen, Madison WI). Dithiothreitol to a concentration of 0.5 mM was added to the cell lysates followed by 3-5 min of sonication in a Branson 1510 sonicator (Branson Ultrasonics, Danbury CT). One third volume of chloroform was then added to the lysates, mixed and separated by centrifugation for 10 min at 17,000 × g at 4°C. Because of the hydrophobic nature of the IQ peptide the chloroform purification step was replaced by centrifugation at 800 × g for 1 min, centrifugation of the resulting supernatant at 66,400 × g for 30 min, and resuspension of the pellet in 3 mL of 0.1 M pH 7 sodium phosphate buffer. VLPs were then precipitated by the per volume addition of 1.5% KCl and 6% polyethylene glycol for one hour at 4°C. VLPs were then pelleted by centrifugation for 10 min at 17,000 × g. The resulting pellet was resuspended by shaking overnight in 0.5 to 2 mls of 0.1 M pH 7 sodium phosphate buffer. Resuspended VLP pellets were then loaded onto a 10 to 40% sucrose gradient in 0.1 M pH 7.0 sodium phosphate buffer and centrifuged for 1 hr at 91,000 × g at 14°C. A diffuse band corresponding to the purified VLP was removed by syringe and

concentrated by centrifugation for 1 hr at 92,000 × g at 4°C. The purified VLP pellet was then resuspended in 0.1 M pH 7 sodium phosphate buffer.

To visualize VLPs within bacteria, cells were induced overnight and subsequently prepared by pelleting, followed by fixing in 2% gluteraldehyde in phosphate buffered saline (PBS) with 0.29 M sucrose. Post-fixing was done in en bloc on the pelleted cells using 1% osmium tetroxide with 2% aqueous uranyl acetate. Dehydration of the pelleted cells was accomplished by treatment with solutions of increasing ethanol content (100% final). The dehydrated pellet was then embedding by solutions of propylene oxide with increasing Spurr's resin content (100% final) and curing at 70°C overnight. Expressed VLPs were visualized in whole fixed bacterial cells and in purified form using a transmission electron microscope at 80 kV.

4.2.3. VLP surface assembly and electroless plating

Purified TMV-VLP1cys was self-assembled onto 1 cm^2 gold-coated silicon chips by incubation overnight at 4°C in a 1 mg/mL solution of the purified VLPs resuspended in 0.1 mM sodium phosphate buffer, pH 7. VLP assembled chips were then dipped in a 0.158 mM solution of Na_2PdCl_4 for 30 minutes at 4°C. The surface-bound VLPs were then coated with nickel by moving the chip directly into an electroless nickel plating solution consisting of 0.05 M $NiCl_2$, 0.12 M glycine, 0.0785 M sodium tetraborate, 0.525 M dimethylamine borane complex at pH 7. Nickel deposition by reduction was allowed to proceed at room temperature until the entire surface of the chip had darkened. Nickel coatings were visualized via field emission electron microscopy.

4.2.4. Chip based enzyme-linked immunosorbent assay (ELISA)

Gold coated 1cm^2 silicon nitrate chips were submerged overnight in purified TMV1cys-VLP or TMV1cys-VLP1cys-FLAG at 4°C to facilitate oriented VLP assembly onto the gold surface. VLP assembled chips were then incubated for an additional 30 min at 4°C in Tris buffered saline (50 mM Tris-HCL, 200 mM NaCl, TBS) pH 7.0 containing 5% non-fat dry milk as a blocking agent. Chips were then rinsed three times by submersion in fresh TBS buffer. Rinsed chips were subsequently incubated for 3 hrs at room temperature in TBS containing 5% non-fat dry milk and a 1/1000 dilution of rabbit anti-flag antibody (Sigma-Aldrich, St. Louis MO). The chip was then rinsed 3 times with TBS buffer and twice with TBS buffer containing 0.05% Tween-20. After rinsing, chips were submerged in TBS with 5% nonfat dry milk containing a 1/5000 dilution of anti-rabbit IgG alkaline phosphatase and incubated at room temperature for 3 hrs. Chips were again rinsed as described above and placed directly in a solution containing 0.15 mg/ml of 5-bromo-4-chloro-3-indoyl phosphate and 0.3 mg/ml NitroBT in substrate buffer (10 mM Tris-HCL pH 9.5, 100 mM NaCl and 5 mM MgCl-6H_2O) and incubated for 10 min at room temperature. The reaction was stopped by immersion in water and the chips dried. Color intensities of individual chips were measured using ImageJ software [167].

4.2.5. Fluorescence binding onto IQ peptide tagged TMV-VLPs

The IQ-tag modified VLPs were tested for preferential binding of the fluorescent imaging agent Genhance^{TM} 680 (PerkinElmer, Waltham MA) as follows. Purified TMV1cys-VLP-AmberFlex-IQ (0.2 mg/ml or 0.02 mg/ml) were incubated overnight at 4°C in 0.5 mL of 0.1 M pH7 phosphate buffer with or without the

addition of 10 μL of 0.1 mg/mL Genhance™ 680. Samples were then centrifuged at 16,000 × g for 45 min. The VLP pellets were then resuspended in 1 mL of 0.1 M pH 7.0 phosphate buffer and centrifuged again for 45 min. Pelleted VLPs were then resuspended in 0.1 M pH 7.0 phosphate buffer to a concentration of 0.5 mg/mL and 0.05 mg/mL. 200 μL of each sample was added to a black-walled 96-well microtiter plate and fluorescence intensity at 690 nm (655 nm excitation and a 665 nm cutoff) was determined using a SpectraMax M2 (Molecular Devices, Sunnyvale, CA).

4.2.6. Design of modified TMV CP genes

The TMV capsid protein gene was modified to substitute neutrally charged or basic amino acid residues for one or more of the negatively charged acidic residues which interact with those on adjacent CP subunits. All modified forms of the TMV capsid protein used in this study were ultimately generated from copies of a DNA open reading frame (ORF) encoding the TMV CP codon optimized for expression in *E. coli* using codon utilization frequency tables. The ORF encoding the E50Q/D77N form was obtained from GenScript (Piscataway, NJ). The ORFs encoding the E95Q/E97Q/E106Q/D109N, E50Q+E95Q/E97Q/D109N, D77N+E106Q, E50K-HA, and D77H and R46G-E50H-HA were generated using Invitrogen™ GeneArt™ Strings™ DNA fragments. All additional variants were generated by sequential polymerase chain reactions using overlap extension PCR with primers encoding the designed modifications and complimentary to regions of the ORF to be modified. These included additional modifications to the carboxylate-containing sites E50, D77, E95, E97, E106, and E109, the insertion of the S1_Y2insC (hereafter denoted as "1cys") modification by the insertion of a cysteine at position three (5′-MSYS…→5′-

MSCYS…), and insertion or replacement of sequences encoding either the FLAG-tag epitope (DYKDDDDK) or the HA-tag (YPYDVPDYA) to the 3′ end of the gene, following the sequence encoding the C-terminal PAT residues. Two endonuclease restriction sites, an *NdeI* restriction site over lapping the ORF start codon and an *XhoI* restriction site at the 3′ end, flanking the ORF were included. For each ORF-interior modification, a set of PCR reactions, each using a primer pair consisting of either a forward primer containing the ORF 5′ end and a reverse primer containing the interior modification or a forward primer containing the interior modification and a reverse primer containing the ORF 3′ end, was performed using *Platinum Taq* DNA Polymerase (Invitrogen): 94 °C for 5min; 32 cycles of 94 °C for 30 s / 55 °C for 30 s / 72 °C for 1 min; 72 °C for 5 min). The PCR product from each of the two PCR reactions was gel-purified using a GENECLEAN III gel purification kit (MP Biomedicals) and used as templates for PCR with the 5′ end forward primer and the 3′ end reverse primer from the previous PCR reactions. Complete PCR products of CP ORFs were isolated and amplified using a TOPO TA cloning kit. pCR-2.0 vector, TOP10 competent cells (Invitrogen).

ORFs were excised from TA clones by restriction with *NdeI* and *XhoI* and isolated from the plasmid vector by agarose gel electrophoresis. Bands were purified using GENECLEAN III gel purification kit and purified DNA fragments were ligated into a similarly cut and purified pET-21a(+) (Novagen, Madison, WI) or pET-DUET expression vector with T4 DNA ligase. Complimentary overhangs between vector and insert were created by using the same restriction enzymes. Ligated plasmid vectors containing the ORFs were transformed into DH5α chemically competent cells

for amplification with ampicillin selection and subsequent miniprep purification. Clones containing inserted genetic material were identified using restriction hydrolysis of ORF-flanking restriction sites and were sequenced to screen for unintended mutations.

4.2.7. Bacterial expression and purification of TMV CP variants

Plasmids containing sequence-verified ORFs encoding the various TMV CPs described above were transformed into chemically competent BL21-CodonPlus *E. coli* K-12 cells. Transformations were spread onto LB-agar plates containing ampicillin (100 μg/mL) and chloramphenicol (20 μg/mL). Colonies were picked and grown in LB containing ampicillin (100 μg/mL) and chloramphenicol (20 μg/mL) at 37 °C overnight. Frozen stocks of cells containing the TMV CP constructs for continued production of modified CP were made by addition of DMSO (70 μl/mL culture) and storage at -80 °C. Cell cultures were grown at 37 °C until reaching an absorbance of 0.5 ± 0.1 at a wavelength of 600 nm. At that point the culture was induced by the addition of IPTG to a concentration of 1 mM and incubated at room temperature with shaking overnight. Induced cells were pelleted by centrifugation at 4 °C and lysed by resuspension in Bugbuster HT Protein Extraction Reagent and the addition of Lysonase according to the manufacturer's protocol (Novagen, Madison WI) and incubation at room temperature for 30 minutes. The bacterial lysate was diluted 10:1 with 0.1 M pH 7 phosphate buffer and pelleted by centrifugation at 91,000 × g for 2 hours. The resulting pellet was resuspended in 2 mL 0.1 M pH 7 phosphate buffer with pipetting and shaking overnight at 4°C. Resuspended pellets were loaded onto a 10 to 40 % sucrose gradient in 0.1 M pH 7 phosphate buffer and

centrifuged at 91,000 × g at 14 °C for either 1 hour (E50Q and D77N variants) or 15 minutes (E50K and D77K variants). The virus-like particles were removed from the center portion of the gradient, where they formed a diffuse visible band, with a syringe and transferred to ~25 mL ultracentrifuge tubes. The samples were diluted with 0.1 M pH 7 phosphate buffer to reduce sucrose concentration and centrifuged at 91,000 × g for 2 hours at 4 °C. The purified VLP pellets were resuspended in 0.1 M pH 7 phosphate buffer.

4.2.8. Determining concentration of TMV and bacterially expressed TMV CP

All determinations of disassembled CP and assembled VLP solution concentrations were made using a Thermo Fisher Scientific™ Nanodrop™ 1000. VLP samples purified from monoclonal cultures of transformed expression strains of *E. coli* (BL21 and BL21 codon plus) all showed a light attenuation peaks at around 280 nm, indicating the relative lack of nucleic acid and in contrast to purified samples of absorption spectrum of encapsidated RNA centered around 260 nm.

Determinations of TMV concentrations, which contain the genomic RNA, were made by measuring the attenuation of the TMV sample at λ = 260 nm, calculating and subtracting the attenuation due to scattering to obtain the attenuation at 260 nm attributable to absorbance alone and using the mass attenuation coefficient and path length to determine concentration using the following form of the Beer-Lambert law

$$C = \frac{(A_{260} - 2.44 \times A_{325})}{\varepsilon_{TMV,260} \times l}$$

Where A_{260} and A_{325} are the sample absorption measurements of 260 nm and 325 nm wavelength light, respectively, $\varepsilon_{TMV,260}$ is the extinction/attenuation coefficient of TMV at wavelength 260 nm, and l is the path length. The expression $2.44 \times A_{325}$ is the estimated attenuation at 260 nm due to scattering. Because neither protein nor RNA has significant absorption at 325 nm, all attenuation at 325 nm is assumed to be due to scattering. Because scattering varies with wavelength with a factor of λ^{-4},the scattering at 260 nm is related to the scattering at 325 nm by a factor of $(260^{-4}/325^{-4})$ = 2.44. The inherited mass attenuation coefficient for TMV, ε_{260}, is 3 $L \cdot g^{-1} \cdot cm^{-1}$.

The concentration of RNA-free, bacterially expressed CP was determined by measuring the optical attenuation at λ = 280 nm, calculating and subtracting the attenuation due to scattering to obtain the attenuation at 280 nm attributable to absorbance alone and using the mass attenuation coefficient and path length to determine concentration using the following form of the Beer-Lambert law

$$C = \frac{A_{280} - (1.8 \times A_{325})}{\varepsilon_{CP,280} \times l}$$

Where A_{280} and A_{325} are the sample absorption measurements of 280 nm and 325 nm wavelength light, respectively, ε_{280}, is the extinction/attenuation coefficient of the relevant CP at wavelength 260 nm (see table), and l is the path length. The expression $1.8 \times A_{325}$ is the estimated attenuation at 280 nm due to scattering. Because protein does not have significant absorption at 325 nm, all attenuation at 325 nm is assumed to be due to scattering. Because scattering varies with wavelength with a factor of λ^{-4},the scattering at 280 nm is related to the scattering at 325 nm by a factor of $(280^{-4}/325^{-4})$ = 1.815.

The attenuation coefficients of the VLP-forming CPs were calculated using the Edelhoch method, according to which

$$\varepsilon(208)(M^{-1}cm^{-1}) = (\#Trp)(5{,}500) + (\#Tyr)(1{,}490) + (\#disulfide)(125)$$

where ε*(280)* is the molar attenuation coefficient, *#Trp*, *#Tyr*, and *#disulfide* are the number of tryptophan residues, tyrosine residues, and disulfide bonds bonds formed by crosslinked cysteine residues, respectively. The corresponding mass attenuation coefficients were obtained by dividing the molar attenuation coefficents by the mass in grams per mole of CP.

	# Trp / CP	# Tyr / CP	# S-S / CP	Molar ε (M^{-1}·cm^{-1})	FW	Mass ε ($L·g^{-1}·cm^{-1}$)
WT CP	3	4	0	22460	17420	1.289
1cys CP	3	4	0	22460	17524	1.281
R46G/E50K-E97Q-FLAG	3	6	0	25440	18405	1.382
D77K-HA	3	5	0	23950	18429	1.299

Table 5: Molar and mass attenuation coefficients at 280 nm for various TMV CPs.

4.2.9. Longitudinal coassembly of neutral carboxylate-substituted CP variants with TMV or VLP with wild-type axial carboxylates

Complexed nanoparticles with distinct and ordered longitudinal domains generated from the coassembly of a nanoparticle retaining wild-type axially interacting carboxylate residues (either infectious TMV or VLP assembled from E95Q/E97Q/D109N+E106Q CP) together with a VLP containing uncharged amino acids substituted at one rod end (E50Q+E95Q/E97Q/D109N-FLAG VLP or D77N+E106-HA VLP) were produced by concentration of a solution containing a mixture of the component nanoparticles.

For the longitudinal coassembly of TMV and D77N+E106Q-HA VLP, 100 µg each of purified 5 mg/mL 1cys TMV and D77N+E106Q-HA VLP in 0.1 M pH 7 sodium phosphate buffer were mixed and diluted with 25 mL 0.1 M pH 7 sodium phosphate buffer in a ultracentrifuge tube. The mixture was centrifuged at 91,000 × g for 2 hours at 4 °C, at which point the supernatant was removed and replaced with 100 µL of 0.1 M pH 7 sodium phosphate buffer. The pellet was allowed to resuspend overnight at 4 °C with gentle rocking, then diluted (1:500) in 0.1 M pH 7 phosphate buffer for immunolabelling and preparation for TEM.

For the longitudinal coassembly of E95Q/E97Q/D109N+E106Q VLP with E50Q+E95Q/E97Q/D109N-FLAG VLP, 50 µL of 1 mg/mL solutions of each of the two purified VLPs in 0.01 M pH 7 sodium phosphate buffer were well mixed in a 1.5 mL centrifuge tube. The mixed sample was then centrifuged under partial vacuum until the sample volume had reduced to ~10 µL (approximately one hour). The concentrated sample was kept at 4 °C overnight before dilution (1:500) in 0.1 M pH 7 sodium phosphate buffer for immunolabelling and preparation for TEM.

4.2.10. Dialysis of samples

All dialysis was performed Spectra/Por® dialysis membrane tubing (MWCO:12-14,000, Spectrum Labs) secured to the opening of a 1.5 mL microcentrifuge tube containing 50-200 µL of plant-expressed TMV and/or bacterially expressed CP. The microcentrifuge tubes were inverted so that sample solution was in contact with dialysis film and placed in a floating microcentrifuge holder on the surface of 500 mL of the solution to be dialyzed against, so that the dialysis tubing was in contact with the target dialysis solution. All dialysis was

performed at 4 °C overnight. For all dialysis experiments, TMV or CP samples, which were initially in 0.1 M pH 7 sodium phosphate buffer were first dialyzed to 0.1 M pH 7 Tris buffer. The pH 7 Tris-buffered samples were then dialyzed against either ultrapure water adjusted to pH 7 with approximately 50 μL of 12 M NaOH per 1 L of water or 0.1 M Tris adjusted to pH 5, 6, 7, 8, or 9 with glacial HCl or 12 M NaOH.

4.2.11. Longitudinal coassembly of positively-charged carboxylate-substituted CP variants with TMV

To generate extended TMV-VLP complexed particles with distinct and ordered longitudinal components, TMV and VLP were dialyzed either separately or in admixture to solution conditions promoting disassembly of the VLP CP and then returned to conditions promoting its assembly, either by dialysis or by the addition of concentrated solution.

For assembly of D77K-HA CP onto TMV, 50 μL of a solution containing 3 mg/mL of D77K-HA CP and 0.6 mg/mL wild-type TMV (a ratio of 5:1 by mass) in 0.1 M pH 7 sodium phosphate buffer was dialyzed as described above first to 0.1 M pH 7 Tris buffer, then to 0.1 M pH 9 Tris buffer to disassemble the D77K CP, and then to 0.1 M pH 7 Tris buffer to initiate reassembly of the D77K CP onto the TMV rod end with each dialysis step taking place overnight at 4 °C. For samples treated with RNase, 0.5 μL of a 1 mg/mL stock solution of RNase A was added to the solution after the dialysis to pH 9, which was hypothesized to have exposed the genomic RNA at the TMV's 5′ rod end, and incubated for 30 min at 37 °C before proceeding with dialysis back to pH 7.

For assembly of R46G/E50K+E97G-FLAG CP onto TMV, 50 µL of a solution containing 1 mg/mL of R46G/E50K+E97G-FLAG and 0.5 mg/mL wild-type TMV (a ratio of 2:1 by mass) in 0.1 M pH 7 sodium phosphate buffer was dialyzed first to 0.1 M pH 7 Tris buffer, then to filtered ultrapure water brought to pH 7 with NaOH to disassemble the R46G/E50K+E97G CP, and then to 0.1 M pH 7 Tris buffer / 0.3 M NaCl to initiate reassembly of R46G/E50K+E97G CP onto the TMV rod end with each dialysis step taking place overnight at 4 °C.

4.2.12. Immunolabelling and electron microscopy

To immunolabel and image samples, assembled TMV and VLP samples were adsorbed onto Formvar-coated Ni TEM grids by floating the grid on 5-10 µL droplets containing the sample arrayed on Parafilm™. Grids were washed with phosphate-buffered saline (PBS: 10 mM sodium phosphate, 150 mM NaCl, pH 7). Surfaces were blocked with Blocking Solution for Goat Antibodies (Aurion, Wageningen, The Netherlands) to reduce nonspecific binding and washed with PBS. Primary antibodies (anti-FLAG antibodies produced in rabbit, anti-HA antibodies produced in mouse, Sigma) were diluted 1:500 in incubation buffer (PBS with 0.1% Tween-20 and 0.1% Aurion BSA-c™) as needed and applied to grids at room temperature for 2 h or at 4 °C overnight. Grids were washed by placing on 50 µL drops of incubation buffer for 5 min three times. Gold nanoparticle (AuNP)-conjugated secondary antibodies (i.e. goat anti-rabbit with 10 nm AuNPs or goat anti-mouse with 6 nm AuNPs), if used, were diluted 1:50 in incubation buffer as needed and applied to grids at room temperature for 2 h or at 4 °C overnight. Grids were washed by placing on 50 µL droplets of incubation buffer for 5 min three times and then on 50 µL droplets of 0.1

M pH 7 Tris. Grids were stained by placing them on a 5 µL droplet of 2% uranyl acetate (UAc) for 1 min. UAc was removed by wicking with filter paper, and the samples were imaged using a Zeiss transmission electron microscope (TEM) at 80 kV.

4.2.13. Light scattering assembly kinetics

Macromolecular assembly kinetics of the D77K and R46G/E50K+E97G CP from the disassembled to the assembled state upon lowering of the pH or increase of the ionic strength of the solution was observed in real time using 90° light scattering to measure the relative degree of rod formation in an aqueous solution of CP. Light scattering was measured on a Varian Cary Eclipse Fluorescence Spectrophotometer. Scattered light was measured at an angle of 90° relative to the angle of incidence using 200 µL of CP solution in a 200 µL capacity quartz cuvette and using the same value of 340 nm for the excitation and emission wavelengths. The dissociation factor D was related to the intensity of scattered light, I, by

$$D = (I_A - I)/(I_A - I_D)$$

where I_A and I_D are the intensity of scattered light for associated and dissociated forms, respectively.

For experiments examining D77K CP assembly, samples were measured by beginning recording of scattered light with baseline measurement of 175 µL of 0.1 M Tris buffer adjusted to pH 5. After 30 s, 25 µL of D77K-HA-tag CP previously dialyzed against 0.1 M Tris buffer adjusted to pH 9 was added and mixed by manual pipetting. Light scattering was recorded for 20 minutes after mixing.

For experiments examining R46G/E50K+E97G CP assembly, samples were

measured by beginning recording of scattered light with baseline measurement of 100 μL of R46G/E50K+E97G-FLAG-tag CP previously dialyzed against filtered water adjusted to pH 7 with NaOH (~50 μL 12 M NaOH / 1 L H_2O). After 30 s, 100 μL of 0.2 M Tris buffer with 0.6 M NaCl adjusted to pH 9 was added and mixed by manual pipetting. Light scattering was recorded for 30 minutes after mixing.

Data was obtained using 340 nm as both the "excitation" (incident light applied to sample from the light source) and "emission" (scattered light measured from sample) wavelength values. This wavelength was chosen after several experiments in which a scan of excitation and emission values were covaried through a range from 200 nm to 700 nm every minute during an assembly reaction of D77K-HA CP. Significant changes in scattered light was observed in the ranges from ~240 nm to ~270 nm and from ~280 nm up to 700 nm, with a dramatically reduced level of scattering observed in the region around 280 nm, presumably due to the high level of absorption by sample CP. The wavelength 340 nm was selected from the candidate ranges as determined by observation due to its use in the literature as a value previously used to study the assembly state of TMV [197, 198].

4.2.14. Surface-bound fabrication of co-assembled nanoparticles

Gold-coated silica wafers (0.5 cm × 0.5 cm), cleaned by sequential 5 min submersions in acetone, methanol, and isopropanol with agitation, were submerged in either a 0.2 mg/mL solution of 1cys TMV in 0.1 M pH 7 sodium phosphate buffer or 0.1 M pH 7 sodium phosphate buffer containing no virus overnight at 4 °C. Residual phosphate buffer was removed by submersion of the wafers in either 0.1 M pH 9 Tris for subsequent addition of D77K-HA CP or filtered water adjusted to pH 7 (by

addition of ~50 µl 12 M NaOH / 1 L water using a pH-meter to monitor pH level) for subsequent addition of R46G/E50K+E97G-FLAG CP.

For longitudinal coassembly of D77K-HA CP onto the TMV base layer: The wafers were placed gold-side-up on Parafilm™ in a 60 mm diameter petri dish. 5 µL of either 0.1 M pH 9 Tris or a 5 mg/ mL solution of D77K-HA CP previously dialyzed with 0.1 M pH 9 Tris to promote VLP disassembly was added to the gold surface by pipet and allowed to sit for 10 minutes at room temperature. Then 35 µL 0.1 M pH 5 Tris buffer was transferred to the gold surface by pipet, and the petri dish was covered with the lid and transferred to 4 °C overnight.

For longitudinal coassembly of R46G/E50K+E97G-FLAG CP onto the TMV base layer: The wafers were placed gold-side-up on Parafilm™ in a 60 mm diameter petri dish. 10 µL of either filtered water adjusted to pH7 or a 10 mg/ mL solution of R46G/E50K+E97G-FLAG CP previously dialyzed with filtered water adjusted to pH7 to promote VLP disassembly was added to the gold surface by pipet and allowed to sit for 10 minutes at room temperature. Then 10 µL 0.6 M NaCl, 0.2 M pH 7 Tris buffer was transferred to the gold surface by pipet, and the petri dish was covered with the lid and transferred to 4 °C overnight.

Excess unbound CP was washed by submersion of the wafers in 1 mL 0.1 M pH 7 Tris (for D77K-HA CP samples) or 1 mL 0.3 M NaCl, 0.1 M pH 7 Tris (for R46G/E50K+E97G-FLAG CP samples) for 5 minutes. The wafers were then placed gold-side-up on Parafilm™ in a 60 mm diameter petri dish, and a 50 µL droplet of Aurion Blocking Solution for Goat Antibodies was gently layered onto each wafer and allowed to block for 1 hour at 4 °C. The wafers were then washed by submersion

of the wafers in 1 mL 0.1 M pH 7 Tris (for D77K-HA CP samples) or 1 mL 0.3 M NaCl, 0.1 M pH 7 Tris (for R46G/E50K+E97G-FLAG CP samples) for 5 minutes, 3 times. The wafers were again transferred to Parafilm™, and 50 μL of primary antibodies (anti-FLAG antibodies produced in rabbit, anti-HA antibodies produced in mouse, Sigma) diluted 1:1000 in incubation buffer (PBS with 0.1% Tween-20 and 0.1% Aurion BSA-c™) was applied to each wafer at room temperature for 2 h or at 4 °C overnight. The wafers were again washed 3 times for 5 minutes each in 1 mL 0.1 M pH 7 Tris (for D77K-HA CP samples) or 1 mL 0.3 M NaCl, 0.1 M pH 7 Tris (for R46G/E50K+E97G-FLAG CP samples). The wafers were then submerged in 500 μL of a 1:1000 solution of secondary antibodies conjugated to horseradish peroxidase (anti-rabbit antibodies produced in goat in 0.1 M pH 7 Tris for D77K-HA CP samples and anti-mouse antibodies produced in goat in 0.3 M NaCl, 0.1 M pH 7 Tris for R46G/E50K+E97G-FLAG CP samples. The wafers were again washed 3 times for 5 minutes each in 1 mL 0.1 M pH 7 Tris (for D77K-HA CP samples) or 1 mL 0.3 M NaCl, 0.1 M pH 7 Tris (for R46G/E50K+E97G-FLAG CP samples). The wafers were then submerged in 1 mL substrate buffer (0.1 M pH 7 Tris, 0.2 M NaCl and 5 mM MgCl) containing 0.15 mg/ml of 5-bromo-4-chloro-3-indoyl phosphate and 0.3 mg/ml NitroBT. The submerged wafers were monitored for color change, and all wafers were removed and washed with 0.3 M NaCl, 0.1 M pH 7 Tris to halt colorimetric reaction after ~12 hours.

Bibliography

[1] K. Gerasopoulos, E. Pomerantseva, M. McCarthy, A. Brown, C. S. Wang, J. Culver*, et al.*, "Hierarchical Three-Dimensional Microbattery Electrodes Combining Bottom-Up Self-Assembly and Top-Down Micromachining," *Acs Nano,* vol. 6, pp. 6422-6432, Jul 2012.

[2] X. L. Chen, K. Gerasopoulos, J. C. Guo, A. Brown, R. Ghodssi, J. N. Culver*, et al.*, "High rate performance of virus enabled 3D n-type Si anodes for lithium-ion batteries," *Electrochimica Acta,* vol. 56, pp. 5210-5213, May 2011.

[3] Y. Zhu, B. Yang, J. Liu, X. Wang, X. Chen, and C. Yang, "An Integrated Flexible Harvester Coupled Triboelectric and Piezoelectric Mechanisms Using PDMS/MWCNT and PVDF," *Journal of Microelectromechanical Systems,* vol. 24, pp. 513-515, 2015.

[4] M. Armand and J. M. Tarascon, "Building better batteries," *Nature,* vol. 451, p. 652, 02/06/online 2008.

[5] X. Z. Fan, K. Gerasopoulos, A. Brown, N. Siwak, J. Culver, R. Ghodssi*, et al.*, "Virus Directed Assembly of Receptor Peptides for Explosive Sensing," in *2010 Ieee Sensors*, ed New York: Ieee, 2010, pp. 2629-2633.

[6] X. Z. Fan, L. Naves, N. P. Siwak, A. Brown, J. Culver, and R. Ghodssi, "Integration of genetically modified virus-like-particles with an optical resonator for selective bio-detection," *Nanotechnology,* vol. 26, May 2015.

[7] A. E. Czapar and N. F. Steinmetz, "Plant viruses and bacteriophages for drug delivery in medicine and biotechnology," *Current Opinion in Chemical Biology,* vol. 38, pp. 108-116, 2017/06/01/ 2017.

[8] A. E. Czapar, Y.-R. Zheng, I. A. Riddell, S. Shukla, S. G. Awuah, S. J. Lippard*, et al.*, "Tobacco Mosaic Virus Delivery of Phenanthriplatin for Cancer therapy," *ACS Nano,* vol. 10, pp. 4119-4126, 2016/04/26 2016.

[9] M. A. Bruckman, S. Hern, K. Jiang, C. A. Flask, X. Yu, and N. F. Steinmetz, "Tobacco mosaic virus rods and spheres as supramolecular high-relaxivity MRI contrast agents," *Journal of Materials Chemistry B: Materials for Biology and Medicine,* vol. 1, pp. 1482-1490, 2013.

[10] M. A. Bruckman, L. N. Randolph, A. VanMeter, S. Hern, A. J. Shoffstall, R. E. Taurog*, et al.*, "Biodistribution, pharmacokinetics, and blood compatibility of native and PEGylated tobacco mosaic virus nano-rods and -spheres in mice," *Virology,* vol. 449, pp. 163-173, 2014/01/20/ 2014.

[11] R. Singh and J. W. Lillard, "Nanoparticle-based targeted drug delivery," *Experimental and Molecular Pathology,* vol. 86, pp. 215-223, 2009/06/01/ 2009.

[12] A. Honigmann and A. Pralle, "Compartmentalization of the Cell Membrane," *Journal of Molecular Biology,* vol. 428, pp. 4739-4748, 2016/12/04/ 2016.

[13] I. Levental and S. L. Veatch, "The Continuing Mystery of Lipid Rafts," *Journal of Molecular Biology,* vol. 428, pp. 4749-4764, 2016/12/04/ 2016.
[14] S. Tanaka, M. R. Sawaya, and T. O. Yeates, "Structure and mechanisms of a protein-based organelle in Escherichia coli," *Science,* vol. 327, pp. 81-4, Jan 1 2010.
[15] A. Kuchler, M. Yoshimoto, S. Luginbuhl, F. Mavelli, and P. Walde, "Enzymatic reactions in confined environments," *Nat Nano,* vol. 11, pp. 409-420, 05//print 2016.
[16] J. N. Culver, A. D. Brown, F. H. Zang, M. Gnerlich, K. Gerasopoulos, and R. Ghodssi, "Plant virus directed fabrication of nanoscale materials and devices," *Virology,* vol. 479, pp. 200-212, May 2015.
[17] X. Z. Fan, E. Pomerantseva, M. Gnerlich, A. Brown, K. Gerasopoulos, M. McCarthy*, et al.*, "Tobacco mosaic virus: A biological building block for micro/nano/bio systems," *Journal of Vacuum Science and Technology A,* vol. 31, Sep 2013.
[18] H. Yan, S. H. Park, G. Finkelstein, J. H. Reif, and T. H. LaBean, "DNA-Templated Self-Assembly of Protein Arrays and Highly Conductive Nanowires," *Science,* vol. 301, p. 1882, 2003.
[19] E. Winfree, F. Liu, L. A. Wenzler, and N. C. Seeman, "Design and self-assembly of two-dimensional DNA crystals," *Nature,* vol. 394, pp. 539-544, 08/06/print 1998.
[20] Y. He, T. Ye, M. Su, C. Zhang, A. E. Ribbe, W. Jiang*, et al.*, "Hierarchical self-assembly of DNA into symmetric supramolecular polyhedra," *Nature,* vol. 452, pp. 198-201, 03/13/print 2008.
[21] Y. Ke, L. L. Ong, W. M. Shih, and P. Yin, "Three-Dimensional Structures Self-Assembled from DNA Bricks," *Science,* vol. 338, p. 1177, 2012.
[22] J. Zheng, J. J. Birktoft, Y. Chen, T. Wang, R. Sha, P. E. Constantinou*, et al.*, "From molecular to macroscopic via the rational design of a self-assembled 3D DNA crystal," *Nature,* vol. 461, pp. 74-77, 09/03/print 2009.
[23] P. W. K. Rothemund, "Folding DNA to create nanoscale shapes and patterns," *Nature,* vol. 440, pp. 297-302, 03/16/print 2006.
[24] S. M. Douglas, H. Dietz, T. Liedl, B. Hogberg, F. Graf, and W. M. Shih, "Self-assembly of DNA into nanoscale three-dimensional shapes," *Nature,* vol. 459, pp. 414-418, 05/21/print 2009.
[25] H. Dietz, S. M. Douglas, and W. M. Shih, "Folding DNA into Twisted and Curved Nanoscale Shapes," *Science (New York, N.Y.),* vol. 325, pp. 725-730, 2009.
[26] D. Han, S. Pal, J. Nangreave, Z. Deng, Y. Liu, and H. Yan, "DNA Origami with Complex Curvatures in Three-Dimensional Space," *Science,* vol. 332, p. 342, 2011.
[27] M. R. Jones, N. C. Seeman, and C. A. Mirkin, "Programmable materials and the nature of the DNA bond," *Science,* vol. 347, 2015.
[28] H. D. Hill and C. A. Mirkin, "The bio-barcode assay for the detection of protein and nucleic acid targets using DTT-induced ligand exchange," *Nat. Protocols,* vol. 1, pp. 324-336, 06//print 2006.

[29] R. J. Macfarlane, B. Lee, M. R. Jones, N. Harris, G. C. Schatz, and C. A. Mirkin, "Nanoparticle Superlattice Engineering with DNA," *Science,* vol. 334, p. 204, 2011.
[30] E. Auyeung, T. I. N. G. Li, A. J. Senesi, A. L. Schmucker, B. C. Pals, M. O. de la Cruz*, et al.*, "DNA-mediated nanoparticle crystallization into Wulff polyhedra," *Nature,* vol. 505, pp. 73-77, 01/02/print 2014.
[31] X. Xu, N. L. Rosi, Y. Wang, F. Huo, and C. A. Mirkin, "Asymmetric Functionalization of Gold Nanoparticles with Oligonucleotides," *Journal of the American Chemical Society,* vol. 128, pp. 9286-9287, 2006/07/01 2006.
[32] M. R. Jones, R. J. Macfarlane, B. Lee, J. Zhang, K. L. Young, A. J. Senesi*, et al.*, "DNA-nanoparticle superlattices formed from anisotropic building blocks," *Nat Mater,* vol. 9, pp. 913-917, 11//print 2010.
[33] J. E. Padilla, C. Colovos, and T. O. Yeates, "Nanohedra: Using symmetry to design self assembling protein cages, layers, crystals, and filaments," *Proceedings of the National Academy of Sciences,* vol. 98, pp. 2217-2221, 2001.
[34] Y.-T. Lai, D. Cascio, and T. O. Yeates, "Structure of a 16-nm Cage Designed by Using Protein Oligomers," *Science,* vol. 336, p. 1129, 2012.
[35] Y.-T. Lai, E. Reading, G. L. Hura, K.-L. Tsai, A. Laganowsky, F. J. Asturias*, et al.*, "Structure of a designed protein cage that self-assembles into a highly porous cube," *Nat Chem,* vol. 6, pp. 1065-1071, 12//print 2014.
[36] N. L. Ogihara, G. Ghirlanda, J. W. Bryson, M. Gingery, W. F. DeGrado, and D. Eisenberg, "Design of three-dimensional domain-swapped dimers and fibrous oligomers," *Proceedings of the National Academy of Sciences,* vol. 98, pp. 1404-1409, 2001.
[37] S. Hirota, Y. Hattori, S. Nagao, M. Taketa, H. Komori, H. Kamikubo*, et al.*, "Cytochrome c polymerization by successive domain swapping at the C-terminal helix," *Proceedings of the National Academy of Sciences,* vol. 107, pp. 12854-12859, 2010.
[38] Y.-W. Lin, S. Nagao, M. Zhang, Y. Shomura, Y. Higuchi, and S. Hirota, "Rational Design of Heterodimeric Protein using Domain Swapping for Myoglobin," *Angewandte Chemie International Edition,* vol. 54, pp. 511-515, 2015.
[39] T. Miyamoto, M. Kuribayashi, S. Nagao, Y. Shomura, Y. Higuchi, and S. Hirota, "Domain-swapped cytochrome cb562 dimer and its nanocage encapsulating a Zn-SO4 cluster in the internal cavity," *Chemical Science,* vol. 6, pp. 7336-7342, 2015.
[40] D. N. Woolfson, G. J. Bartlett, M. Bruning, and A. R. Thomson, "New currency for old rope: from coiled-coil assemblies to α-helical barrels," *Current Opinion in Structural Biology,* vol. 22, pp. 432-441, 8// 2012.
[41] J. M. Fletcher, R. L. Harniman, F. R. H. Barnes, A. L. Boyle, A. Collins, J. Mantell*, et al.*, "Self-Assembling Cages from Coiled-Coil Peptide Modules," *Science,* vol. 340, pp. 595-599, 2013.
[42] N. C. Burgess, T. H. Sharp, F. Thomas, C. W. Wood, A. R. Thomson, N. R. Zaccai*, et al.*, "Modular Design of Self-Assembling Peptide-Based

Nanotubes," *Journal of the American Chemical Society,* vol. 137, pp. 10554-10562, 2015/08/26 2015.
[43] F. Thomas, N. C. Burgess, A. R. Thomson, and D. N. Woolfson, "Controlling the Assembly of Coiled–Coil Peptide Nanotubes," *Angewandte Chemie International Edition,* vol. 55, pp. 987-991, 2016.
[44] A. Sciore, M. Su, P. Koldewey, J. D. Eschweiler, K. A. Diffley, B. M. Linhares*, et al.*, "Flexible, symmetry-directed approach to assembling protein cages," *Proceedings of the National Academy of Sciences,* vol. 113, pp. 8681-8686, August 2, 2016 2016.
[45] A. Leaver-Fay, M. Tyka, S. M. Lewis, O. F. Lange, J. Thompson, R. Jacak*, et al.*, "Rosetta3," *Methods in Enzymology,* vol. 487, pp. 545-574, 2011/01/01/ 2011.
[46] N. Koga, R. Tatsumi-Koga, G. Liu, R. Xiao, T. B. Acton, G. T. Montelione*, et al.*, "Principles for designing ideal protein structures," *Nature,* vol. 491, pp. 222-227, 11/08/print 2012.
[47] Y.-R. Lin, N. Koga, R. Tatsumi-Koga, G. Liu, A. F. Clouser, G. T. Montelione*, et al.*, "Control over overall shape and size in de novo designed proteins," *Proceedings of the National Academy of Sciences,* vol. 112, pp. E5478-E5485, 2015.
[48] N. P. King, W. Sheffler, M. R. Sawaya, B. S. Vollmar, J. P. Sumida, I. André*, et al.*, "Computational Design of Self-Assembling Protein Nanomaterials with Atomic Level Accuracy," *Science,* vol. 336, p. 1171, 2012.
[49] N. P. King, J. B. Bale, W. Sheffler, D. E. McNamara, S. Gonen, T. Gonen*, et al.*, "Accurate design of co-assembling multi-component protein nanomaterials," *Nature,* vol. 510, pp. 103-108, 06/05/print 2014.
[50] Y. Hsia, J. B. Bale, S. Gonen, D. Shi, W. Sheffler, K. K. Fong*, et al.*, "Design of a hyperstable 60-subunit protein icosahedron," *Nature,* vol. 535, pp. 136-139, 07/07/print 2016.
[51] J. B. Bale, S. Gonen, Y. Liu, W. Sheffler, D. Ellis, C. Thomas*, et al.*, "Accurate design of megadalton-scale two-component icosahedral protein complexes," *Science,* vol. 353, p. 389, 2016.
[52] S. Franzen and S. A. Lommel, "Targeting cancer with 'smart bombs': equipping plant virus nanoparticles for a 'seek and destroy' mission," *Nanomedicine,* vol. 4, pp. 575-588, Jul 2009.
[53] C. S. Rae, I. W. Khor, Q. Wang, G. Destito, M. J. Gonzalez, P. Singh*, et al.*, "Systemic trafficking of plant virus nanoparticles in mice via the oral route," *Virology,* vol. 343, pp. 224-235, Dec 20 2005.
[54] K. S. Raja, Q. Wang, M. J. Gonzalez, M. Manchester, J. E. Johnson, and M. G. Finn, "Hybrid virus-polymer materials. 1. Synthesis and properties of PEG-decorated cowpea mosaic virus," *Biomacromolecules,* vol. 4, pp. 472-476, May-Jun 2003.
[55] C. Mao, A. Liu, and B. Cao, "Virus-Based Chemical and Biological Sensing," *Angewandte Chemie International Edition,* vol. 48, pp. 6790-6810, 2009 2009.

[56] K. Gerasopoulos, M. McCarthy, P. Banerjee, X. Fan, J. N. Culver, and R. Ghodssi, "Biofabrication methods for the patterned assembly and synthesis of viral nanotemplates," *Nanotechnology,* vol. 21, Feb 5 2010.

[57] X. L. Chen, K. Gerasopoulos, J. C. Guo, A. Brown, C. S. Wang, R. Ghodssi*, et al.*, "A Patterned 3D Silicon Anode Fabricated by Electrodeposition on a Virus-Structured Current Collector," *Advanced Functional Materials,* vol. 21, pp. 380-387, Jan 2011.

[58] S. Sirotkin, A. Mermet, M. Bergoin, V. Ward, and J. Van Etten, "Viruses as nanoparticles: Structure versus collective dynamics," 2014.

[59] A. Chatterji, W. F. Ochoa, T. Ueno, T. Lin, and J. E. Johnson, "A Virus-Based Nanoblock with Tunable Electrostatic Properties," *Nano Letters,* vol. 5, pp. 597-602, 2005/04/01 2005.

[60] C. M. Soto, A. S. Blum, G. J. Vora, N. Lebedev, C. E. Meador, A. P. Won*, et al.*, "Fluorescent Signal Amplification of Carbocyanine Dyes Using Engineered Viral Nanoparticles," *Journal of the American Chemical Society,* vol. 128, pp. 5184-5189, 2006/04/01 2006.

[61] M. Allen, J. W. M. Bulte, L. Liepold, G. Basu, H. A. Zywicke, J. A. Frank*, et al.*, "Paramagnetic viral nanoparticles as potential high-relaxivity magnetic resonance contrast agents," *Magnetic Resonance in Medicine,* vol. 54, pp. 807-812, 2005.

[62] Q. Wang, E. Kaltgrad, T. Lin, J. E. Johnson, and M. G. Finn, "Natural Supramolecular Building Blocks," *Chemistry & Biology,* vol. 9, pp. 805-811, 2002/07/01/ 2002.

[63] N. F. Steinmetz, M. E. Mertens, R. E. Taurog, J. E. Johnson, U. Commandeur, R. Fischer*, et al.*, "Potato virus X as a novel platform for potential biomedical applications," *Nano Lett,* vol. 10, pp. 305-12, Jan 2010.

[64] M. B. Sherman, R. H. Guenther, F. Tama, T. L. Sit, C. L. Brooks, A. M. Mikhailov*, et al.*, "Removal of divalent cations induces structural transitions in Red clover necrotic mosaic virus, revealing a potential mechanism for RNA release," *Journal of Virology,* vol. 80, pp. 10395-10406, Nov 2006.

[65] L. Loo, R. H. Guenther, S. A. Lommel, and S. Franzen, "Infusion of dye molecules into Red clover necrotic mosaic virus," *Chemical Communications,* pp. 88-90, 2008.

[66] D. M. Lockney, R. N. Guenther, L. Loo, W. Overton, R. Antonelli, J. Clark*, et al.*, "The Red clover necrotic mosaic virus Capsid as a Multifunctional Cell Targeting Plant Viral Nanoparticle," *Bioconjugate Chemistry,* vol. 22, pp. 67-73, 2011/01/19 2011.

[67] J. A. Speir, S. Munshi, G. Wang, T. S. Baker, and J. E. Johnson, "Structures of the native and swollen forms of cowpea chlorotic mottle virus determined by X-ray crystallography and cryo-electron microscopy," *Structure,* vol. 3, pp. 63-78, 1995/01/01/ 1995.

[68] F. Tama and C. L. Brooks, "The Mechanism and Pathway of pH Induced Swelling in Cowpea Chlorotic Mottle Virus," *Journal of Molecular Biology,* vol. 318, pp. 733-747, 2002/05/03/ 2002.

[69] R. Usha, J. B. Rohll, V. E. Spall, M. Shanks, A. J. Maule, J. E. Johnson*, et al.*, "Expression of an animal virus antigenic site on the surface of a plant virus particle," *Virology,* vol. 197, pp. 366-74, Nov 1993.

[70] C. Porta, V. E. Spall, J. Loveland, J. E. Johnson, P. J. Barker, and G. P. Lomonossoff, "Development of Cowpea Mosaic Virus as a High-Yielding System for the Presentation of Foreign Peptides," *Virology,* vol. 202, pp. 949-955, 1994/08/01/ 1994.

[71] G. Lomonossoff and J. E. Johnson*†, "Eukaryotic viral expression systems for polypeptides," *Seminars in Virology,* vol. 6, pp. 257-267, 1995/08/01/ 1995.

[72] J. Johnson, T. Lin, and G. Lomonossoff, "PRESENTATION OF HETEROLOGOUS PEPTIDES ON PLANT VIRUSES: Genetics, Structure, and Function," *Annual Review of Phytopathology,* vol. 35, pp. 67-86, 1997/09/01 1997.

[73] G. P. Lomonossoff and J. E. Johnson, "Use of macromolecular assemblies as expression systems for peptides and synthetic vaccines," *Current Opinion in Structural Biology,* vol. 6, pp. 176-182, 1996/04/01/ 1996.

[74] S. N. Shah, N. F. Steinmetz, A. A. A. Aljabali, G. P. Lomonossoff, and D. J. Evans, "Environmentally benign synthesis of virus-templated, monodisperse, iron-platinum nanoparticles," *Dalton Transactions,* pp. 8479-8480, 2009.

[75] N. F. Steinmetz, S. N. Shah, J. E. Barclay, G. Rallapalli, G. P. Lomonossoff, and D. J. Evans, "Virus-Templated Silica Nanoparticles," *Small,* vol. 5, pp. 813-816, 2009/04/06 2009.

[76] N. Carette, H. Engelkamp, E. Akpa, S. J. Pierre, N. R. Cameron, P. C. M. Christianen*, et al.*, "A virus-based biocatalyst," *Nat Nano,* vol. 2, pp. 226-229, 04//print 2007.

[77] H. Morin, M.-H. Tremblay, É. Plante, C. Paré, N. Majeau, R. Hogue*, et al.*, "High avidity binding of engineered papaya mosaic virus virus-like particles to resting spores of Plasmodiophora Brassicae," *Journal of Biotechnology,* vol. 128, pp. 423-434, 2007/02/01/ 2007.

[78] K. Namba, R. Pattanayek, and G. Stubbs, "Visualization of protein-nucleic acid interactions in a virus," *Journal of Molecular Biology,* vol. 208, pp. 307-325, 1989/07/20/ 1989.

[79] T. M. T. Schuster, R. B. Scheele, M. L. Adams, S. J. Shire, and J. J. Steckert, "Studies on the mechanism of assembly of tobacco mosaic virus," *Biophysical Journal,* vol. 32, pp. 313-29.

[80] G. G. Lebeurier, A. Nicolaieff, and K. E. Richards, "Inside-out model for self-assembly of tobacco mosaic virus," *Proceedings of the National Academy of Sciences of the United States of America,* vol. 74, pp. 149-53.

[81] B. Bhyravbhatla, S. J. Watowich, and D. L. D. Caspar, "Refined atomic model of the four-layer aggregate of the tobacco mosaic virus coat protein at 2.4-angstrom resolution," *Biophysical Journal,* vol. 74, pp. 604-615, Jan 1998.

[82] A. C. Bloomer, J. N. Champness, G. Bricogne, R. Staden, and A. Klug, "Protein disk of tobacco mosaic virus at 2.8 Å resolution showing the interactions within and between subunits," *Nature,* vol. 276, pp. 362-368, 1978 1978.

[83] M. B. Sherman, R. H. Guenther, F. Tama, T. L. Sit, C. L. Brooks, A. M. Mikhailov*, et al.*, "Removal of Divalent Cations Induces Structural Transitions in Red Clover Necrotic Mosaic Virus, Revealing a Potential Mechanism for RNA Release," *Journal of Virology,* vol. 80, pp. 10395-10406, November 1, 2006 2006.

[84] J. M. Alonso, M. Ł. Górzny, and A. M. Bittner, "The physics of tobacco mosaic virus and virus-based devices in biotechnology," *Trends in Biotechnology,* vol. 31, pp. 530-538, 2013/09/01/ 2013.

[85] X. L. Chen, K. Gerasopoulos, J. C. Guo, A. Brown, C. S. Wang, R. Ghodssi*, et al.*, "Virus-Enabled Silicon Anode for Lithium-Ion Batteries," *Acs Nano,* vol. 4, pp. 5366-5372, Sep 2010.

[86] C. Y. Chiang, J. Epstein, A. Brown, J. N. Munday, J. N. Culver, and S. Ehrman, "Biological Templates for Antireflective Current Collectors for Photoelectrochemical Cell Applications," *Nano Letters,* vol. 12, pp. 6005-6011, Nov 2012.

[87] M. McCarthy, K. Gerasopoulos, R. Enright, J. N. Culver, R. Ghodssi, and E. N. Wang, "Biotemplated hierarchical surfaces and the role of dual length scales on the repellency of impacting droplets," *Applied Physics Letters,* vol. 100, Jun 25 2012.

[88] E. Royston, A. Ghosh, P. Kofinas, M. T. Harris, and J. N. Culver, "Self-Assembly of Virus-Structured High Surface Area Nanomaterials and Their Application as Battery Electrodes," *Langmuir,* vol. 24, pp. 906-912, 2008/02/01 2008.

[89] D. Zimmern and P. J. G. Butler, "The isolation of tobacco mosaic virus RNA fragments containing the origin for viral assembly," *Cell,* vol. 11, pp. 455-462, 1977/07/01/ 1977.

[90] S. Eiben, N. Stitz, F. Eber, J. Wagner, P. Atanasova, J. Bill*, et al.*, "Tailoring the surface properties of tobacco mosaic virions by the integration of bacterially expressed mutant coat protein," *Virus Research,* vol. 180, pp. 92-96, 2014/02/13/ 2014.

[91] Y. Tian, S. Gao, M. Wu, X. Liu, J. Qiao, Q. Zhou*, et al.*, "Tobacco Mosaic Virus-Based 1D Nanorod-Drug Carrier via the Integrin-Mediated Endocytosis Pathway," *ACS Applied Materials & Interfaces,* vol. 8, pp. 10800-10807, 2016/05/04 2016.

[92] F. C. Geiger, F. J. Eber, S. Eiben, A. Mueller, H. Jeske, J. P. Spatz*, et al.*, "TMV nanorods with programmed longitudinal domains of differently addressable coat proteins," *Nanoscale,* vol. 5, pp. 3808-3816, 2013.

[93] S. Shukla, F. J. Eber, A. S. Nagarajan, N. A. DiFranco, N. Schmidt, A. M. Wen*, et al.*, "The Impact of Aspect Ratio on the Biodistribution and Tumor Homing of Rigid Soft-Matter Nanorods," *Advanced Healthcare Materials,* vol. 4, pp. 874-82, Apr 22 2015.

[94] K. Saunders and G. P. Lomonossoff, "In Planta Synthesis of Designer-Length Tobacco Mosaic Virus-Based Nano-Rods That Can Be Used to Fabricate Nano-Wires," *Frontiers in Plant Science,* vol. 8, 2017-August-18 2017.

[95] F. J. Eber, S. Eiben, H. Jeske, and C. Wege, "RNA-controlled assembly of tobacco mosaic virus-derived complex structures: from nanoboomerangs to tetrapods," *Nanoscale,* vol. 7, pp. 344-355, 2015.
[96] B. Lu, G. Stubbs, and J. N. Culver, "Carboxylate interactions involved in the disassembly of tobacco mosaic tobamovirus," *Virology,* vol. 225, pp. 11-20, Nov 1 1996.
[97] D. L. D. Caspar, "Assembly and Stability of the Tobacco Mosaic Virus Particle," in *Advances in Protein Chemistry*. vol. 18, C. B. Anfinsen, M. L. Anson, and J. T. Edsall, Eds., ed: Academic Press, 1964, pp. 37-121.
[98] B. Lu, Z. F. Taraporewala, G. Stubbs, and J. N. Culver, "Intersubunit interactions allowing a carboxylate mutant coat protein to inhibit tobamovirus disassembly," *Virology,* vol. 244, pp. 13-19, Apr 25 1998.
[99] A. Kadri, E. Maiß, N. Amsharov, A. M. Bittner, S. Balci, K. Kern*, et al.*, "Engineered Tobacco mosaic virus mutants with distinct physical characteristics in planta and enhanced metallization properties," *Virus Research,* vol. 157, pp. 35-46, 2011/04/01/ 2011.
[100] A. Kadri, C. Wege, and H. Jeske, "In vivo self-assembly of TMV-like particles in yeast and bacteria for nanotechnological applications," *Journal of Virological Methods,* vol. 189, pp. 328-340, 2013/05/01/ 2013.
[101] K. Zhou, F. Li, G. Dai, C. Meng, and Q. Wang, "Disulfide Bond: Dramatically Enhanced Assembly Capability and Structural Stability of Tobacco Mosaic Virus Nanorods," *Biomacromolecules,* vol. 14, pp. 2593-2600, 2013/08/12 2013.
[102] J. Zhang, K. Zhou, and Q. Wang, "Tailoring the Self-Assembly Behaviors of Recombinant Tobacco Mosaic Virus by Rationally Introducing Covalent Bonding at the Protein–Protein Interface," *Small,* vol. 12, pp. 4955-4959, 2016.
[103] R. A. Miller, A. D. Presley, and M. B. Francis, "Self-Assembling Light-Harvesting Systems from Synthetically Modified Tobacco Mosaic Virus Coat Proteins," *Journal of the American Chemical Society,* vol. 129, pp. 3104-3109, 2007/03/01 2007.
[104] D. J. Hwang, I. M. Roberts, and T. M. Wilson, "Expression of tobacco mosaic virus coat protein and assembly of pseudovirus particles in Escherichia coli," *Proceedings of the National Academy of Sciences,* vol. 91, pp. 9067-9071, 1994.
[105] A. C. H. Durham, J. T. Finch, and A. Klug, "States of Aggregation of Tobacco Mosaic Virus Protein," *Nature New Biology,* vol. 229, p. 37, 01/13/online 1971.
[106] K. Wadu-Mesthrige, B. Pati, W. M. McClain, and G.-Y. Liu, "Disaggregation of Tobacco Mosaic Virus by Bovine Serum Albumin," *Langmuir,* vol. 12, pp. 3511-3515, 1996/01/01 1996.
[107] Z. Niu, M. Bruckman, V. S. Kotakadi, J. He, T. Emrick, T. P. Russell*, et al.*, "Study and characterization of tobacco mosaic virus head-to-tail assembly assisted by aniline polymerization," *Chemical Communications,* pp. 3019-3021, 2006.

[108] Z. Niu, M. A. Bruckman, S. Li, L. A. Lee, B. Lee, S. V. Pingali*, et al.*, "Assembly of Tobacco Mosaic Virus into Fibrous and Macroscopic Bundled Arrays Mediated by Surface Aniline Polymerization," *Langmuir,* vol. 23, pp. 6719-6724, 2007/06/01 2007.
[109] Z. Niu, J. Liu, L. A. Lee, M. A. Bruckman, D. Zhao, G. Koley*, et al.*, "Biological Templated Synthesis of Water-Soluble Conductive Polymeric Nanowires," *Nano Letters,* vol. 7, pp. 3729-3733, 2007/12/01 2007.
[110] Q. Zhou, X. Liu, Y. Tian, M. Wu, and Z. Niu, "Mussel-Inspired Polydopamine Coating on Tobacco Mosaic Virus: One-Dimensional Hybrid Nanofibers for Gold Nanoparticle Growth," *Langmuir,* vol. 33, pp. 9866-9872, 2017/09/26 2017.
[111] A. M. Bittner, X. C. Wu, S. Balci, M. Knez, A. Kadri, and K. Kern, "Bottom-Up Synthesis and Top-Down Organisation of Semiconductor and Metal Clusters on Surfaces," *European Journal of Inorganic Chemistry,* vol. 2005, pp. 3717-3728, 2005.
[112] S. P. Wargacki, B. Pate, and R. A. Vaia, "Fabrication of 2D Ordered Films of Tobacco Mosaic Virus (TMV): Processing Morphology Correlations for Convective Assembly," *Langmuir,* vol. 24, pp. 5439-5444, 2008/05/01 2008.
[113] A. Ghosh, J. Guo, A. D. Brown, E. Royston, C. Wang, P. Kofinas*, et al.*, "Virus-Assembled Flexible Electrode-Electrolyte Interfaces for Enhanced Polymer-Based Battery Applications," *Journal of Nanomaterials,* 2012 2012.
[114] S. Y. Lee, E. Royston, J. N. Culver, and M. T. Harris, "Improved metal cluster deposition on a genetically engineered tobacco mosaic virus template," *Nanotechnology,* vol. 16, pp. S435-S441, Jul 2005.
[115] P. Lu and M.-G. Feng, "Bifunctional enhancement of a beta-glucanase-xylanase fusion enzyme by optimization of peptide linkers," *Applied Microbiology and Biotechnology,* vol. 79, pp. 579-587, Jun 2008.
[116] A. Mueller, F. J. Eber, C. Azucena, A. Petershans, A. M. Bittner, H. Gliemann*, et al.*, "Inducible Site-Selective Bottom-Up Assembly of Virus-Derived Nanotube Arrays on RNA-Equipped Wafers," *ACS Nano,* vol. 5, pp. 4512-4520, 2011/06/28 2011.
[117] M. L. Smith, W. P. Fitzmaurice, T. H. Turpen, and K. E. Palmer, "Display of Peptides on the Surface of Tobacco Mosaic Virus Particles," in *Plant-produced Microbial Vaccines*, A. V. Karasev, Ed., ed Berlin, Heidelberg: Springer Berlin Heidelberg, 2009, pp. 13-31.
[118] L. A. Lee, H. G. Nguyen, and Q. Wang, "Altering the landscape of viruses and bionanoparticles," *Organic & Biomolecular Chemistry,* vol. 9, pp. 6189-6195, 2011.
[119] K. L. Lee, B. L. Carpenter, A. M. Wen, R. A. Ghiladi, and N. F. Steinmetz, "High Aspect Ratio Nanotubes Formed by Tobacco Mosaic Virus for Delivery of Photodynamic Agents Targeting Melanoma," *ACS Biomaterials Science & Engineering,* vol. 2, pp. 838-844, 03/23 2016.
[120] A. M. Wen, M. Infusino, A. De Luca, D. L. Kernan, A. E. Czapar, G. Strangi*, et al.*, "Interface of Physics and Biology: Engineering Virus-Based Nanoparticles for Biophotonics," *Bioconjugate Chemistry,* vol. 26, pp. 51-62, 2015/01/21 2015.

[121] X. Liu, B. Liu, S. Gao, Z. Wang, Y. Tian, M. Wu*, et al.*, "Glyco-decorated tobacco mosaic virus as a vector for cisplatin delivery," *Journal of Materials Chemistry B,* vol. 5, pp. 2078-2085, 2017.
[122] L. Chen, X. Zhao, Y. Lin, Y. Huang, and Q. Wang, "A supramolecular strategy to assemble multifunctional viral nanoparticles," *Chemical Communications,* vol. 49, pp. 9678-9680, 2013.
[123] T. L. Schlick, Z. Ding, E. W. Kovacs, and M. B. Francis, "Dual-Surface Modification of the Tobacco Mosaic Virus," *Journal of the American Chemical Society,* vol. 127, pp. 3718-3723, 2005/03/01 2005.
[124] M. L. Smith, J. A. Lindbo, S. Dillard-Telm, P. M. Brosio, A. B. Lasnik, A. A. McCormick*, et al.*, "Modified Tobacco mosaic virus particles as scaffolds for display of protein antigens for vaccine applications," *Virology,* vol. 348, pp. 475-488, 2006/05/10/ 2006.
[125] K. Altintoprak, A. Seidenstucker, A. Welle, S. Eiben, P. Atanasova, N. Stitz*, et al.*, "Peptide-equipped tobacco mosaic virus templates for selective and controllable biomineral deposition," *Beilstein Journal of Nanotechnology,* vol. 6, pp. 1399-412, 2015.
[126] C. Koch, K. Wabbel, F. J. Eber, P. Krolla-Sidenstein, C. Azucena, H. Gliemann*, et al.*, "Modified TMV Particles as Beneficial Scaffolds to Present Sensor Enzymes," *Frontiers in Plant Science,* vol. 6, 2015-December-24 2015.
[127] F. H. Zang, K. Gerasopoulos, X. Z. Fan, A. D. Brown, J. N. Culver, and R. Ghodssi, "An electrochemical sensor for selective TNT sensing based on Tobacco mosaic virus-like particle binding agents," *Chemical Communications,* vol. 50, pp. 12977-12980, 2014.
[128] F. Zang, K. Gerasopoulos, A. D. Brown, J. N. Culver, and R. Ghodssi, "Capillary Microfluidics-Assembled Virus-like Particle Bionanoreceptor Interfaces for Label-Free Biosensing," *ACS Applied Materials & Interfaces,* vol. 9, pp. 8471-8479, 2017/03/15 2017.
[129] L. A. Lee, S. M. Muhammad, Q. L. Nguyen, P. Sitasuwan, G. Horvath, and Q. Wang, "Multivalent Ligand Displayed on Plant Virus Induces Rapid Onset of Bone Differentiation," *Molecular Pharmaceutics,* vol. 9, pp. 2121-2125, 2012/07/02 2012.
[130] L. A. Lee, Q. L. Nguyen, L. Wu, G. Horvath, R. S. Nelson, and Q. Wang, "Mutant Plant Viruses with Cell Binding Motifs Provide Differential Adhesion Strengths and Morphologies," *Biomacromolecules,* vol. 13, pp. 422-431, 2012/02/13 2012.
[131] M. A. Bruckman, J. Liu, G. Koley, Y. Li, B. Benicewicz, Z. Niu*, et al.*, "Tobacco mosaic virus based thin film sensor for detection of volatile organic compounds," *Journal of Materials Chemistry,* vol. 20, pp. 5715-5719, 2010.
[132] M. A. Bruckman, G. Kaur, L. A. Lee, F. Xie, J. Sepulveda, R. Breitenkamp*, et al.*, "Surface Modification of Tobacco Mosaic Virus with "Click" Chemistry," *ChemBioChem,* vol. 9, pp. 519-523, 2008/03/03 2008.
[133] H. Yi, S. Nisar, S.-Y. Lee, M. A. Powers, W. E. Bentley, G. F. Payne*, et al.*, "Patterned Assembly of Genetically Modified Viral Nanotemplates via

Nucleic Acid Hybridization," *Nano Letters,* vol. 5, pp. 1931-1936, 2005/10/01 2005.
[134] M. Demir and M. H. B. Stowell, "A chemoselective biomolecular template for assembling diverse nanotubular materials," *Nanotechnology,* vol. 13, p. 541, 2002.
[135] G. P. Pogue, J. A. Lindbo, S. J. Garger, and W. P. Fitzmaurice, "Making an ally from an enemy: plant virology and the new agriculture," *Annual Review of Phytopathology,* vol. 40, pp. 45-74, 2002/09/01 2002.
[136] O. Y. Frolova, I. V. Petrunia, T. V. Komarova, V. S. Kosorukov, E. V. Sheval, Y. Y. Gleba*, et al.*, "Trastuzumab-binding peptide display by Tobacco mosaic virus," *Virology,* vol. 407, pp. 7-13, 2010/11/10/ 2010.
[137] T. H. Turpen, S. J. Reinl, Y. Charoenvit, S. L. Hoffman, V. Fallarme, and L. K. Grill, "Malaria Epitopes Expressed on the surface of Recombinant Tobacco Mosaic Virus," *Bio/Technology,* vol. 13, p. 53, 01/01/online 1995.
[138] S. S. Cruz, S. Chapman, A. G. Roberts, I. M. Roberts, D. A. Prior, and K. J. Oparka, "Assembly and movement of a plant virus carrying a green fluorescent protein overcoat," *Proceedings of the National Academy of Sciences of the United States of America,* vol. 93, pp. 6286-6290, 1996.
[139] J. Tilsner, O. Linnik, M. Louveaux, I. M. Roberts, S. N. Chapman, and K. J. Oparka, "Replication and trafficking of a plant virus are coupled at the entrances of plasmodesmata," *The Journal of Cell Biology,* vol. 201, pp. 981-995, 2013.
[140] R. d. Bruin, K. Spelt, J. Mol, R. Koes, and F. Quattrocchio, "Selection of high-affinity phage antibodies from phage display libraries," *Nature Biotechnology,* vol. 17, p. 397, 04/01/online 1999.
[141] G. Å. Løset, B. Bogen, and I. Sandlie, "Expanding the Versatility of Phage Display I: Efficient Display of Peptide-Tags on Protein VII of the Filamentous Phage," *PLOS ONE,* vol. 6, p. e14702, 2011.
[142] G. Å. Løset, N. Roos, B. Bogen, and I. Sandlie, "Expanding the Versatility of Phage Display II: Improved Affinity Selection of Folded Domains on Protein VII and IX of the Filamentous Phage," *PLOS ONE,* vol. 6, p. e17433, 2011.
[143] K. Saunders and G. P. Lomonossoff, "Exploiting plant virus-derived components to achieve in planta expression and for templates for synthetic biology applications," *The New phytologist,* Mar 4 2013.
[144] Z. Liu, J. Qiao, Z. Niu, and Q. Wang, "Natural supramolecular building blocks: from virus coat proteins to viral nanoparticles," *Chemical Society reviews,* vol. 41, pp. 6178-94, Sep 21 2012.
[145] J. K. Pokorski and N. F. Steinmetz, "The art of engineering viral nanoparticles," *Molecular pharmaceutics,* vol. 8, pp. 29-43, Feb 7 2011.
[146] C. E. Flynn, S. W. Lee, B. R. Peelle, and A. M. Belcher, "Viruses as vehicles for growth, organization and assembly of materials," *Acta Materialia,* vol. 51, pp. 5867-5880, Nov 25 2003.
[147] K. Saunders and G. P. Lomonossoff, "Exploiting plant virus-derived components to achieve in planta expression and for templates for synthetic biology applications," *The New phytologist,* Mar 4 2013.

[148] I. Yildiz, S. Shukla, and N. F. Steinmetz, "Applications of viral nanoparticles in medicine," *Current opinion in biotechnology,* vol. 22, pp. 901-8, Dec 2011.
[149] M. T. Dedeo, D. T. Finley, and M. B. Francis, "Viral capsids as self-assembling templates for new materials," *Progress in molecular biology and translational science,* vol. 103, pp. 353-92, 2011.
[150] S. Y. Lee, J. S. Lim, and M. T. Harris, "Synthesis and application of virus-based hybrid nanomaterials," *Biotechnology and bioengineering,* vol. 109, pp. 16-30, Jan 2012.
[151] K. Namba, R. Pattanayek, and G. Stubbs, "Visualization of protein-nucleic acid interactions in a virus - refined structure of intact tobacco mosaic virus at 2.9 A resolution by X-ray fiber diffraction," *Journal of Molecular Biology,* vol. 208, pp. 307-325, 1989.
[152] G. Stubbs, "Molecular structures of viruses from the tobacco mosaic virus group," *Seminars in Virology,* vol. 1, pp. 405-412, 1990.
[153] M. L. Smith, W. P. Fitzmaurice, T. H. Turpen, and K. E. Palmer, "Display of peptides on the surface of tobacco mosaic virus particles," *Curr Top Microbiol Immunol,* vol. 332, pp. 13-31, 2009.
[154] V. Yusibov, S. Shivprasad, T. H. Turpen, W. Dawson, and H. Koprowski, "Plant viral vectors based on tobamoviruses," *Current topics in microbiology and immunology,* vol. 240, pp. 81-94, 1999.
[155] S. Rabindran and W. O. Dawson, "Assessment of recombinants that arise from the use of a TMV-based transient expression vector," *Virology,* vol. 284, pp. 182-9, Jun 5 2001.
[156] D. J. Hwang, I. M. Roberts, and T. M. Wilson, "Assembly of tobacco mosaic virus and TMV-like pseudovirus particles in Escherichia coli," *Archives of virology. Supplementum,* vol. 9, pp. 543-58, 1994.
[157] M. T. Dedeo, K. E. Duderstadt, J. M. Berger, and M. B. Francis, "Nanoscale protein assemblies from a circular permutant of the tobacco mosaic virus," *Nano letters,* vol. 10, pp. 181-6, Jan 2010.
[158] M. A. Bruckman, C. M. Soto, H. McDowell, J. L. Liu, B. R. Ratna, K. V. Korpany*, et al.*, "Role of hexahistidine in directed nanoassemblies of tobacco mosaic virus coat protein," *ACS nano,* vol. 5, pp. 1606-16, Mar 22 2011.
[159] D. J. Hwang, I. M. Roberts, and T. M. Wilson, "Expression of tobacco mosaic virus coat protein and assembly of pseudovirus particles in Escherichia coli," *Proc Natl Acad Sci U S A,* vol. 91, pp. 9067-71, Sep 13 1994.
[160] A. Durham, J. Finch, and A. Klug, "States of aggregation of tobacco mosaic virus," *Nature,* vol. 229, pp. 37-42, 1971.
[161] J. N. Culver, W. O. Dawson, K. Plonk, and G. Stubbs, "Site-Directed Mutagenesis Confirms the Involvement of Carboxylate Groups in the Disassembly of Tobacco Mosaic-Virus," *Virology,* vol. 206, pp. 724-730, Jan 10 1995.
[162] E. Royston, A. Ghosh, P. Kofinas, M. T. Harris, and J. N. Culver, "Self-assembly of virus-structured high surface area nanomaterials and their application as battery electrodes," *Langmuir : the ACS journal of surfaces and colloids,* vol. 24, pp. 906-912, Feb 5 2008.

[163] A. Einhauer and A. Jungbauer, "The FLAG peptide, a versatile fusion tag for the purification of recombinant proteins," *Journal of biochemical and biophysical methods,* vol. 49, pp. 455-65, Oct 30 2001.
[164] P. Lu and M. G. Feng, "Bifunctional enhancement of a beta-glucanase-xylanase fusion enzyme by optimization of peptide linkers," *Applied microbiology and biotechnology,* vol. 79, pp. 579-87, Jun 2008.
[165] K. A. Kelly, J. Carson, J. R. McCarthy, and R. Weissleder, "Novel peptide sequence ("IQ-tag") with high affinity for NIR fluorochromes allows protein and cell specific labeling for in vivo imaging," *PLoS One,* vol. 2, p. e665, 2007.
[166] B. J. Bachmann, K. B. Low, and A. L. Taylor, "Recalibrated linkage map of Escherichia coli K-12," *Bacteriological reviews,* vol. 40, pp. 116-67, Mar 1976.
[167] C. A. Schneider, W. S. Rasband, and K. W. Eliceiri, "NIH Image to ImageJ: 25 years of image analysis," *Nature methods,* vol. 9, pp. 671-5, Jul 2012.
[168] A. Ghosh, J. C. Guo, A. D. Brown, E. Royston, C. S. Wang, P. Kofinas*, et al.*, "Virus-Assembled Flexible Electrode-Electrolyte Interfaces for Enhanced Polymer-Based Battery Applications," *Journal of Nanomaterials,* 2012.
[169] Y. Liu, H. Wang, J. Huang, J. Yang, B. Liu, and P. Yang, "Microchip-based ELISA strategy for the detection of low-level disease biomarker in serum," *Anal Chim Acta,* vol. 650, pp. 77-82, Sep 14 2009.
[170] T. H. Turpen, S. J. Reinl, Y. Charoenvit, S. L. Hoffman, V. Fallarme, and L. K. Grill, "Malarial epitopes expressed on the surface of recombinant tobacco mosaic virus," *Biotechnology (N Y),* vol. 13, pp. 53-7, Jan 1995.
[171] N. V. Petukhova, T. V. Gasanova, L. A. Stepanova, O. A. Rusova, M. V. Potapchuk, A. V. Korotkov*, et al.*, "Immunogenicity and protective efficacy of candidate universal influenza A nanovaccines produced in plants by tobacco mosaic virus-based vectors," *Current pharmaceutical design,* Feb 1 2013.
[172] L. Wu, L. Jiang, Z. Zhou, J. Fan, Q. Zhang, H. Zhu*, et al.*, "Expression of foot-and-mouth disease virus epitopes in tobacco by a tobacco mosaic virus-based vector," *Vaccine,* vol. 21, pp. 4390-8, Oct 1 2003.
[173] M. Paschke, "Phage display systems and their applications," *Appl Microbiol Biotechnol,* vol. 70, pp. 2-11, Mar 2006.
[174] A. S. Khan, R. Thompson, C. Cao, and J. J. Valdes, "Selection and characterization of peptide memitopes binding to ricin," *Biotechnol Lett,* vol. 25, pp. 1671-5, Oct 2003.
[175] P. Samuelson, H. Wernerus, M. Svedberg, and S. Stahl, "Staphylococcal surface display of metal-binding polyhistidyl peptides," *Appl Environ Microbiol,* vol. 66, pp. 1243-8, Mar 2000.
[176] T. Ide, S. H. Baik, T. Matsuba, and S. Harayama, "Identification by the phage-display technique of peptides that bind to H7 flagellin of Escherichia coli," *Biosci Biotechnol Biochem,* vol. 67, pp. 1335-41, Jun 2003.
[177] Z. Han, G. Su, and C. Huang, "Screening and identification of receptor antagonist for shiga toxin from random peptides displayed on filamentous bacteriophages," *Sci China C Life Sci,* vol. 42, pp. 43-9, Feb 1999.

[178] E. A. Soykut, F. C. Dudak, and I. H. Boyaci, "Selection of staphylococcal enterotoxin B (SEB)-binding peptide using phage display technology," *Biochem Biophys Res Commun,* vol. 370, pp. 104-8, May 23 2008.
[179] H. Ma, B. Zhou, Y. Kim, and K. D. Janda, "A cyclic peptide-polymer probe for the detection of Clostridium botulinum neurotoxin serotype A," *Toxicon,* vol. 47, pp. 901-8, Jun 15 2006.
[180] V. A. Petrenko and V. J. Vodyanoy, "Phage display for detection of biological threat agents," *J Microbiol Methods,* vol. 53, pp. 253-62, May 2003.
[181] A. D. Brown, L. Naves, X. Wang, R. Ghodssi, and J. N. Culver, "Carboxylate-Directed In Vivo Assembly of Virus-like Nanorods and Tubes for the Display of Functional Peptides and Residues," *Biomacromolecules,* vol. 14, pp. 3123-3129, Sep 2013.
[182] R. Kay, A. Chan, M. Daly, and J. McPherson, "Duplication of CaMV 35S promoter sequences creates a strong enhancer for plant genes," *Science,* vol. 236, pp. 1299-1302, 1987.
[183] J. N. Culver, A. D. Brown, F. Zang, M. Gnerlich, K. Gerasopoulos, and R. Ghodssi, "Plant virus directed fabrication of nanoscale materials and devices," *Virology,* vol. 479-480, pp. 200-12, May 2015.
[184] S.-M. Kim and H.-S. Kim, "Engineering of extracellular vesicles as drug delivery vehicles," *Stem Cell Investigation,* vol. 4, p. 74, 09/12
07/20/received
08/21/accepted 2017.
[185] F. Hong, F. Zhang, Y. Liu, and H. Yan, "DNA Origami: Scaffolds for Creating Higher Order Structures," *Chem Rev,* vol. 117, pp. 12584-12640, Oct 25 2017.
[186] W. Pfeifer and B. Sacca, "From Nano to Macro through Hierarchical Self-Assembly: The DNA Paradigm," *Chembiochem,* vol. 17, pp. 1063-1080, Jun 16 2016.
[187] N. P. King and Y. T. Lai, "Practical approaches to designing novel protein assemblies," *Curr Opin Struct Biol,* vol. 23, pp. 632-8, Aug 2013.
[188] B. Schwarz, M. Uchida, and T. Douglas, "Biomedical and Catalytic Opportunities of Virus-Like Particles in Nanotechnology," *Adv Virus Res,* vol. 97, pp. 1-60, 2017.
[189] A. M. Wen and N. F. Steinmetz, "Design of virus-based nanomaterials for medicine, biotechnology, and energy," *Chem Soc Rev,* vol. 45, pp. 4074-126, Jul 25 2016.
[190] X. Z. Fan, E. Pomerantseva, M. Gnerlich, A. Brown, K. Gerasopoulos, M. McCarthy*, et al.*, "Tobacco mosaic virus: A biological building block for micro/nano/bio systems," *Journal of Vacuum Science & Technology A,* vol. 31, pp. 1-24, Sep 2013.
[191] E. Strable and M. G. Finn, "Chemical Modification of Viruses and Virus-Like Particles," *Viruses and Nanotechnology,* vol. 327, pp. 1-21, 2009.
[192] K. Zhou, F. Li, G. L. Dai, C. Meng, and Q. B. Wang, "Disulfide Bond: Dramatically Enhanced Assembly Capability and Structural Stability of Tobacco Mosaic Virus Nanorods," *Biomacromolecules,* vol. 14, pp. 2593-2600, Aug 2013.

[193] A. Mueller, F. J. Eber, C. Azucena, A. Petershans, A. M. Bittner, H. Gliemann*, et al.*, "Inducible site-selective bottom-up assembly of virus-derived nanotube arrays on RNA-equipped wafers," *ACS nano,* vol. 5, pp. 4512-20, Jun 28 2011.
[194] F. C. Geiger, F. J. Eber, S. Eiben, A. Mueller, H. Jeske, J. P. Spatz*, et al.*, "TMV nanorods with programmed longitudinal domains of differently addressable coat proteins," *Nanoscale,* vol. 5, pp. 3808-16, May 07 2013.
[195] A. Schneider, F. J. Eber, N. L. Wenz, K. Altintoprak, H. Jeske, S. Eiben*, et al.*, "Dynamic DNA-controlled "stop-and-go" assembly of well-defined protein domains on RNA-scaffolded TMV-like nanotubes," *Nanoscale,* vol. 8, pp. 19853-19866, Dec 01 2016.
[196] F. J. Eber, S. Eiben, H. Jeske, and C. Wege, "RNA-controlled assembly of tobacco mosaic virus-derived complex structures: from nanoboomerangs to tetrapods," *Nanoscale,* vol. 7, pp. 344-355, 2015.
[197] C. F. S. Bonafe, C. M. R. Vital, R. C. B. Telles, M. C. Gonçalves, M. S. A. Matsuura, F. B. T. Pessine*, et al.*, "Tobacco Mosaic Virus Disassembly by High Hydrostatic Pressure in Combination with Urea and Low Temperature," *Biochemistry,* vol. 37, pp. 11097-11105, 1998/08/01 1998.
[198] J. L. R. Santos, J. A. C. Bispo, G. F. Landini, and C. F. S. Bonafe, "Proton dependence of tobacco mosaic virus dissociation by pressure," *Biophysical Chemistry,* vol. 111, pp. 53-61, 2004/09/01/ 2004.
[199] J. N. Culver, W. O. Dawson, K. Plonk, and G. Stubbs, "Site-directed mutagenesis confirms the involvement of carboxylate groups in the disassembly of tobacco mosaic virus," *Virology,* vol. 206, pp. 724-730, 1995/01/10/ 1995.
[200] P. J. Butler, "Self-assembly of tobacco mosaic virus: the role of an intermediate aggregate in generating both specificity and speed," *Philosophical transactions of the Royal Society of London. Series B, Biological sciences,* vol. 354, pp. 537-550, 1999.